AFCRL-63-662

DYNAMIC PROPERTIES OF ROCKS

V. G. Gregson
T. J. Ahrens
C. F. Petersen

Stanford Research Institute
Menlo Park, California

Contract No. AF 19(604)-8419

Final Report
August 15, 1963

Prepared for

AIR FORCE CAMBRIDGE RESEARCH LABORATORIES
OFFICE OF AEROSPACE RESEARCH
UNITED STATES AIR FORCE
BEDFORD, MASSACHUSETTS

WORK SPONSORED BY ADVANCED RESEARCH PROJECTS AGENCY
PROJECT VELA-UNIFORM

ARPA Order No. 180-61 (Amendment 2)
Project 8100, Task 2
ARPA Order No. 292-62
Project 8652
Task 865201

AFCRL-63-662

DYNAMIC PROPERTIES OF ROCKS

V. G. Gregson
T. J. Ahrens
C. F. Petersen

Stanford Research Institute
Menlo Park, California

Contract No. AF 19(604)-8419

Final Report
August 15, 1963

Prepared for

AIR FORCE CAMBRIDGE RESEARCH LABORATORIES
OFFICE OF AEROSPACE RESEARCH
UNITED STATES AIR FORCE
BEDFORD, MASSACHUSETTS

WORK SPONSORED BY ADVANCED RESEARCH PROJECTS AGENCY
PROJECT VELA-UNIFORM

ARPA Order No. 180-61 (Amendment 2)
Project 8100, Task 2
ARPA Order No. 292-62
Project 8652
Task 865201

ABSTRACT

Hugoniot equation of state data in the pressure range 5 to 250 kb have been obtained for quartzite, sandstone, calcite, marble, limestone, plagioclase, and basalt. The data were obtained by conventional shock wave techniques which measure shock and associated free-surface velocities. Impedance match solutions were obtained for porous rocks.

High values of the Hugoniot elastic limit were observed in solid rocks—50 to 100 kb in quartzite, 40 to 50 kb in feldspar and basalt, and 20 kb in calcite and marble. Porous rocks show considerably reduced values amounting to approximately 5 kb in sandstone and limestone.

Four phase transitions, indicated by multiple shock fronts, are observed in calcite. No simple relation between these and the reported transitions observed in static experiments is evident. An indication of a phase transition in sandstone at 68 kb was also obtained and is interpreted as the quartz-stishovite transition.

Decay of the elastic precursor wave amplitude, implying a time-dependent yield stress, is observed in quartzite, calcite, and marble.

CONTENTS

ABSTRACT ii

LIST OF ILLUSTRATIONS iv

LIST OF TABLES vi

I INTRODUCTION 1

II SUMMARY 3

III SHOCK WAVE EXPERIMENTS 5
- A. Inclined Mirror Method 6
- B. Impedance Match Solution 9
- C. Quartz Transducer Method 10

IV RESULTS 15
- A. Quartz Rocks 15
  - 1. Quartz and Quartzites 15
  - 2. Sandstones 16
  - 3. Calculation of Shock Temperature in Sandstones 22
  - 4. Relaxation Velocity 30
  - 5. Water Saturated Sandstone 34
  - 6. Discussion, Shock Compression of Sandstone 35
- B. Carbonate Rocks 37
  - 1. Calcite 37
  - 2. Marbles and Limestones 41
- C. Plagioclase and Basalt 51
  - 1. Plagioclase 51
  - 2. Basalt 56

V STATIC MEASUREMENTS 60
- A. Experiments 60
- B. Results 63
  - 1. St. Peter Sandstone 63
  - 2. Massillon Sandstone 69
  - 3. Coconino Sandstone 70
  - 4. Solenhofen Limestone 70

REFERENCES 71

ILLUSTRATIONS

Fig. 1 Inclined Mirror Assembly 7

Fig. 2 Inclined Mirror Method 8

Fig. 3 Impedance Match Solution 10

Fig. 4 Impedance Match Solution 11

Fig. 5 Experimental Configuration for Quartz Transducer Stress-Time Profiles in Porous Rock. 12

Fig. 6 Graphical Solution, Quartz Transducer Data 13

Fig. 7 Stress-Volume Relations, Nonporous Quartz. 16

Fig. 8 Hugoniot, Sandstone. 18

Fig. 9 Stress-Particle Velocity, Sandstone. 19

Fig. 10 Inclined Mirror Cutoff Coconino Sandstone, Double Wave. 21

Fig. 11 Inclined Mirror Cutoff Coconino Sandstone, Single Wave. 21

Fig. 12 Hugoniot, Porous Rock. 23

Fig. 13 Specific Heat *vs.* Temperature, SiO_2 (α-Quartz) 25

Fig. 14 Shock Stress *vs.* Shock Temperature and SiO_2 Phases 29

Fig. 15 Lateral Relaxation Velocity *vs.* Maximum Shock Stress 31

Fig. 16 Relaxation Particle Velocity from Lateral and Free-Surface Velocity, Coconino Sandstone. 33

Fig. 17 Quartz Transducer Stress-Time Profiles, Coconino Sandstone 34

Fig. 18 Hugoniot for Calcite and Carbonates. 38

Fig. 19 Stress-Particle Velocity Plot for Calcite. 39

Fig. 20 Stress-ρ_0/ρ Plot for Calcite 40

Fig. 21 Decay of Hugoniot Elastic Limits 44

Fig. 22 Hugoniot for a Solid Having a Yield Point and Two Phase Transitions. 46

Fig. 23 Inclined Mirror Trace for Solenhofen Limestone 47

Fig. 24 Inclined Mirror Trace for Quartz 47

Fig. 25 Inclined Mirror Trace for Vermont Marble 49

Fig. 26 Idealized Shock Front for Marble 49

Fig. 27 Hugoniot for Plagioclase and Basalt. 53

Fig. 28 Stress-Particle Velocity Curve for Plagioclase 54

Fig. 29 Stress-ρ_0/ρ Plot of Plagioclase Rocks. 55

ILLUSTRATIONS

Fig. 30 Particle Velocity Curve for Basalt 58

Fig. 31 Shock-Particle Velocity Curve for Plagioclase Rocks. 59

Fig. 32 Experimental Pressure Vessel for Ultrasonic Measurements with Two-Dimensional Stress Systems 61

Fig. 33 Schematic of System. 62

Fig. 34 Two-Inch Specimen of St. Peter Sandstone After Failure. 65

Fig. 35 One-Inch Specimen of the St. Peter Sandstone After Failure. 65

Fig. 36 St. Peter Sandstone—Raw Ultrasonic Data for Compressional Wave Arrivals. 66

Fig. 37 St. Peter Sandstone—Calculated and Measured Length Decrease. 67

Fig. 38 St. Peter Sandstone—Compressional Velocity Measurements 68

TABLES

Table I	Hugoniot Data for Sandstone	20
Table II	Shock Compression Temperatures, Coconino Sandstone	28
Table III	Hugoniot Data for Carbonate Rocks	43
Table IV	Hugoniot Data for Plagioclase	52
Table V	Hugoniot Data for Basalt	57

I INTRODUCTION

The problem of distinguishing an underground explosion from an earthquake on the basis of seismic recordings is a complex one and is being studied by a variety of approaches. Since the two phenomena differ primarily in the mode of energy release to the surrounding rock, it is clear that a complete understanding of the differences in seismic behavior must include detailed knowledge of shock propagation and decay in the vicinity of an explosion.

The mathematical description of shock propagation is based, in general, on three relations, *viz.*, the equation of continuity, the equation of motion, and a constitutive relation among the stress and strain tensors and the internal energy of the medium. The first two are universal and independent of the particular medium except insofar as the properties of the medium may dictate whether certain simplifications may reasonably be made. The third must, in general, be determined for each medium experimentally, since theory is not yet capable of providing adequate predictions.

In this report we describe work performed during the past year to determine the constitutive relation for several simple rocks and minerals in the pressure range 0 to 250 kb. These are: quartzite, sandstone and water-saturated sandstone; calcite, marble, and limestone, single and polycrystalline plagioclase, and basalt.

Most of this work has involved measuring the Hugoniot equation of state; this is the locus of equilibrium stress-density states attainable from a given initial state through a single shock transition, where "stress" refers to that component of the stress tensor normal to the shock front. These data were obtained by conventional shock wave techniques in which measurements are made of shock wave velocities and associated free-surface velocities.

An important feature of these measurements was the observation of multiple shock fronts due to yield at the elastic limit for each material, and, in the case of carbonate rocks, due also to several polymorphic phase

transitions. In addition, stress relaxation in the elastic waves was observed in quartzite, marble and calcite; some indication of relaxation was also obtained for feldspar.

A major goal of this program is to determine the constitutive relation for simple minerals which occur commonly in the earth's crust. With this information as a basis, it is hoped that theoretical models can be found for estimating the relations obtaining for more complicated rocks composed of mixtures of these minerals. The work thus far has dealt primarily with minerals and mono-mineralic rocks; intensive investigation of mixtures has not yet been undertaken. However, some preliminary experiments on water-saturated sandstone were performed.

The stress-density relations that are obtained during unloading from a shocked state are more difficult to measure than the Hugoniot and, while several techniques can, in principle, provide this information, these are not yet well-established. A few preliminary experiments for this purpose were performed on sandstone during the reporting period. These indicate that high accuracy is required in order to obtain meaningful results.

Section II of this report presents a summary of the major results. A brief description of experimental techniques, described in more detail in an earlier report,[1] appears in Section III. Section IV-A deals with the experimental results and interpretation for quartz rocks, Section IV-B with carbonate rocks, and Section IV-C with feldspars and basalt.

The results of static compression experiments on porous rocks are given in Section V.

II SUMMARY

The major results and conclusions may be listed as:

1. Data on the Rankine-Hugoniot equation of state have been obtained to 250 kb for quartzites and sandstones, for calcite, marble and limestone, for single and polycrystalline plagioclase, and for basalt.

2. Quartz rocks have an elastic wave amplitude which ranges from 5 kb in sandstone to 40 kb in Sioux quartzite, to 60 kb in Eureka quartzite, and to 100 kb novaculite. The elastic wave amplitude decreases as the porosity increases. In addition, decay of the elastic wave amplitude with distance of travel is observed in the quartzites. The temperatures attained in porous sandstones,* when shock loaded, are much higher than those attained in quartz or quartzites. Temperatures of 900°K are estimated in Coconino sandstone, shocked to 95 kb. A possible interpretation for some of the results for sandstone is that the quartz-stishovite transition is observed.

3. Calcite and carbonate rocks have an elastic wave amplitude that varies from about 20 kb in calcite, to about 12 kb in Yule and Vermont marble, to about 10 kb in Solenhofen limestone, and to about 5 kb in Spergen limestone. Besides the Hugoniot elastic limit, there are three additional transitions in calcite which are indicated by multiple shock fronts. These occur at about 30, 45, and 95 kb; values at each transition vary slightly depending upon crystal orientation. The 45 and 95 kb transitions also occur in marble; no evidence was obtained for the 30 kb transition. However, a 22 kb transition is observed in marble (the Hugoniot elastic limit is 12 kb). Calcite and Vermont marble show decay of the elastic wave amplitude with distance of travel.

4. Plagioclase and basalt have Hugoniot elastic limits of about 40 kb and have no other observed transitions for pressures as high as 250 kb. There is some indication that the elastic amplitude decays with distance of travel.

5. Transitions recorded by Adadurov, Balashov, and Dremin[2] in marble and by Hughes and McQueen[3] in gabbro may require some reinterpretation. Similar transitions in calcite and basalt were not observed.

---

* The earlier sandstone Hugoniots obtained using the two-dimensional wedge (Ref. 1, Figs. 18 and 19, and Table IV, pages 35 and 36) are now known to be *incorrect* above 15 kb.

a. The transition at 150 kb in marble reported by Adadurov *et al.* is probably the transition we recorded at about 95 kb, 150 kb being the upper limit at which the multiple shock from the 95 kb transition may be observed.

b. The estimated transition at 150 kb in gabbro reported by Hughes and McQueen may be the result of elastic yield at about 50 kb. This is indicated by data using basalt--a rock similar to gabbro, and plagioclase--a mineral occurring in sizable amounts in gabbro.

6. Yield stress in static one-dimensional strain experiments for sandstone is nearly the same value as that obtained in shock experiments. This correlation is not observed for limestones.

III SHOCK-WAVE EXPERIMENTS

The methods used in determining Hugoniot equations of state are discussed in Semiannual Technical Report No. 2, April 15, 1962. These methods, as well as methods reviewed by Rice *et al.*,[4] are based on the Rankine-Hugoniot jump conditions expressing conservation of mass, momentum, and energy across a shock front.

$$\frac{V_1}{V_0} = 1 - \frac{u_1 - u_0}{U_1 - u_0} \tag{1}$$

$$\sigma_1 - \sigma_0 = \rho_0 (U_1 - u_0)(u_1 - u_0) \tag{2}$$

$$E_1 - E_0 = \frac{\sigma_1 + \sigma_0}{2} (V_0 - V_1) \tag{3}$$

where V is specific volume, u is mass velocity, U is shock velocity, σ is compressive stress normal to the shock front, and E is specific internal energy. All shock front and particle velocities used in this report refer to laboratory coordinates. Subscripts "0" refer to the state ahead of the shock front, and subscripts "1" to the state immediately behind the front.

Assuming the state ahead of a shock front to be known, there are five unknown quantities and three relations to describe the state behind the shock. Hence, measurement of any two allows all quantities to be computed. In the method used, the shock wave velocity and the velocity from a free surface are measured. These, together with a relation between free-surface velocity and particle velocity prior to reflection, are sufficient to determine the stress-density-energy state behind the shock front. A series of measurements with different shock pressures determines the Hugoniot equation of state.

The particle velocity prior to reflection is, to an adequate approximation, one-half the free surface velocity. This approximation is based on the condition that entropy changes are small.[5] In essence, this means

that the unloading states should follow the mirror image of the Hugoniot states represented in the pressure-particle velocity plane. This assumption is satisfactory for crystals and non-porous rock, but is not for porous rocks, *i.e.*, limestones and sandstones.

The pressure region from a few kilobars to a few hundred kilobars is the region in which the elastic strength and phase transitions affect the shock. This is the region in which we have made our measurements. Such measurements in rocks are difficult because of the wide range in amplitudes of elastic precursors, and because rock surfaces are nonconducting, brittle, and poor reflectors. Occurrence of phase transitions makes problems more difficult. Desirable techniques are those that measure continuously shock and free-surface velocity. The techniques that were used are briefly described below.

A. INCLINED MIRROR METHOD

The inclined mirror method was used in most experiments. More detail is presented in Semiannual Technical Report No. 2, April 15, 1962, and in a paper by G. R. Fowles.[6]

The rock specimens are usually about ¼-inch or ½-inch thick by 1½-inches square. A specimen is cemented to a backing plate and a plane shock wave is driven through the backing plate and into the specimen. An explosive assembly,* which produces a plane detonation wave, is cemented to one surface of the backing plate; specimen and mirrors are cemented to the other surface (Fig. 1 and 2). The experiment is designed to determine shock and particle velocity. Shock wave velocity is measured by observing the transit time of a shock wave through a known thickness of sample. Particle velocity is determined by measuring the free-surface velocity produced upon interaction of a shock wave with a free boundary and converting to particle velocity as discussed above.

Figure 2 is a simplified diagram of the interaction of the assembly with a plane shock wave. The shock front, S_1 in the backing plate, generated by the explosive lens travels with a velocity U_1. Mirrors along with the aluminized lower surface of the specimen (if the specimen is transparent) record the arrival of the shock wave at the upper surface of the

* Manufactured by Mason and Hanger, Inc., Amarillo, Texas.

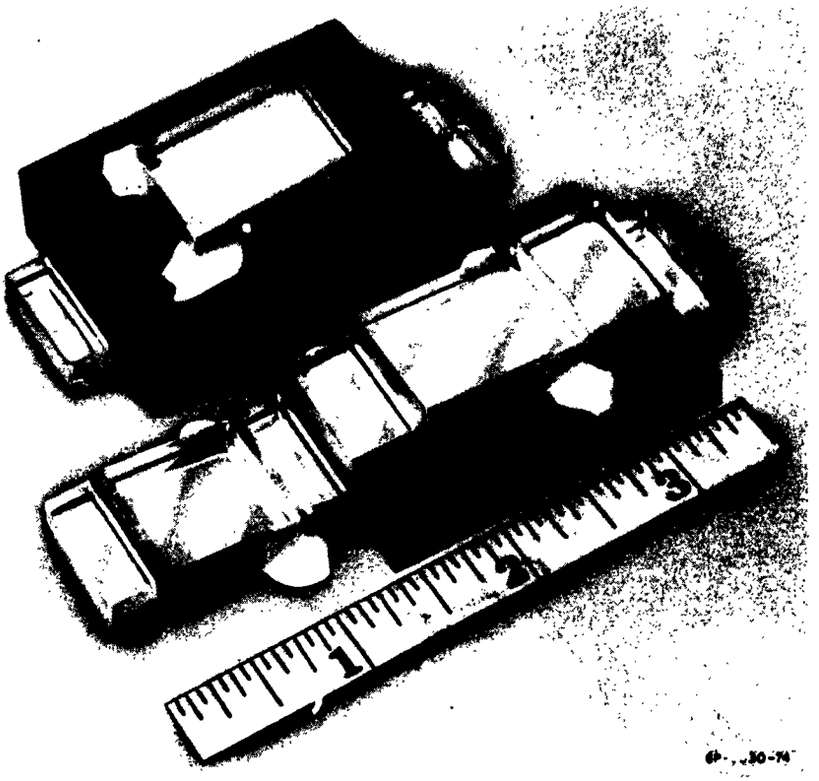

FIG. 1 INCLINED MIRROR ASSEMBLY
(Vacuum chamber not shown)

backing plate. This is recorded as a change in the intensity of reflected light when the shock wave destroys the aluminized surface of the mirrors.

When the shock wave traveling in the backing plate reaches the boundary between the plate and specimen, it interacts to transmit a shock wave of different pressure into the specimen. Assume the shock wave in the specimen is unstable and forms a double shock, S_2 and S_3, indicating a phase change or failure at the elastic limit. The two shock waves, S_2 and S_3, in the sample travel with velocities U_2 and U_3. The reflection of the shock wave with velocity U_2 at the surface of the sample accelerates the surface to velocity u_{f2}, which is much slower than the shock wave velocity; then the shock wave, S_3 with velocity U_3, overtakes the free surface and further accelerates it to velocity u_{f3}.

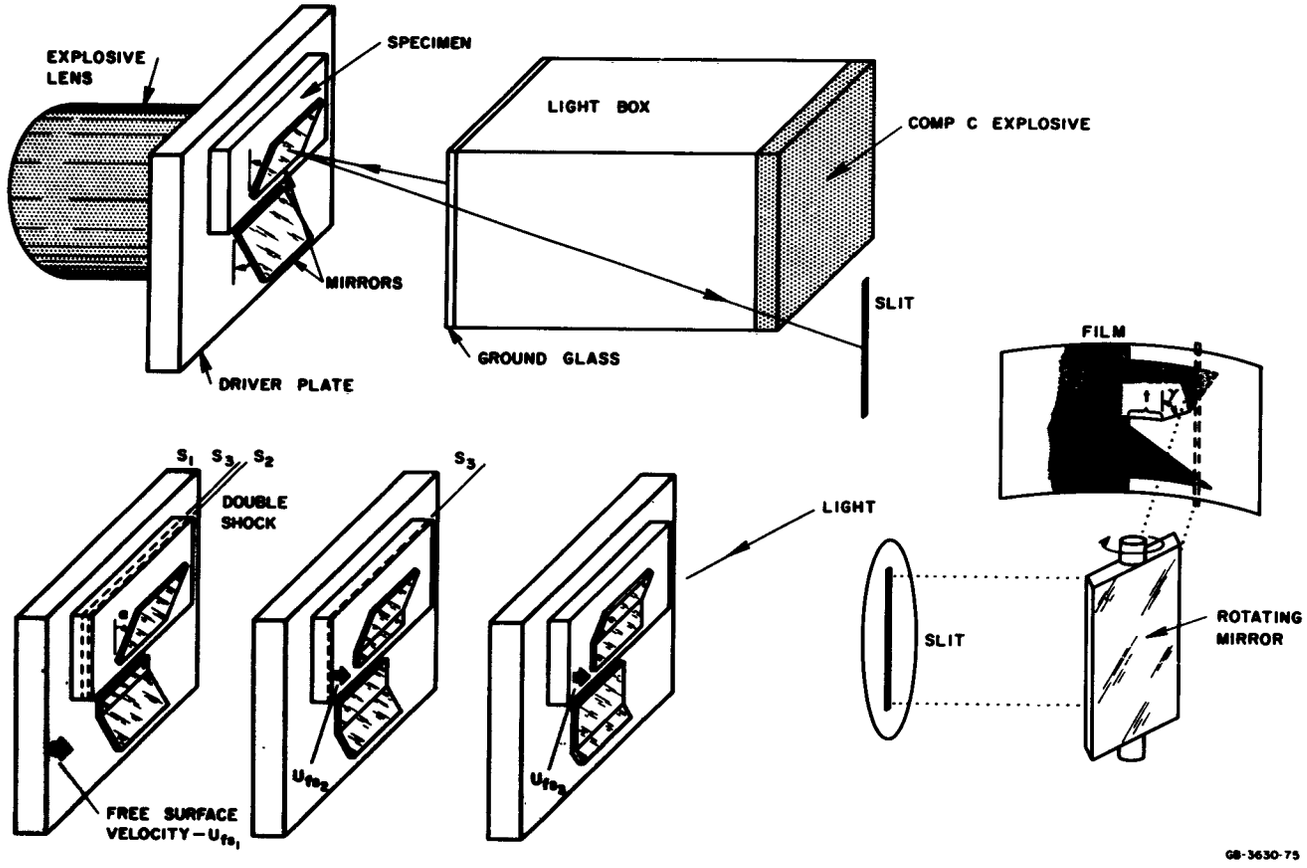

FIG. 2 INCLINED MIRROR METHOD

Initially, the inclined mirror on the sample is turned by the impact of the surface traveling with velocity u_{f2}, and if the angle between mirror and specimen surface is α, the point of collision travels along the mirror with apparent velocity $U_{a1} = u_{f2}/\sin\alpha$. When the second shock accelerates the free surface to velocity u_{f3}, the apparent velocity, U_{a2}, is increased to $u_{f3}/\sin\alpha$. These apparent velocities are recorded with a streak camera. Thus distances indicated by t on the film in Fig. 2 are related to shock velocities. The angles, γ, are related to particle velocities. From the measured shock and particle velocities the other quantities describing the shocked state can be computed. Note, too, that this technique provides a continuous measurement of free-surface velocity.

B. IMPEDANCE MATCH SOLUTION

The impedance-match solution for the stress-particle velocity state in the specimen is obtained by the method shown in Fig. 3. The curve OA is the previously determined locus of points which can be attained by passing a shock through the backing plate. The point A represents the state behind the shock which is incident on the boundary between the backing plate and the specimen. The particle velocity, u, is obtained from the free-surface velocity of the backing plate and is measured with an inclined mirror. A reflected wave is generated when the shock reaches the interface between the backing plate and specimen. The states which can be attained by the reflected wave can be calculated from the known Hugoniot of the backing plate; they are very close to AB, a mirror image of the curve OA. Since normal stress and particle velocity must be continuous across the interface, the state in the sample must lie on AB. From the equation for conservation of momentum, $\sigma_1 = \rho_0 U_1 u_1$, the state in the specimen must also be on a straight line with a slope $(\sigma_1/u_1) = \rho_0 U_1$. The intersection of this line with AB determines B, the state in the specimen. The associated compression and specific energy may be calculated from the equations for conservation of mass and energy across the shock front.

Sometimes free-surface velocities from two different metals placed on top of the specimen, or the free-surface velocity from the backing plate and the particle velocity from a metal on top of the specimen are measured. The particle velocities are measured with inclined mirrors, optical lever techniques[1] or quartz transducers. For example, assume the

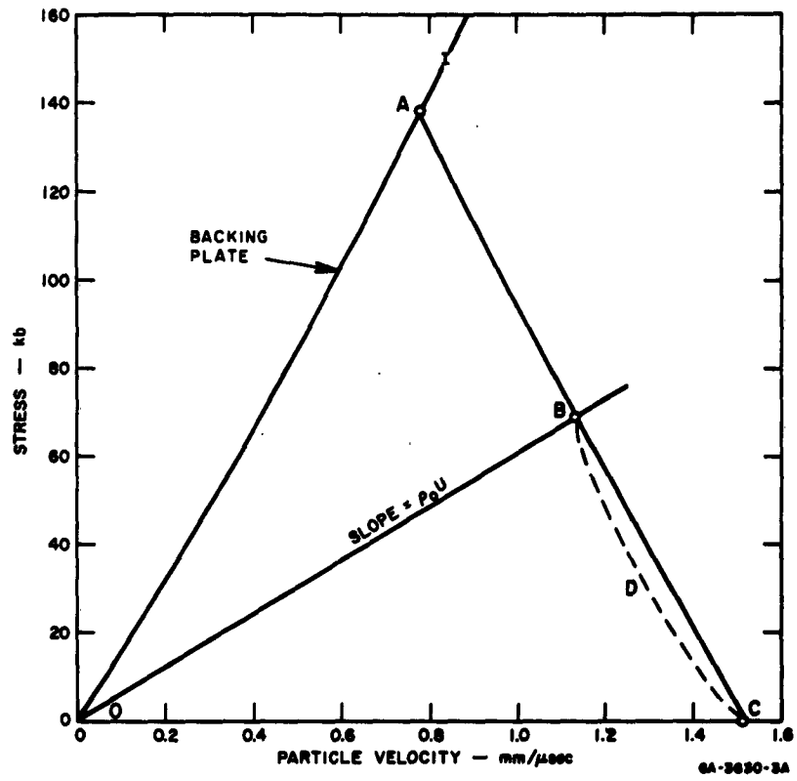

FIG. 3 IMPEDANCE MATCH SOLUTION

shock velocity in the sample and particle velocities of two metals on top of the specimen have been measured. The free-surface approximation is used to obtain particle velocities in the two metal mirrors on the rock specimen, giving points *A* and *B* on the known $\sigma - u$ loci of these metals (Fig. 4). *A* lies on the locus of states attainable by reflected shocks in the rock and *B* lies on the locus of reflected rarefactions from the rock. If *A* and *B* are close to one another, the straight line *AB* is a good approximation to the cross curve of reflected wave states of the rock Hugoniot. The intersection at *C* of *AB* with the line from the origin of slope $\rho_0 U$ determines the state from the rock.

C. QUARTZ TRANSDUCER METHOD

The measurement of shock wave profiles in aluminum, various steels, iron, and barium titanate by means of *X*-cut quartz transducers has been described by Jones *et al.*,[7] and Halpin *et al.*[8] These quartz transducers

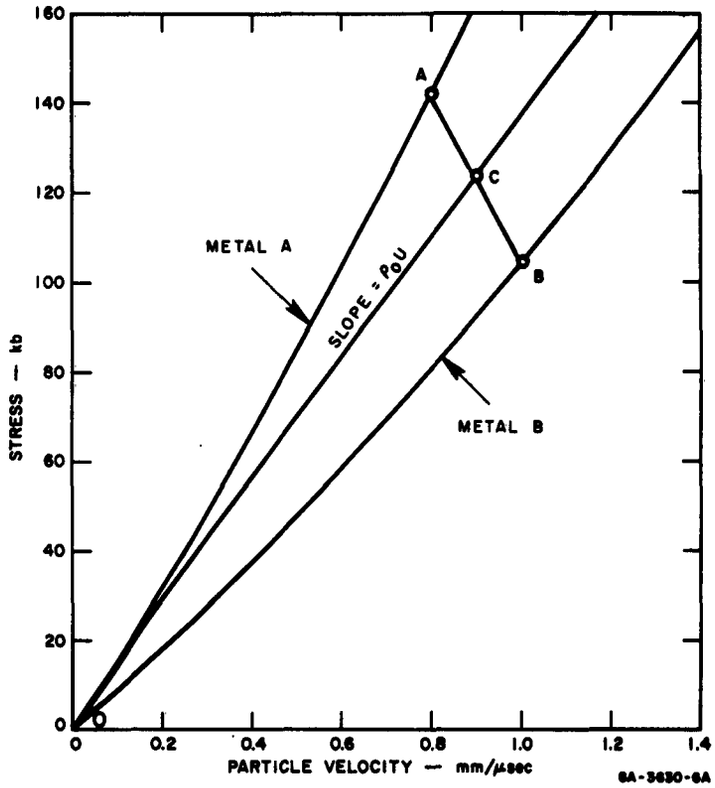

FIG. 4 IMPEDANCE MATCH SOLUTION

operate up to a stress level of 21 kb. A longitudinal stress difference parallel to the X direction generates a displacement current by piezoelectric polarization. A longitudinal stress wave impinging on the quartz transducer (Fig. 5) generates a current.[8]

$$i(t) = \frac{Akv_q}{h_q} [\sigma_q(0,t) - \sigma_q(h,t)] \qquad (4)$$

where A is the effective area of the transducer, h_q is the transducer thickness, v_q the longitudinal elastic-wave velocity in quartz in the X direction, σ_q the longitudinal stress in the quartz (a function of position and time), and k is the piezoelectric coefficient for strain in the X direction. By using Eq. (4) it is assumed that the strain and the displacement field are one-dimensional, and the dielectric constant, piezoelectric coefficient, and longitudinal wave velocity are independent of the stress.

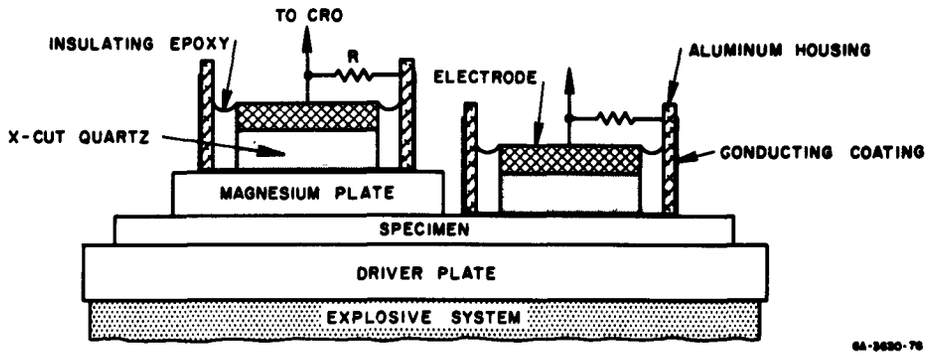

FIG. 5 EXPERIMENTAL CONFIGURATION FOR QUARTZ TRANSDUCER STRESS-TIME PROFILES IN POROUS ROCK

The stress-wave generator, specimen, and quartz transducer dimensions are adjusted so that the duration of the stress-wave profile of interest is less than the one-way travel time of a stress wave through the quartz transducer. For this arrangement the time interval of interest is,

$$0 < t < h_q/v_q \quad , \quad \text{and}$$

the stress on the side of the quartz away from the specimen,

$$\sigma_q(h,t) = 0$$

Then Eq. (4) may be written in the form

$$\sigma_q(0,t) = \frac{h_q i(t)}{Akv_q} \tag{5}$$

where the current generated by the quartz transducer is now proportional to the stress at the specimen-quartz interface.

In practice the one-dimensional geometry implicitly required in the above discussion is experimentally obtained by using only the central portion of the quartz transducer. A guard-ring arrangement in which the electrode covers only the central region of the disk was used in one of the present experiments (Section IV-A-2). Specific electrode arrangements are discussed by Halpin *et al.*[8]

If, as depicted in Fig. 5, the entire surface of the quartz is used to obtain the current from the transducer, significant errors due to edge effects are introduced. In the present experiment these errors may be evaluated from the work of Jones *et al.*[7] For a transducer diameter-to-thickness ratio of 5 to 1, and in the recording time interval of 0.00 to 0.35 μsec, the stress indicated by the quartz transducer using Eq. (5) is approximately 3% too low.

The stress-time record in the quartz transducer requires some additional assumptions if we wish to obtain stress as a function of time for the specimen. Consider a point *A* on the pressure-particle velocity curve of *X*-cut quartz [Fig. 6(a)] where *A* represents the state in the quartz at the quartz-specimen interface at a given instant of time.

In order that the state *A* in the quartz be related to the state *B* in the specimen it is necessary that the shock reflection path *AB* be known. Generally the shock reflection curve *AB* as well as the shock compression curve *OB* are unknown. For a specimen of higher shock impedance (not shown in Fig. 6) than the quartz, a rarefaction wave will connect the state in the specimen to the state in the quartz. For a multiple step shock front, the impedance match solution is computed stepwise. Through the use of the appropriate electronic timing, the relative shock velocity $(U - u_E)$,

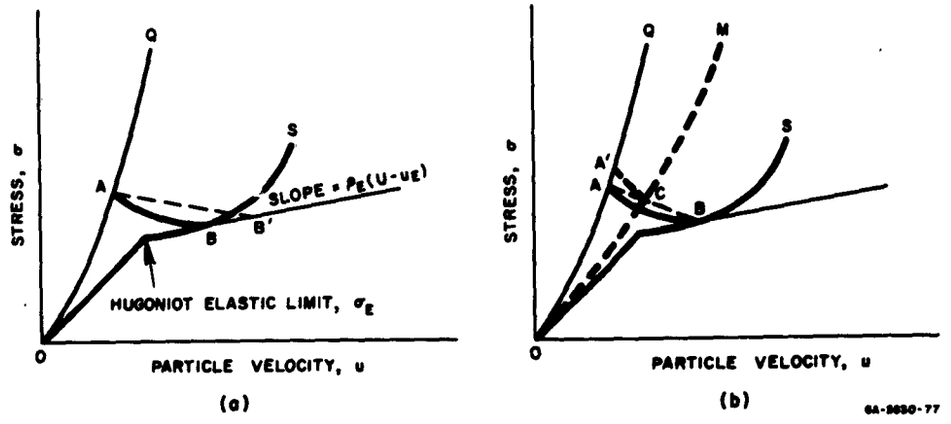

FIG. 6 GRAPHICAL SOLUTION, QUARTZ TRANSDUCER DATA
(a) Erroneous result obtained at B'; BA is actual shock reflection path rather than mirror approximation B'A;
(b) State A' is observed by transducer mounted on material of stress-particle velocity curve OM; C on OM corresponds to A'; for solution, ACB is drawn as approximation to shock reflection curve AB

appropriate to the stress level A and, hence Section III-B, the slope of the line through σ_g is known.

In the present experiments, on dry and wet sandstone, shock reflection such as depicted in Fig. 6(a), occurs since the sandstones are of lower shock impedance than the X-cut quartz. For an initially porous material such as sandstone, the use of the mirror image line, AB' [Fig. 6(a)], can give a poor approximation of the specimen shock reflection curve. One technique for obtaining the shock reflection curve AB and the state B in the specimen is to place another material of known equation of state on top of the specimen (Section III-B). Another pressure versus time record is obtained using a second quartz transducer placed on the material surface as depicted in Fig. 5. At a given time, the state A' is obtained in the quartz transducer from the material of known equation of state. In the present experiment, magnesium is used for the material of known equation of state. The mirror image of the magnesium pressure-particle velocity loading curve is used as an approximation of the shock reflection curve. The state C in the magnesium corresponding to the state A' in the quartz may be obtained graphically [Fig. 6(b)]. In order to relate the corresponding states in the stress-time profile observed from the two transducers, it is convenient to assume that the stress profile does not change shape in the magnesium, i.e.,

$$\sigma_m(0, t_0) = \sigma_m\left(x_m, t_0 + \frac{x_m}{v_m}\right) \tag{6}$$

Here σ_m is the stress in the magnesium, a function of position x_m and time t, and v_m is the magnesium shock velocity which is assumed constant.* The points A and A', which correspond to the same state B in the specimen, can be correlated on the basis of equal time, as measured from the beginning of the shock-wave profile. By assuming that the appropriate segment of the reflected shock pressure-particle velocity curve in the specimen may be approximated by a straight line, the line AC is constructed. The intersection of AC with the line of slope $\rho_g(U - u_g)$, where ρ_g and u_g are the density and particle velocity at the Hugoniot elastic limit, determines [Fig. 6(b)] the state in the specimen.

* Below 10 kb the change in shock velocity in magnesium with stress is on the order of 0.4%/kb.

IV RESULTS

A. QUARTZ ROCKS

1. Quartz and Quartzites

The agreement between Fowles'[6] and Wackerle's[9] shock compression data for crystal quartz demonstrates that the Hugoniot is repeatable within experimental accuracy. The Hugoniot of novaculite and quartzite is also reproducible and in general agreement with average values for crystal quartz (Fig. 7).

For different cuts of quartz it is not clear how Hugoniot data are best represented in the stress-volume or stress-particle velocity plane so that the results may be compared to those for polycrystalline quartz. Comparison with Bridgman's[10] dilatometric isothermal measurements is also useful in interpretation of shock wave results.

Wackerle has calculated the shock and particle velocity in quartz appropriate for hypothetical shock transition directly from zero stress to states normally achieved only via a second wave. These hypothetical shock and particle velocities are combined for *X*-, *Y*-, and *Z*-cuts and the result is analytically fit to straight lines in different stress ranges. Below 144 kb, Wackerle's straight line was fitted to a Murnaghan equation of state of the form of Eq. (16), the result is shown in Fig. 7. The Bridgman data has also been put in the form of Eq. (16) and is shown in Fig. 7. The agreement among the reduced Hugoniot data of Wackerle, the static Bridgman data, and the states achieved by the second wave in polycrystalline quartz, here represented by Arkansas novaculite, is noteworthy.

Although the general behavior of single and polycrystalline nonporous quartz rock at relatively low pressures is thought to be understood, several phenomena at high stresses have not been explained. These include:

(1) The differences in Hugoniots above the elastic limit for various crystal directions of quartz cannot be explained in terms of present models of material behavior under shock compression.

(2) The question of shock induced polymorphism in quartz, which is suggested by Wackerle and recently discussed by McQueen *et al.*[11]

(3) The stress relaxation phenomenon and the variation of the precursor wave amplitude in different polycrystalline quartz materials require further investigation.

2. SANDSTONES

The shock compression of Coconino sandstone has been examined up to 186 kb. The results for the Coconino sandstone and those from several

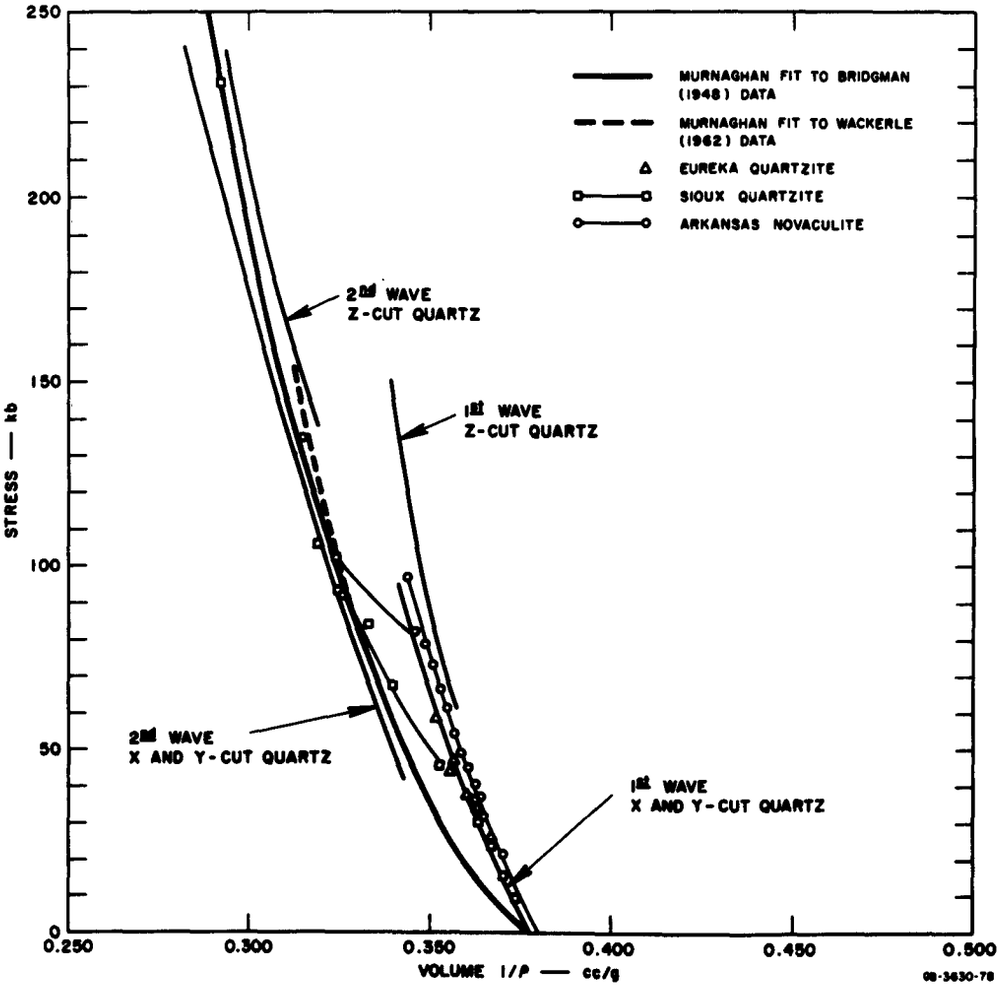

FIG. 7 STRESS-VOLUME RELATIONS, NONPOROUS QUARTZ

experiments below 25 kb using Massillon and St. Peter sandstone are shown in Figs. 8 and 9.

Coconino sandstone is composed of 97% quartz grains ranging in diameter from 0.12 to 0.15 mm. The impurities, 3% of the solid volume, are principally microcline and orthoclase. Porosity of this rock varies from 22.5- to 24.1%. The present data (Table I) have been obtained from material in which the best estimate of the porosity is 24.1%.

Massillon sandstone is composed of 94% (of the solid volume) quartz grains ranging from 0.01 to 0.5 mm. The 6% impurities are chiefly feldspar, iron oxide, and clay. Variations in color suggest the clay and iron oxide content changes in the rock. The rock has a porosity of 23.5%.

St. Peter sandstone is composed of 99% (of the solid volume) of rounded grains ranging in diameter from 0.05 to 0.4 mm. Impurities consisting of feldspar, sphene, zircon, tourmaline, and clinozoisite amount to less than 0.5%. The porosity is 19.5%.

The Hugoniots of Coconino and Massillon sandstones do not appear to differ significantly for shocks below 25 kb. The greater shock impedance of the St. Peter sandstone is probably due to the lower porosity. At zero pressure the longitudinal wave velocity determined by conventional ultrasonic travel-time methods is 3.254 ± 0.178 mm/μsec, 3.183 ± 0.216 mm/μsec, and 3.333 ± 0.103 mm/μsec, for Massillon, St. Peter, and Coconino sandstone, respectively. These velocities are in fair agreement with those of the elastic precursor listed in Table I. The relatively lower porosity of St. Peter sandstone is thought to produce the relatively high precursor velocity of approximately 3.63 mm/μsec; however, this high value has not been observed in the longitudinal ultrasonic velocities.

For shock states up to the Hugoniot elastic limit (Table I, Figs. 8 and 9) the inclined mirror technique was used to obtain free-surface velocity. The free-surface approximation was applied in order that the initial state for the following second shock could be calculated. In the experiments in which two waves were observed, the final state was calculated using the impedance-match solution with the initial state assumed to be that of the precursor. The free-surface velocities which correspond to the final state, for shocks in which two waves were present, are indicated in Fig. 8. These data were obtained from the slope of the inclined mirror cut-off on the streak camera records; the records of Figs. 10 and 11 being

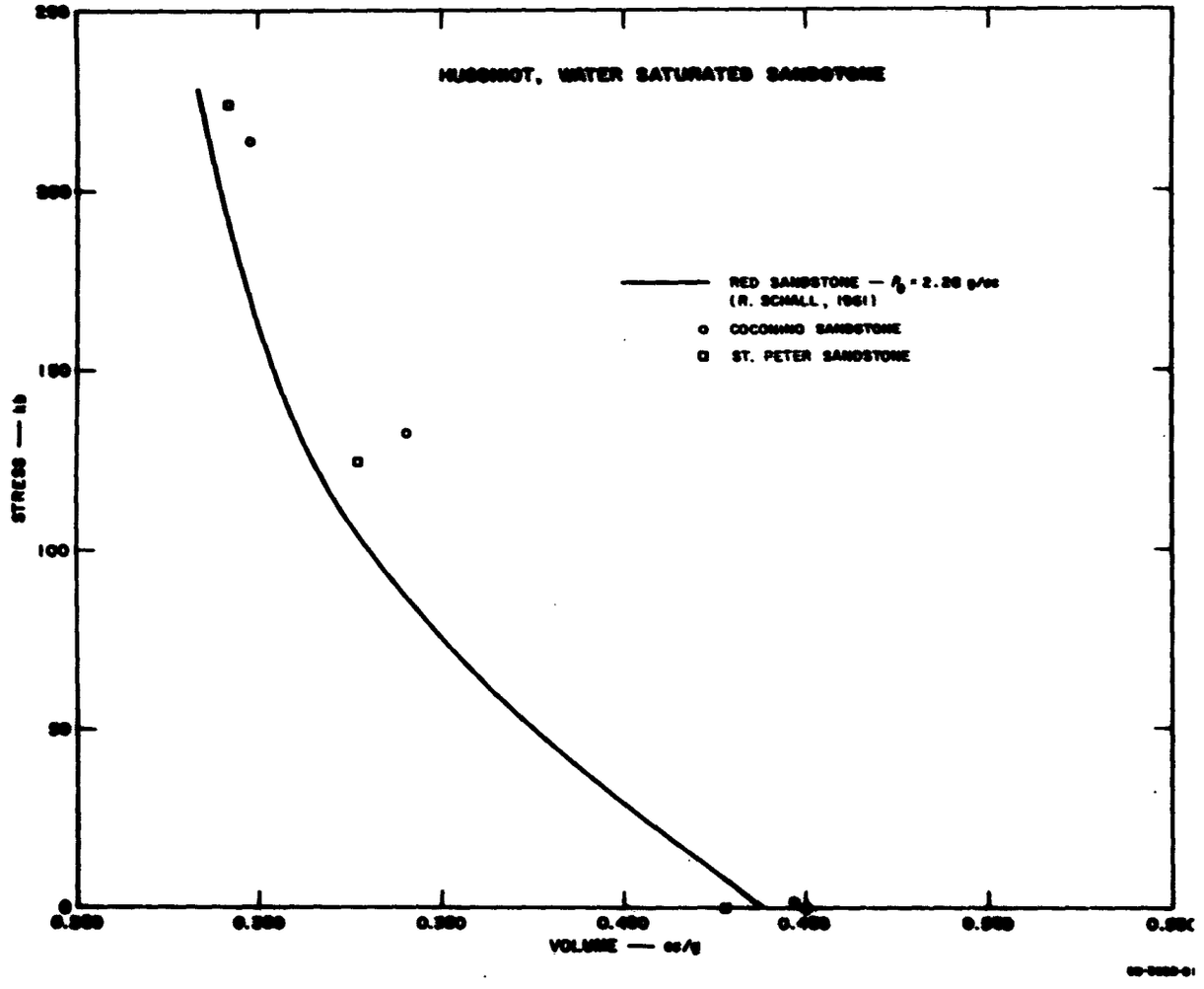
HUGONIOT, WATER SATURATED SANDSTONE
RED SANDSTONE — ρ_0 = 2.26 g/cc
(R. SCHALL, 1961)
COCONINO SANDSTONE
ST. PETER SANDSTONE
STRESS — kb
VOLUME — cc/g

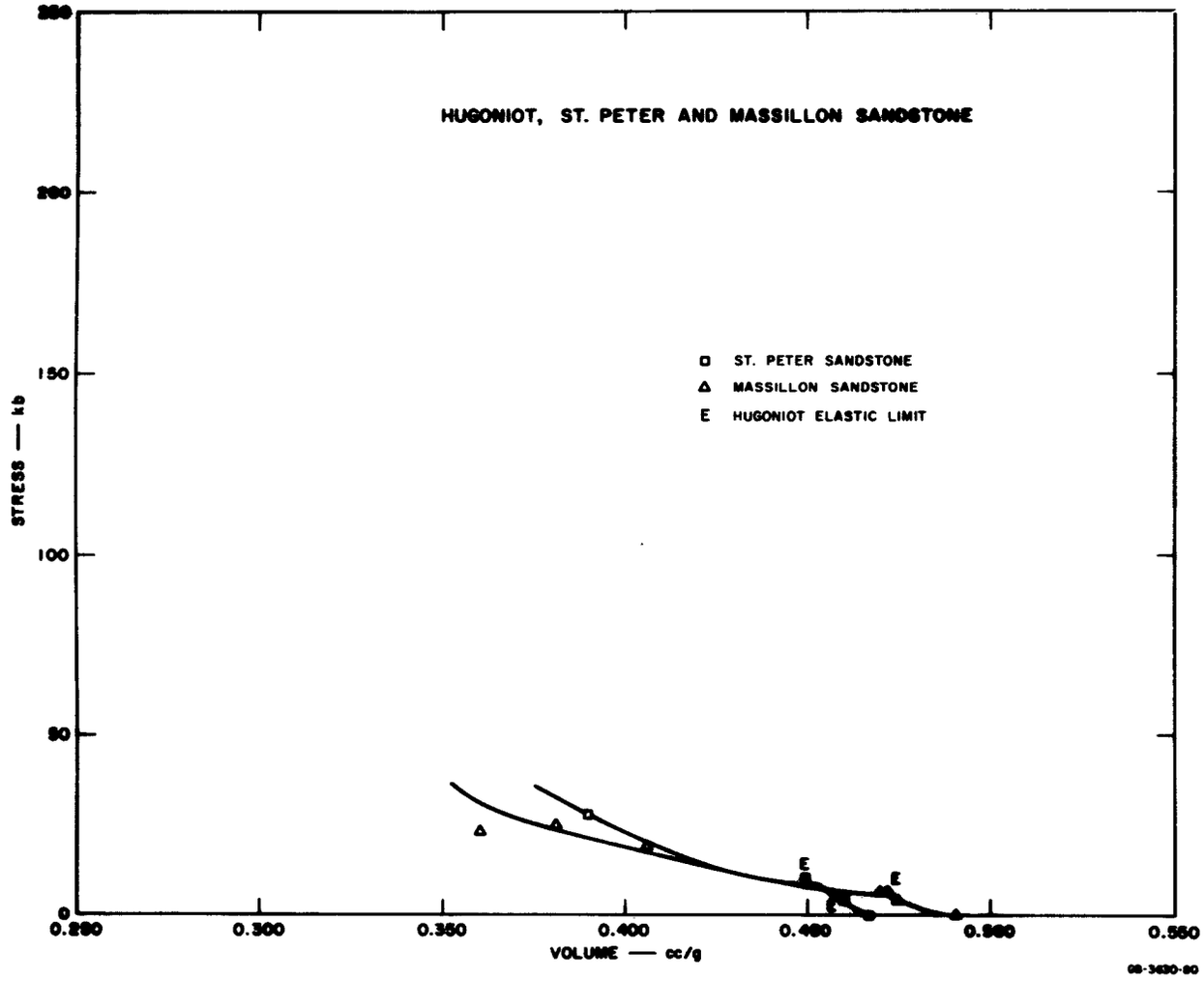
HUGONIOT, ST. PETER AND MASSILLON SANDSTONE
ST. PETER SANDSTONE
MASSILLON SANDSTONE
E HUGONIOT ELASTIC LIMIT
STRESS — kb
VOLUME — cc/g
0
50
100
150
200
250
0.250
0.300
0.350
0.400
0.450
0.500
0.550
E
E
E
68-3630-80

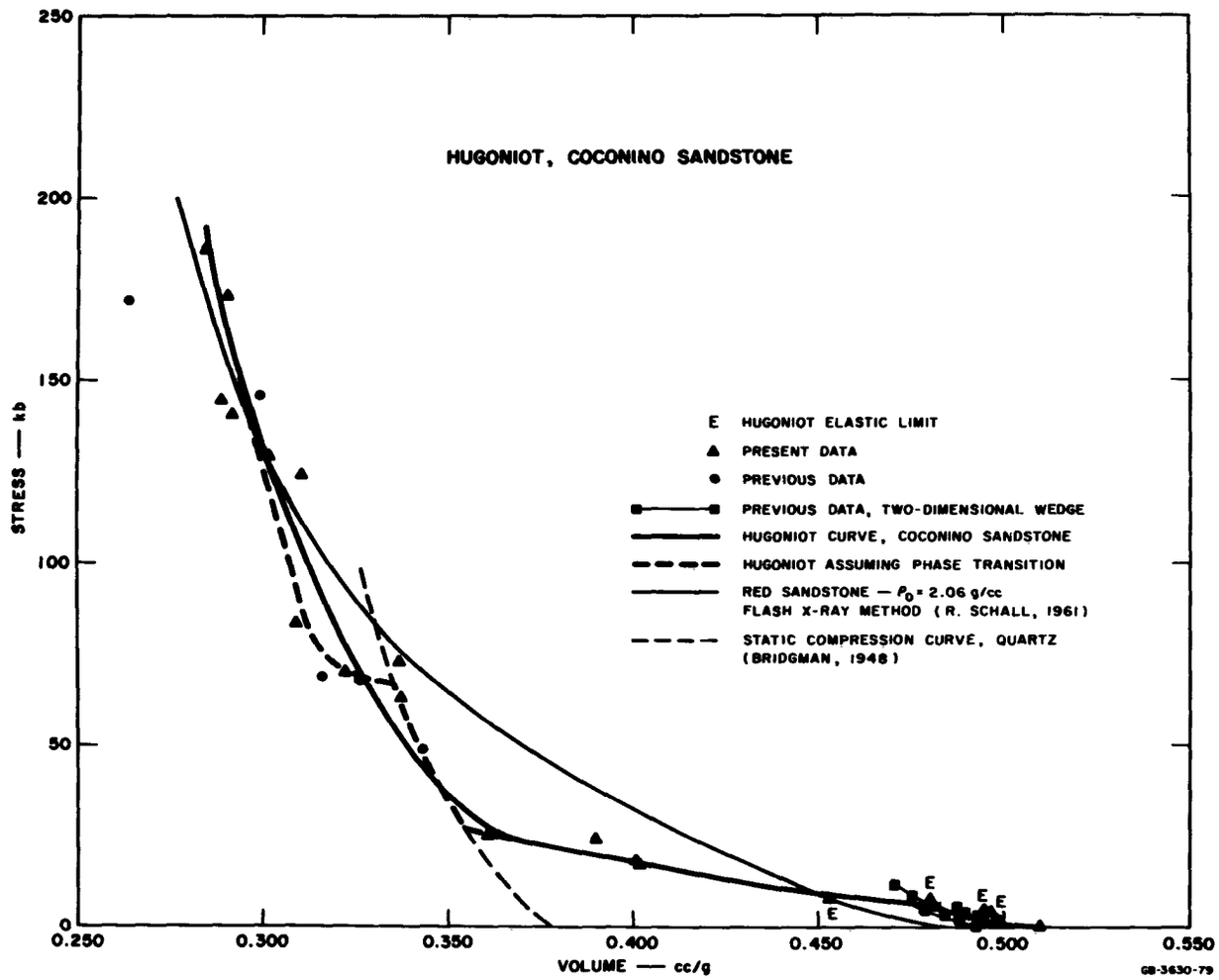

FIG. 8 HUGONIOT, SANDSTONE

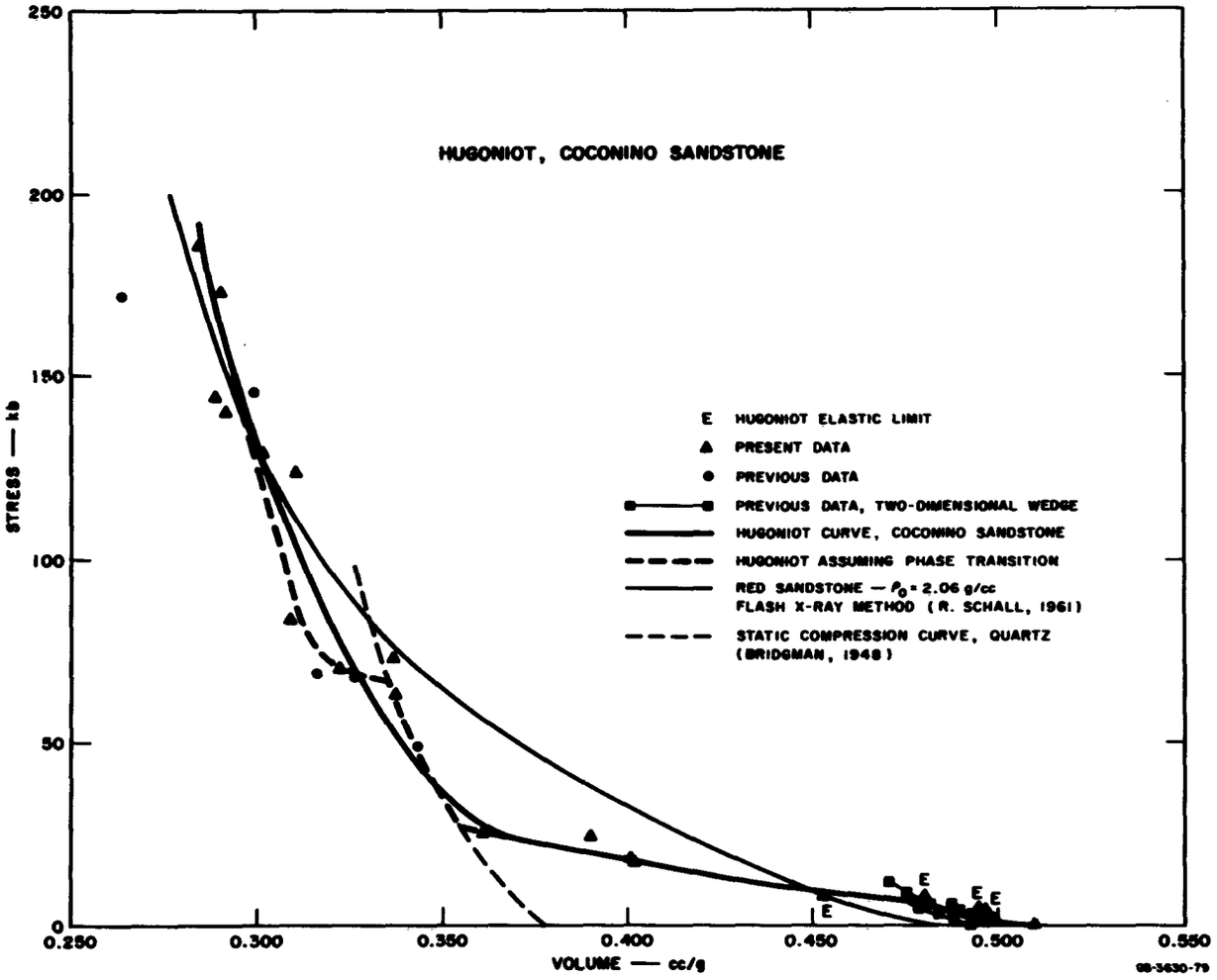

FIG. 8 HUGONIOT, SANDSTONE

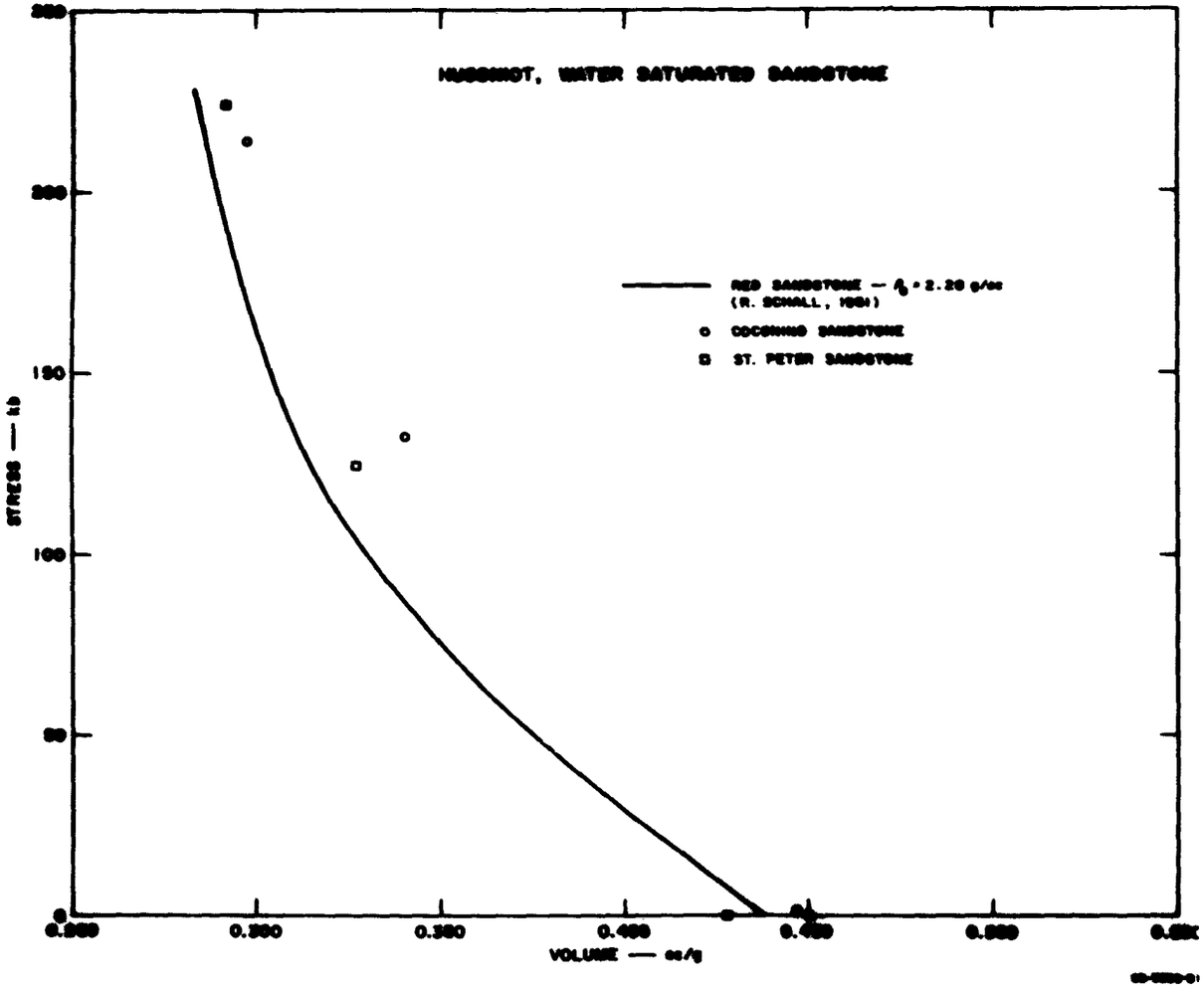
HUGONIOT, WATER SATURATED SANDSTONE
RED SANDSTONE — ρ_0 = 2.20 g/cc
(R. SCHALL, 1964)
COCONINO SANDSTONE
ST. PETER SANDSTONE
STRESS — kb
200
150
100
50
0
0.300
0.350
0.400
VOLUME — cc/g

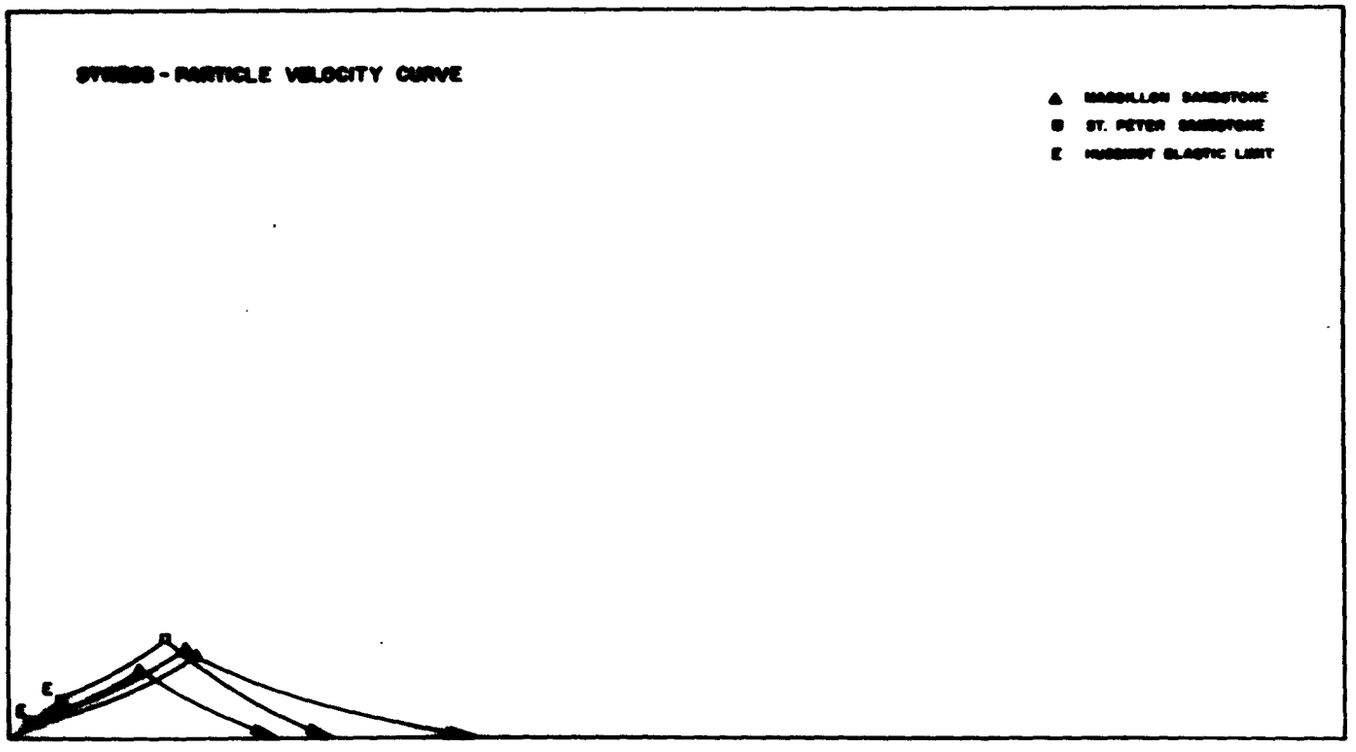
STRESS - PARTICLE VELOCITY CURVE
▲ MAGALLON SANDSTONE
■ ST. PETER SANDSTONE
E HUGONIOT ELASTIC LIMIT
D
E

GD-3630-83

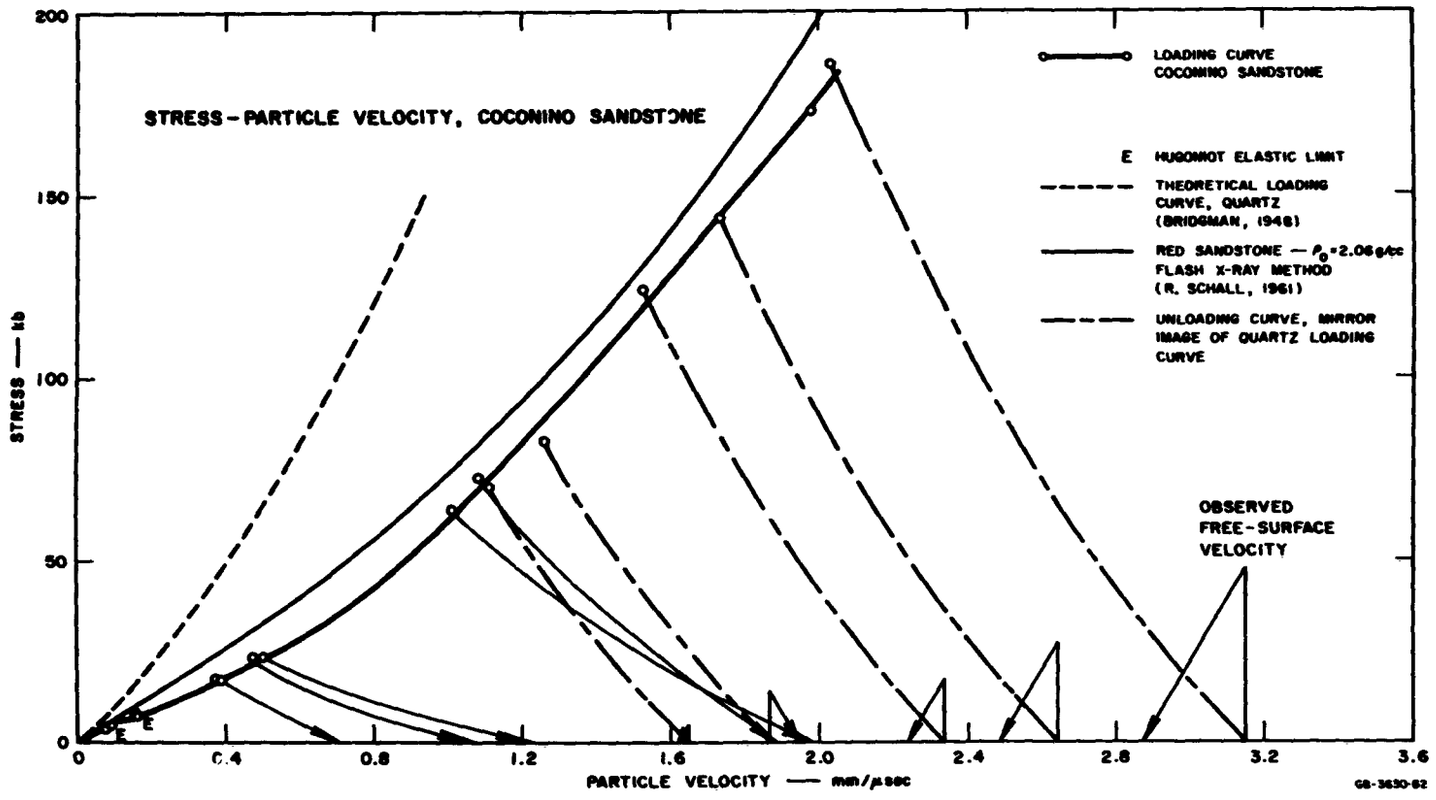

FIG. 9 STRESS-PARTICLE VELOCITY, SANDSTONE

SPECIMEN TYPE	SPECIMEN THICKNESS (mm)	FIRST FRONT					
		½ (Free-Surface Velocity (mm/μsec)	Shock Velocity (mm/μsec)	Stress (kb)	Volume (cc/g)	Particle Velocity (mm/μsec)	Free-Surface Velocity (mm/μsec
Coconino Sandstone	6.32					1.74	2.50
	6.35					1.53	2.24
Coconino Sandstone	6.63					1.26	1.95
	6.43					1.11	1.63
Coconino Sandstone	6.35					1.09	1.88
	6.32					1.02	1.99
Coconino Sandstone	5.07	0.156	2.622	(8.0)	0.480	0.371	0.699
	9.29	0.074	2.853	4.1	0.497	0.371	0.499
Massillon Sandstone	6.60	0.109	2.861	(6.4)	0.472	0.354	(0.732)
Coconino Sandstone	6.61						4.481
	12.79						3.837
	0.00†					1.98	
Coconino Sandstone	6.34	0.151	2.705	(8)	0.453	0.475	1.08
	9.58	0.086	3.027	5.1	0.495	0.500	1.22
Massillon Sandstone	5.21	0.080	2.540	4.2	0.475	0.508	0.423
	9.59	0.120	2.857	(6.9)	0.4697	0.472	(1.270)
St. Peter Sandstone	6.35	0.142	3.579	(10.9)	0.449		0.879
	9.57	0.058	3.670	4.5	0.460		0.480
	0.00†					0.420	
Coconino Sandstone	6.35						2.872
	9.53						2.540
	0.00†					2.041	
St. Peter Sandstone (Water Saturated)	7.23						
	4.81						
	0.00†					1.756	
Coconino Sandstone (Water Saturated)	7.20						
	4.81						
	0.00†					1.80	
Coconino Sandstone (Water Saturated)	9.54	0.021 Particle Velocity	3.222	1.5 ± 0.2	0.447	0.628	
Coconino Sandstone	8.37	0.043 Particle Velocity	1.881	1.8 ± 0.2	0.498		
Coconino Sandstone	6.38					1.20	
	9.58						
St. Peter Sandstone	6.49						
	12.69					1.16	

NOTE: ρ_0 from 9107, 9106, 9209 used for all calculations.

( ) indicates less reliable data.

†Linear Extrapolation.

•Separate observation.

Table I

HUGONIOT DATA FOR SANDSTONE

N TYPE	SPECIMEN THICKNESS (mm)	FIRST FRONT				FINAL STATE					EXPLOSIVE SYSTEM P-60 +	DRIVER		SH
		½ (Free-Surface Velocity (mm/μsec)	Shock Velocity (mm/μsec)	Stress (kb)	Volume (cc/g)	Particle Velocity (mm/μsec)	Free-Surface Velocity (mm/μsec)	Shock Velocity (mm/μsec)	Stress (kb)	Volume (cc/g)		Material (inch)	Free-Surface Velocity (mm/μsec)	
andstone	6.32					1.74	2.50	4.126	144	0.289	1" Comp B	0.5 Al	2.568	
	6.35					1.53	2.24	4.039	124	0.311	1" Comp B	1 Al	2.206	
andstone	6.63					1.26	1.95	3.285	83	0.309	2" Baratol	0.25 Al	1.77	
	6.43					1.11	1.63	3.141	70	0.323	2" Baratol	0.75 Al	1.54	
andstone	6.35					1.09	1.88	3.321	73	0.337		0.5 Lucite	2.46	
	6.32					1.02	1.99	3.136	64	0.337		1 Lucite	2.25	
andstone	5.07	0.156	2.622	(8.0)	0.480	0.371	0.699	2.305	18	0.402	P-80 (instead of P-60)	0.5 Brass + 1 Lucite	0.836	
	9.29	0.074	2.853	4.1	0.497	0.371	0.499	2.385	18	0.402	↓	↓	↓	
Sandstone	6.60	0.109	2.861	(6.4)	0.472	0.354	(0.732)	2.553	19	0.406				
andstone	6.61						4.481	4.386			2" Comp B	0.5 Al	(3.38)	
	12.79						3.837	4.481						
	0.00†					1.98		4.600	173	0.290	↓	↓	↓	
ndstone	6.34	0.151	2.705	(8)	0.453	0.475	1.08	2.354	23.8	0.3902		0.5 Brass + 0.75 Lucite	1.076 (assumed)	
	9.58	0.086	3.027	5.1	0.495	0.500	1.22	2.357	24.9	0.3615		↓	↓	
andstone	5.21	0.080	2.540	4.2	0.475	0.508	0.423	2.111	23.0	0.3606				
	9.59	0.120	2.857	(6.9)	0.4697	0.472	(1.270)	2.503	25.0	0.3811				
andstone	6.35	0.142	3.579	(10.9)	0.449		0.879	2.920						
	9.57	0.058	3.670	4.5	0.460		0.480	2.888						
	0.00†					0.420		2.980	27.9	0.3899		↓	↓	
idstone	6.35						2.872	4.615			2" Comp B	0.25 Al	(2.872)	
	9.53						2.540	4.599						
	0.00 †					2.041		4.633	186	0.285	↓	↓	↓	
ndstone rated)	7.23							5.268			↓	0.5 Al	2.935 (assumed)	
	4.81							5.344						
	0.00†					1.756		5.494	224	0.2915		↓	↓	
idstone rated)	7.20							5.215						
	4.81							5.256						
	0.00†					1.80		5.227	214	0.2983		↓	↓	
idstone rated)	9.54	0.021 Particle Velocity	3.222	1.5 ± 0.2	0.447	0.628		3.00	39.5(?)	0.358		0.5 Brass + 0.75 Lucite	↓	93
dstone	8.37	0.043 Particle Velocity	1.881	1.8 ± 0.2	0.498							0.5 Brass + 0.75 Lucite	1.076	94
dstone	6.38					1.20		4.92 (Avg.)	133	0.340	½" Comp B + 1" Baratol	0.5 Al	1.910*	94
	9.58													
ndstone	6.49													
	12.69					1.16		4.92 (Avg.)	125	0.327	↓	↓	↓	↓

1 9107, 9106, 9209 used for all calculations.

less reliable data.

olation.

rvation.

Table I

HUGONIOT DATA FOR SANDSTONE

FINAL STATE					EXPLOSIVE SYSTEM P-60 +	DRIVER		SHOT NO.	NOTES
article Velocity (mm/μsec)	Free-Surface Velocity (mm/μsec)	Shock Velocity (mm/μsec)	Stress (kb)	Volume (cc/g)		Material (inch)	Free-Surface Velocity (mm/μsec)		
1.74	2.50	4.126	144	0.289	1" Comp B	0.5 Al	2.568	8974	
1.53	2.24	4.039	124	0.311	1" Comp B	1 Al	2.206	8974	
1.26	1.95	3.285	83	0.309	2" Baratol	0.25 Al	1.77	8975	
1.11	1.63	3.141	70	0.323	2" Baratol	0.75 Al	1.54	8975	
1.09	1.88	3.321	73	0.337		0.5 Lucite	2.46	8989	
1.02	1.99	3.136	64	0.337		1 Lucite	2.25	8989	
0.371	0.699	2.305	18	0.402	P-80 (instead of P-60)	0.5 Brass + 1 Lucite	0.836	9107	
0.371	0.499	2.385	18	0.402	↓	↓	↓	↓	
0.354	(0.732)	2.553	19	0.406	↓	↓	↓	↓	ρ_0 = 2.0386 ± 0.0030 g/cc
	4.481	4.386			2" Comp B	0.5 Al	(3.38)	9106	ρ_0 = 1.961 ± 0.006 g/cc
	3.837	4.481			↓	↓	↓	↓	
1.98		4.600	173	0.290	↓	↓	↓	↓	
0.475	1.08	2.354	23.8	0.3902		0.5 Brass + 0.75 Lucite	1.076 (assumed)	9208	
0.500	1.22	2.357	24.9	0.3615		↓	↓	9208	
0.508	0.423	2.111	23.0	0.3606				9215	
0.472	(1.270)	2.503	25.0	0.3811				9215	
	0.879	2.920						9209	ρ = 2.141 ± 0.013 g/cc
	0.480	2.888						↓	
0.420		2.980	27.9	0.3899					
	2.872	4.615			2" Comp B	0.25 Al	(2.872)	9342	
	2.540	4.599							
0.041		4.633	186	0.285	↓	↓	↓	↓	
		5.268			↓	0.5 Al	2.935 (assumed)	9259	ρ_0 = 2.334 g/cc (Calculated)
		5.344							↓
0.756		5.494	224	0.2915		↓	↓	↓	
		5.215							ρ_0 = 2.222 g/cc (Calculated)
		5.256							↓
80		5.227	214	0.2983		↓	↓	↓	
628		3.00	39.5(?)	0.358		0.5 Brass + 0.75 Lucite		9334	Quarts Transducer ρ_0 = 2.222 g/cc (Calculated)
						0.5 Brass + 0.75 Lucite	1.076	9402	Quarts Transducer Precursor Rise Time 0.21 μsec
20		4.92 (Avg.)	133	0.340	½" Comp B + 1" Baratol	0.5 Al	1.910*	9410	ρ_0 = 2.222 g/cc (Calculated)
16		4.92 (Avg.)	125	0.327	↓	↓	↓	↓	ρ_0 = 2.334 g/cc (Calculated)

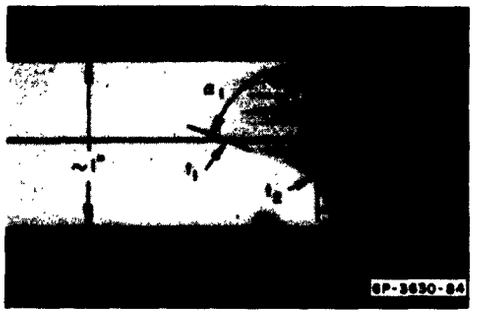

FIG. 10 INCLINED MIRROR CUTOFF COCONINO SANDSTONE, DOUBLE WAVE
First wave 4.1 kb; second wave 18 kb

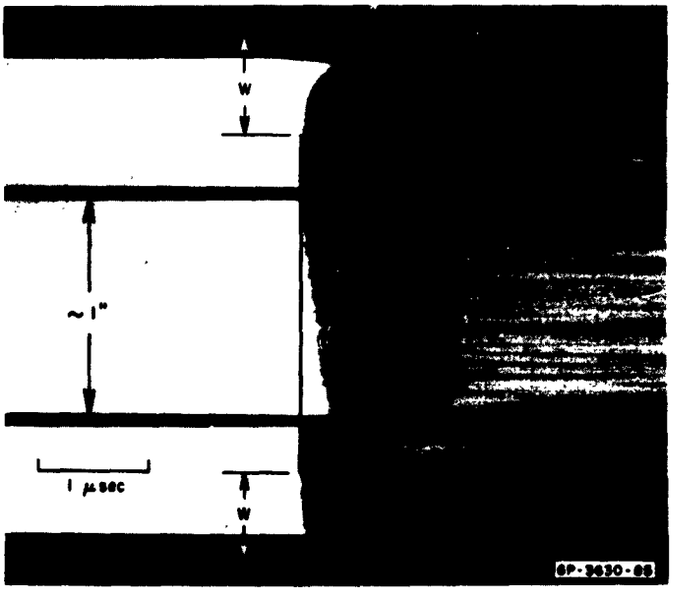

FIG. 11 INCLINED MIRROR CUTOFF COCONINO SANDSTONE, SINGLE WAVE
Single wave, showing lateral relaxation wave interaction width, W

typical. The general indistinctness and unevenness in Fig. 10 are thought to produce some of the scatter in the data, particularly at free-surface velocities of less than 2 mm/μsec. Shock attenuation and edge effects in porous rocks have limited most of the experiments to specimens between 5- and 13-mm thick with a 6- or 8-inch diameter explosive lens. For these dimensions the grain size of the rocks, particularly when on the order of 0.5 mm, undoubtedly affects the reproducibility of the free-surface velocity measurements.

The porous sandstones studied may be characterized as displaying a Hugoniot elastic limit in the vicinity of 5 kb.* Above the elastic limit and up to 25 kb, successfully higher stress states are achieved by irreversible crushing of the sandstone until the quartz density is reached.† Although the free surface velocity data are not entirely self-consistent (Fig. 8, see also Section IV-A-4), they imply that the material shocked to states between 50 and 130 kb relaxes along stress-particle velocity curves which are nearly those which would be expected if the material produced by the shock were solid quartz.

Above 65 kb the Hugoniot for Coconino sandstone lies at smaller volumes than that of either single or polycrystalline quartz. The implication of this behavior in relation to the temperature achieved during shock compression is considered below (Section IV-A-6).

3. Calculation of Shock Temperature in Sandstones

The temperatures achieved in nonporous rocks and minerals during shock compression are rather moderate. For many nonporous solids the temperature achieved upon a shock compression and upon subsequent adiabatic relaxation may be calculated using the method described by Walsh and Christian.[12] To date, temperatures reached by shock wave compression of porous rocks have not been specifically discussed. Temperature calculations in porous metals are briefly discussed by Kormer *et al.*[13]

Consider the shock compression of a porous rock initially in a state, given by V_0, $\sigma_0 = 0$, to a state V, σ (Fig. 12). From Eq. (3) the difference

---

* On the basis of streak camera record quality (Fig. 10) the best determination of the precursor amplitude for all three sandstones lies between 4.1 and 5.1 kb (Table I).

† Previous two-dimensional wedge and plane-wave experiments gave strongly discordant densities above 40 kb. The earlier results using the two-dimensional wedge (Ref. 1, Figs. 18 and 19, and Table IV, pages 35 and 36) are now known to be *incorrect* above 15 kb.

in internal energy per unit mass across the shock wave interface is given by

$$E = \sigma(V_0 - V)/2$$

The difficulty in calculating the temperature in a shock transition lies in determining how E is partitioned into compressional energy, denoted by E_k, and thermal energy, denoted by E_t.

Thus,

$$E = E_t + E_k \quad . \tag{7}$$

It is convenient to discuss the energies of shock compression in terms of three regimes on the Hugoniot curve (Fig. 12).

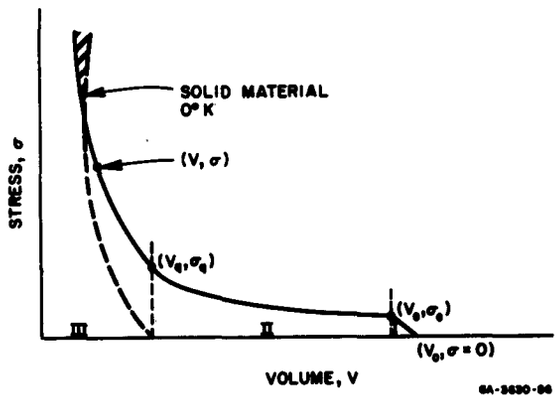

FIG. 12 HUGONIOT, POROUS ROCK: I, elastic regime; II, collapse regime; III, energy partition regime. Shaded area, error in energy from greater compression of porous material

The elastic regime, or regime I, extends from $(V_0, 0)$ to (V_e, σ_e) where the subscript e refers to the Hugoniot elastic limit. For a shock in which the highest stress attained is below σ_e, the temperatures may be estimated if adiabatic compression is assumed. This is justified for the low-level elastic precursor observed in porous sandstones and in limestones, since the precursor shock velocity is close to the measured adiabatic longitudinal wave velocity. The Hugoniot, therefore, may be assumed

to lie close to the adiabat. The adiabatic heating is thus estimated from

$$T_H\big|_I = T_0 \exp \frac{\gamma(V_0 - V)}{V} \tag{8}$$

where T_H is the temperature along the Hugoniot, T_0 is the initial temperature and γ is Gruneisen's ratio given by

$$\gamma = V\left(\frac{\partial P}{\partial E}\right)_V = \frac{V}{C_V}\left(\frac{\partial P}{\partial T}\right)_V \tag{9}$$

For several nonporous solids γ/V is nearly constant;[14] therefore, because of the small variation of σ and V even for porous media in regime I, the use of Eq. (8) appears justified. For Coconino sandstone the temperature increase achieved upon shock compression to the Hugoniot elastic limit, from Eq. (8), is approximately 15°C. This temperature increase can be neglected when it is compared to the much greater temperature increase resulting from stronger shocks.

The second regime may be defined as consisting of compressed states lying between volumes V_e and V_g. In this region the shock compression may be considered as primarily consisting of crushing porous sandstone to the volume of uncompressed single-crystal quartz. The inherent irreversibility of such a process suggests that nearly the entire energy of the shock will go into thermal energy. With this simplifying assumption, the recoverable mechanical energy and contributions to E from the quartz-grain surface energy are neglected. The shock energy may then be written as

$$E\big|_{II} = E_t = \sigma(V_0 - V)/2 \tag{10}$$

For regime II in the case for silicate minerals, the Debye temperature is higher than the shock temperature; therefore a constant value of the specific heat—such as 6 calorie/mol. deg., the Dulong-Petit value—is inappropriate to calculate T_H from E_t. In quartz, typical of the common silicates, the specific heat at constant volume, c_v, varies by a factor of 1.6 between room temperature and 800°K (Fig. 13). It should also be noted that, as in the calculation of shock temperature in porous metals,[13] the specific heat of the porous rock or mineral is given in terms of mass rather than volume and is assumed to be the same as

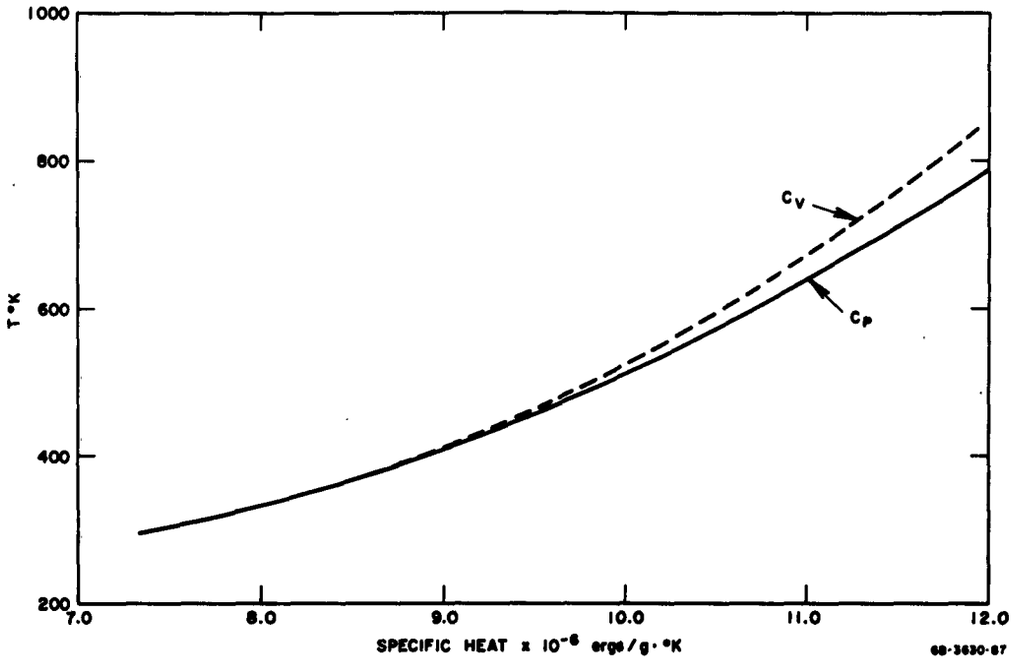

FIG. 13 SPECIFIC HEAT vs. TEMPERATURE, SiO_2 (α-Quartz)
(Data from Kelley, 1949)

that of the solid material; this being consistent with the assumptions used in obtaining Eq. (10). Pressure affects specific heat, within a rough approximation discussed by Birch, by an amount proportional to the square root of the density ratio of compressed to uncompressed solid material.[14] In the following, therefore, the specific heat is assumed to be independent of stress, since the compression of the solid quartz is small. Thus the specific heat is assumed to be only a function of the temperature achieved in shock compression.

At constant pressure c_p is related to c_v by

$$c_p = c_v - T\left(\frac{\partial P}{\partial V}\right)_T \alpha^2 V^2 \qquad (11)$$

where α is the volume coefficient of expansion.

The measurements of Kelley[15] provide c_p as a function of temperature. It is then possible to calculate c_v as a function of temperature (Fig. 13),

although the difference, generally, is negligible. Often c_v or c_p are expressed as a function of temperature in the form

$$c_v = a + bT - c/T^2 \tag{12}$$

where a, b, and c are experimentally determined constants.

Then

$$E_T|_{II} = \int_{T_0}^{T_H} c_v dT \quad . \tag{13}$$

For states in regime II (Fig. 12) the temperature may be implicitly expressed as

$$0 = T_H^3 + \frac{2a}{b} T_H^2 - \frac{2}{b}\left[\sigma\frac{(V_0 - V)}{2} + aT_0 + \frac{bT_0^2}{2} + \frac{c}{T_0}\right]T_H + \frac{2c}{b} \tag{14}$$

where Eqs. (12) and (10) were substituted into Eq. (13). Eq. (14) is a cubic equation and may be solved for T_H, the temperature achieved in any shock compression to volumes in the range

$$V_q < V < V_e$$

In regime III (Fig. 12) a partition of shock energy is assumed. The total energy of a shock may be written as

$$E|_{III} = (V_0 - V)\sigma/2 = \int_{T_0}^{T_H} C_v(T)dT + E_h \tag{15}$$

The low value of the thermal expansion coefficient for nonmetallic materials such as silicates and, in particular, quartz, suggests that the 0°K isotherm may be approximated by the isothermal compression curve, such as the one determined statically by Bridgman.[10] The 0°K isotherm may be expressed in terms of a Murnaghan equation of state. For this equation of state, the pressure-volume relation is written in the form

$$P|_{0°K} = \beta\left[\left(\frac{V_q}{V}\right)^{\xi} - 1\right] \tag{16}$$

where β and ξ are empirical constants. The compressional shock energy is given by

$$E_k = \int_{V_g}^{V} - [PdV]_{0^\circ K} \tag{17}$$

which, upon substitution of Eq. (16) and integration becomes

$$E_k = V_g \beta \left[\frac{(V_g/V)^{\xi-1} - 1}{\xi - 1} + V/V_g - 1 \right] \tag{18}$$

Therefore, the temperature of a porous sandstone at final states of shock compression in regime III, may be written implicitly as

$$0 = T_H^3 + \frac{2a}{b} T_H^2 - \frac{2}{b} \left\{ \sigma \frac{(V_0 - V)}{2} - V_g \beta \left[\frac{(V_g/V)^{\xi-1} - 1}{\xi - 1} + V/V_g - 1 \right] \right.$$

$$\left. + aT_0 + \frac{bT_0^2}{2} + \frac{c}{T_0} \right\} T_H + 2c/b \tag{19}$$

where Eq. (12) and Eq. (17) are substituted into Eq. (15). The form of Eq. (19) is similar to Eq. (14).

The shock temperatures for Coconino sandstone were calculated using Eqs. (14) and (19) and are tabulated in Table II. These results and the temperature obtained by Wackerle for quartz using the Walsh and Christian development are shown in Fig. 14.

The temperatures shown in Table II should be considered as being **minimum** temperatures for the following reasons:

(1) It is implicitly assumed in regimes II and III that thermal equilibrium behind the shock has been achieved; *i.e.*, the shock energy density is evenly distributed within the shocked material. In a coarse aggregate, more thermal energy should be concentrated at the grain boundaries of the shocked material than in the volume within the center of the quartz grains, the characteristic relaxation time being determined by the grain size and thermal properties of the shocked material.

Table II

SHOCK COMPRESSION TEMPERATURES, COCONINO SANDSTONE

STRESS (kb)	E (ergs/g x 10^{-9})	E_K (ergs/g x 10^{-9})	$E - E_K$ (ergs/g x 10^{-9})	T ($^{\circ}$K)
0.0	0.0	0.0	0.0	300
2.4	0.0119	0.0	0.0119	305
6.8	0.0749	0.0	0.0749	310
8.3	0.145	0.0	0.145	322
12.5	0.374	0.0	0.374	348
17.0	0.722	0.0	0.722	390
22.0	1.20	0.0	1.20	443
30.0	2.00	0.0	2.00	524
33.0	2.31	0.025	2.28	556
39.0	2.92	0.15	2.77	598
47.0	3.76	0.42	2.34	656
57.5	4.89	0.89	4.00	713
73.5	6.61	1.61	5.00	800

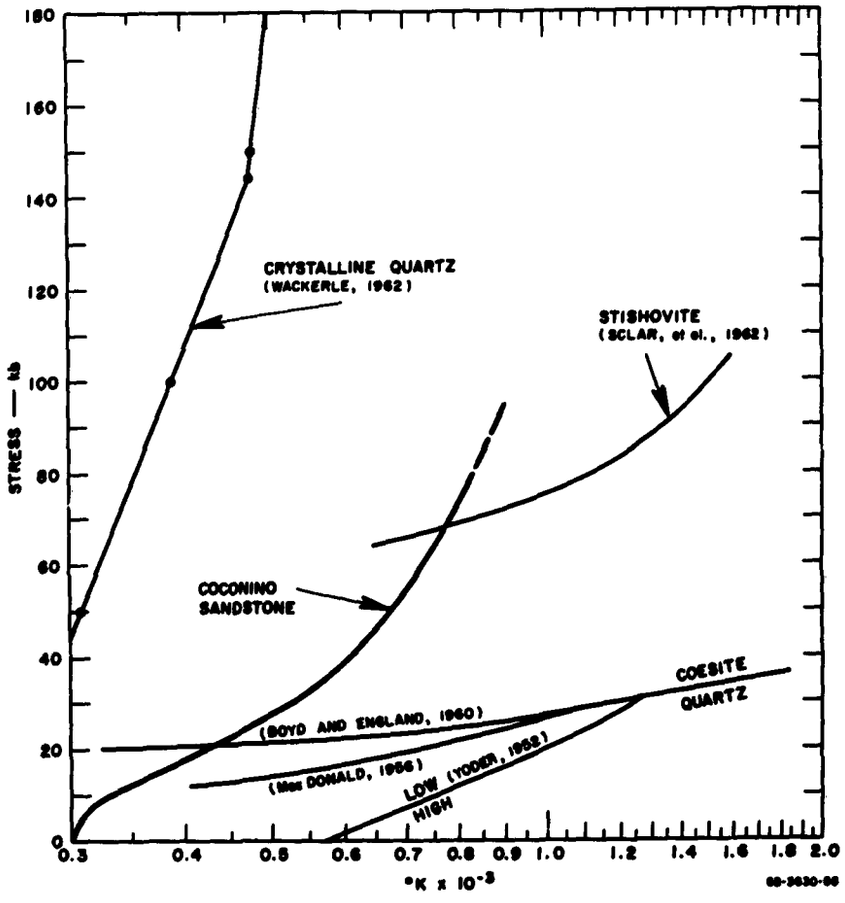

FIG. 14 SHOCK STRESS vs. SHOCK TEMPERATURE AND SiO_2 PHASES

(2) In general, the mineral in a porous rock may not remain in the same polymorphic phase as the solid material shocked to the same pressure. In the present case, for Coconino sandstone, the solid Hugoniot of Fig. 8 appears to cross over the curve (Bridgman's) for the 0°K isotherm used in the calculation at approximately 75 kb. An error produced by too large a value for E_K and therefore too low a temperature estimate will result from using Eq. (19); the magnitude of the error in E_K is equal to the cross-hatched area in Fig. 12.

(3) If the quartz in the Coconino sandstone is partially converted to stishovite when shocked to above 67 kb, as suggested in Section IV-A-6 (see also Fig. 14), additional inaccuracies may arise in the estimate of T_H, as follows:

(*a*) The °K isotherm of stishovite is of significantly lower volume than that of quartz; thus an error may result by using too high a value for E_K in Eq. (19). This, in turn, produces too low a value of T_H.

(*b*) At the temperature of the hypothetical stishovite transition the specific heat calculated for quartz has risen to that of the classical Dulong-Petit solid; an additional underestimate could result if the specific heat of stishovite were actually lower than that of quartz.

(*c*) If the transformation is exothermic, as implied by the slope of the quartz-stishovite phase line (Fig. 14), still another temperature underestimate will be made. For a latent heat of 2.8×10^9 ergs/g (Section IV-A-6), significant compared to the thermal energies available above 68 kb listed in Table II, the phase transition itself could provide an important contribution to the shock temperature.

Finally, it should be noted that it is not presently clear whether the surface energy of a porous rock will increase or decrease during shock compression. Thus, a temperature error of unknown sign or magnitude resulting from surface effects may be present in Table II.

4. Relaxation Velocity

The velocity of relaxation waves emanating from the lateral free-surfaces of shock-compressed sandstone specimens has been examined for shock amplitudes in the 60-186 kb range. A study of these unloading

velocities can provide information on the properties of the shocked solid which are not obtainable from the Hugoniot.

For a plane shock impinging on a specimen with a lateral boundary oriented at 90° to the shock front, the extent of the region of the interaction of relaxation waves with the shock may be determined by measuring the point at which the planarity of the emerging wave is affected by the specimen edge. The velocity of the relaxation wave, C, is related to the width of disturbed region, W, by

$$C = U\sqrt{(W/D)^2 + (U - u)^2/(U)^2} \qquad (20)$$

where D is the thickness of the specimen. Even under ideal conditions, it is difficult to estimate W—a typical smear camera record is shown in Fig. 11. The problems which arise in applying this method to metals are discussed by Al'tshuler *et al.*[16] Due to the inherent nonplanarity of the shock driven through a porous rock (Figs. 10 and 11) the application of this technique to porous rocks especially at low shock stresses is more difficult than for metals. Although complete results were not obtained for all the experiments performed, those available are plotted in Fig. 15.

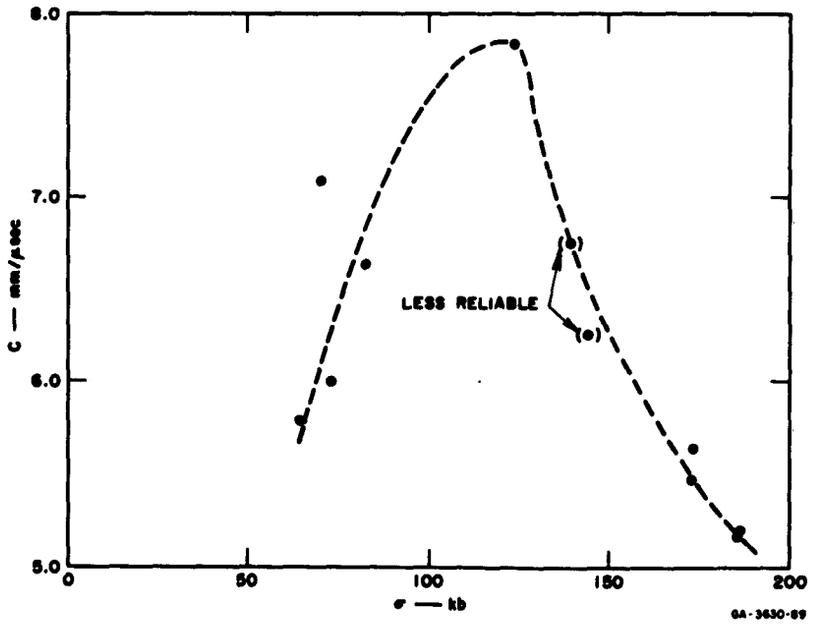

FIG. 15 LATERAL RELAXATION VELOCITY vs. MAXIMUM SHOCK STRESS

The increase in relaxation velocity up to 134 kb is expected. Above that stress level the results are surprising. They could indicate a phase change but this speculation seems at present inappropriate in view of the inherent inaccuracies in the porous rock measurements, as well as an inconsistency which is noted below between the lateral relaxation and the free-surface velocity data.

The free-surface velocity obtained in the various experiments may be compared to a velocity which is estimated from the lateral relaxation data. For a simple shock, the free-surface velocity is given by

$$U_{fs} = \frac{V}{\rho_0 U} + u_r \tag{21}$$

the first term on the right is the usual particle velocity for shock compression from the Rankine-Hugoniot jump conditions, and u_r is the relaxation particle velocity.

If the relaxation process is assumed to be adiabatic, the relaxation particle velocity may be written as[17]

$$U_r = \int_{\rho_0}^{\rho} C d\rho/\rho \tag{22}$$

If C is assumed a function of ρ only (independent of temperature) the integral on the right (Eq. 22) may be evaluated for the data in Fig. 15. Since C has not been obtained below 60 kb, the integral in Eq. 22 is unknown for densities less than 2.958 g/cc, and the vertical position of the curve segment representing u_r in Fig. 16 is undetermined. The point of inflection at a density of approximately 3.25 g/cc (Fig. 16) corresponds to the apparent maximum relaxation velocity at 134 kb (Fig. 15). From comparing Figs. 15 and 16 it is evident that the value of the integral in Eq. (22) is relatively insensitive to the possible large errors in the determination of C.

When u_r is calculated using Eq. (21) the slope of the u_r versus σ curve predicted by the free-surface velocity is in disagreement with that obtained from the lateral relaxation velocity. The factors producing this apparent discrepancy are not at present known; however it is possible that aside from an error in the experimental technique, which cannot be

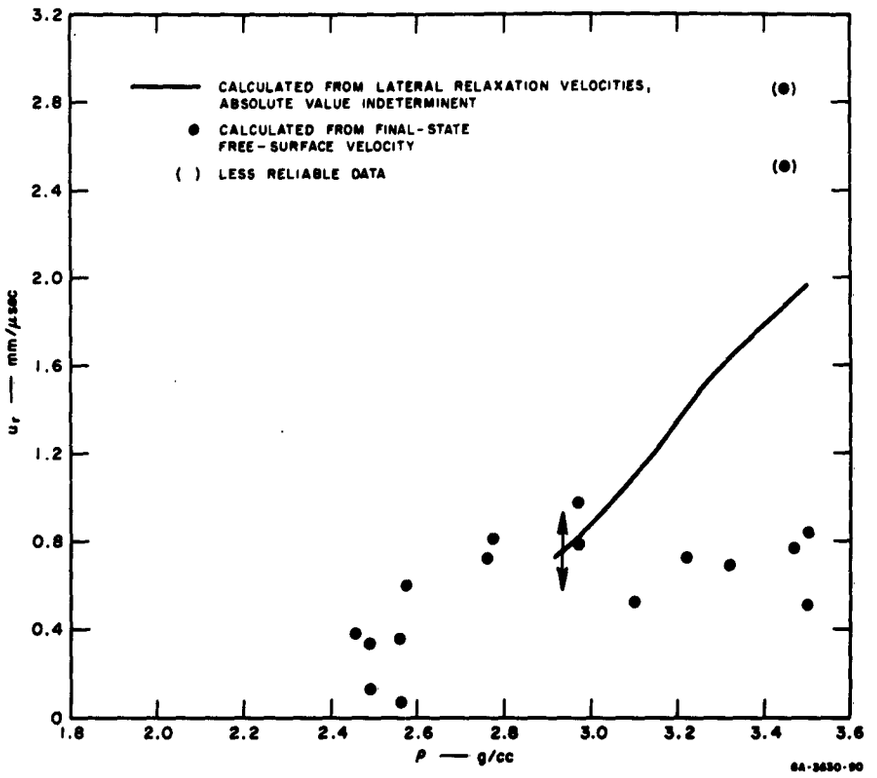

FIG. 16 RELAXATION PARTICLE VELOCITY FROM LATERAL AND FREE-SURFACE VELOCITY, COCONINO SANDSTONE

completely ruled out, two of the assumptions in the foregoing treatment may be invalid. These are:

(1) The shock-compressed rock into which relaxation waves propagate may be anisotropic with respect to the directions parallel and perpendicular to plane of the shock. In consideration of the anisotropy exhibited by single crystal quartz above shock stresses of 200 kb, it seems reasonable to suppose that the relaxation path may actually differ for lateral relaxation waves and free-surface reflection relaxation waves.

(2) The lateral relaxation velocity may be strongly dependent on shock temperature rather than being only dependent on the final compressed density; in this case the application of Eq. (26) would be invalid since relaxation could proceed along a different path for each temperature.

In view of these and other uncertainties, it seems imprudent to speculate on this comparison—at least until more data are available.

5. Water Saturated Sandstone

Three exploratory experiments at high-shock stress on the effect of water saturation on the equation of state of porous sandstone (Table I and Fig. 8) have given points in a fair agreement with the stress-volume curve obtained by Schall[18] using a flash X-ray technique. The rocks were saturated by means of first subjecting them to vacuum and then, using water, increasing the ambient pressure to atmospheric pressure. On the basis of the uniformity of shock velocity, saturation was believed to be essentially complete.

At shock stresses sufficiently high to overdrive the Hugoniot elastic limit, no major experimental difficulties arise. The impedance-match technique is applied to obtain the equation of state point.

At low stress levels, where a two-wave shock is likely, the use of the inclined mirror technique (Section III-A) for measuring free-surface velocity does not seem appropriate for the following reasons:

(1) To avoid observation of an air shock, inclined mirror measurements are usually performed in a vacuum; and

(2) It seems apparent that when a shock wave impinges on the free-surface of a saturated rock, the water exposed on the surface and the quartz grains in the sandstone will move with different particle velocities appropriate to the shock impedance of each of the components.

Because of these difficulties, two of the low-shock stress experiments, one with saturated Coconino sandstone, and the other unsaturated, were performed using the quartz transducer technique (Section III-C). The pressure-time profiles of the shock transitions (Fig. 17) are believed to

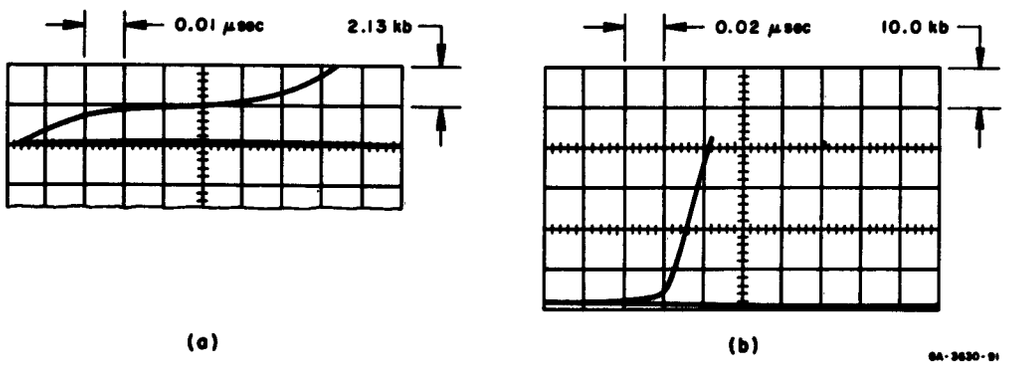

FIG. 17 QUARTZ TRANSDUCER STRESS-TIME PROFILES, COCONINO SANDSTONE
Nominal stress scale refers to rock; (a) dry; (b) water saturated

be quantitatively reliable as far as the inherent times in the shocks are concerned. The anomalously low values of the precursor amplitude observed for dry sandstone as compared to those obtained using the inclined mirror method (Table I), which are thought to be the correct values, indicate a discrepancy presently unexplained.

The elastic precursor rise-time of 0.21 μsec (Fig. 17), almost a factor of 10 greater than can be attributed to tilt or nonplanarity of the shock, is a particularly interesting result for both experiments.

The quartz transducer was in the nonlinear stress-current range for the stress level of the main shock in both experiments; however, the *CRO* records imply that the rise times of the main shocks are also approximately 0.22 μsec. A rise time of the main shock of the order of 0.2 μsec has also been observed using the inclined mirror cutoff (Figs. 10 and 23), in both the sandstone and limestone experiments. The precursor rise-time is difficult to observe in a smear camera record, although its presence may account for some of the nonreproducibility in the measurement of the precursor velocity.

6. Discussion, Shock Compression of Sandstone

The behavior of the Hugoniot for Coconino sandstone above 67 kb is particularly interesting. Normally the Hugoniot of the porous material would be expected to lie toward greater volume states than that of the isotherm and Hugoniot of the solid material because of the heat generated and the entropy gained in shock transition. In contrast, for shocks greater than 67 kb, the volume achieved by the shock transition in Coconino sandstone is less than that achieved at the same pressure with the solid material or that observed in isothermal static compression.

The locus of pressure-temperatures states shown in Fig. 14 implies that at approximately 68 kb and 770°K the stishovite stability regime* [19] is achieved by shock compression. Because of what appears to be essentially coincidence in shock stress between the predicted quartz (or coesite?)—stishovite transition and an apparent anomalous density increase observed on the Hugoniot, the hypothesis that stishovite is produced is quite suggestive. The close agreement in stress levels is undoubtedly fortuitous. A parallel hypothesis has been put forward by McQueen *et al.*[11] for the formation of stishovite at 144 kb and 523°K in Wackerle's shock compression experiment on quartz.

* The Solar *et al.* phase line (Fig. 14) may suggest too high an equilibrium temperature and pressure for stishovite since the starting material was silica gel rather than coesite or quartz.

The dashed curve of Fig. 8 is a possible configuration of the Hugoniot which is compatible with the data points and implies a polymorphic transition at 67 kb. The polymorphic transition indicated by the dashed curve (Fig. 8) is not likely to give rise to a multiwaved shock (see Section IV-B-2).

The stishovite-quartz energy difference at the stress-level at which the transition may have been partially achieved in the present experiment can be estimated from the Sclar *et al.*[19] results and the pressure-volume curves for quartz and stishovite assumed by McQueen *et al.* The internal energy difference is

$$E_s - E_q = T(S_s - S_q) - \sigma(V_s - V_q) \qquad (23)$$

where the subscripts s and q refer to stishovite and quartz, and S is entropy. Applying the Clausius-Clapeyron relation to the Sclar *et al.*, phase line, the entropy change,

$$S_s - S_q \cong -3.6 \times 10^6 \text{ ergs/(°K)g}$$

The volume change,

$$V_s - V_q \cong -0.108 \text{ cc/g}$$

is obtained from McQueen *et al.*, and may then be used to estimate the energy difference in Eq. (23). For $T = 770$°K and $\sigma = 68$ kb,

$$E_s - E_q = 4.6 \times 10^9 \text{ ergs/g} \qquad (24)$$

which may be compared with the value

$$E_{0s} - E_{0q} = 1.5 \times 10^{10} \text{ ergs/g}$$

given by McQueen *et al.* for the energy difference at $\sigma = 0$. In the McQueen estimate (*a*), the quartz-stishovite phase line is assumed to pass through the point ($\sigma = 144$ kb, $T = 523$°K), at which the Wackerle data indicates a transition, and, (*b*) the first term in Eq. (23) is negligible. The validity of these assumptions and those used in the present calculation could be critically considered when more SiO_2 phase equilibrium data are available.

B. CARBONATE ROCKS

1. Calcite

Much of this information is taken from Semiannual Report No. 3, October 20, 1962.[20] The calcite specimens come from naturally occurring "Iceland Spar" found in Chihuahua, Mexico. Only crystals that are colorless, free from cleavage, parting, and obvious defects are used. The specimens, usually about ¼-inch thick and 1¼ inches on a side, are cut into four different orientations: *X*, *Y*, *Z*, and $(01\bar{1}2)$-cleavage plane. The designation of a particular cut means that the shock travels parallel to the designated crystallographic axis.

A plot of the experimental data in the stress-volume plane is shown as Fig. 18; the corresponding stress-particle velocity plot is shown as Fig. 19. In Fig. 20, hydrostatic data reported by Bridgman[10] and both static and dynamic data reported by Adadurov, *et al.*,[2] are shown.

The Hugoniot elastic limit lies between 18.5 and 23.7 kb for the cuts investigated—a conclusion based on more than twenty measurements. This transition is termed the Hugoniot elastic limit because it is the first observed and the velocities with which the wave front travels in various crystallographic directions correspond within 3% to elastic wave velocities computed from elastic constants. Thus it would seem that the value of 20 kb is the maximum normal stress that calcite can support without exceeding the maximum values of lateral shear stresses that can exist in calcite, *i.e.*, a true Hugoniot elastic limit. But this may not be so. In Vermont and in Yule marble a Hugoniot elastic limit of about 12 kb is measured and a transition at 22 kb. Hence maximum elastic amplitudes in calcite may be controlled by a polymorphic transition at 22 kb rather than being limited by the maximum lateral shear stresses that calcite would otherwise support.

Good evidence exists in all orientations for a phase transition at 30 to 32 kb; about eight measurements are available. The transition at 95 kb is also well documented; about four measurements are available for all orientations in calcite. The transition at 45 kb is least documented; only two reliable values are available in *Z*-cut calcite, with some evidence that there is a transition at about 45 kb in three other calcite experiments.

Dremin and Adadurov[21] record a transition in marble at 150 kb. Their technique measures only an average free-surface velocity; *i.e.*, above 150 kb the free-surface velocity of a single wave front was measured, and below 150 kb the average free-surface velocity of a multiple wave front was measured. We did not observe a transition at 150 kb but did

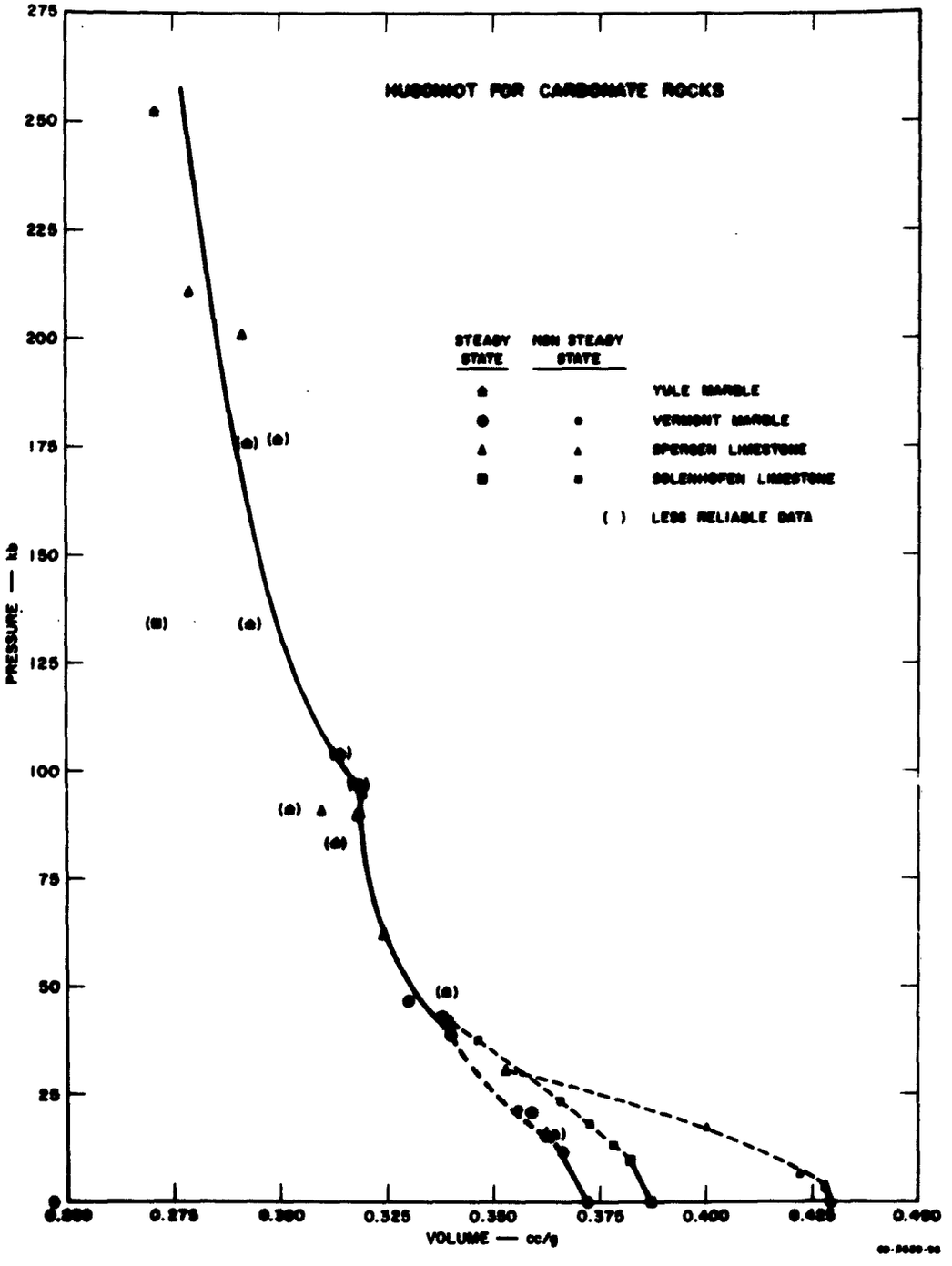
HUGONIOT FOR CARBONATE ROCKS
STEADY STATE
NON STEADY STATE
YULE MARBLE
VERMONT MARBLE
SPERGEN LIMESTONE
SOLENHOFEN LIMESTONE
( ) LESS RELIABLE DATA
PRESSURE — kb
VOLUME — cc/g
275
250
225
200
175
150
125
100
75
50
25
0
0.275
0.300
0.325
0.350
0.375
0.400
0.425
0.450

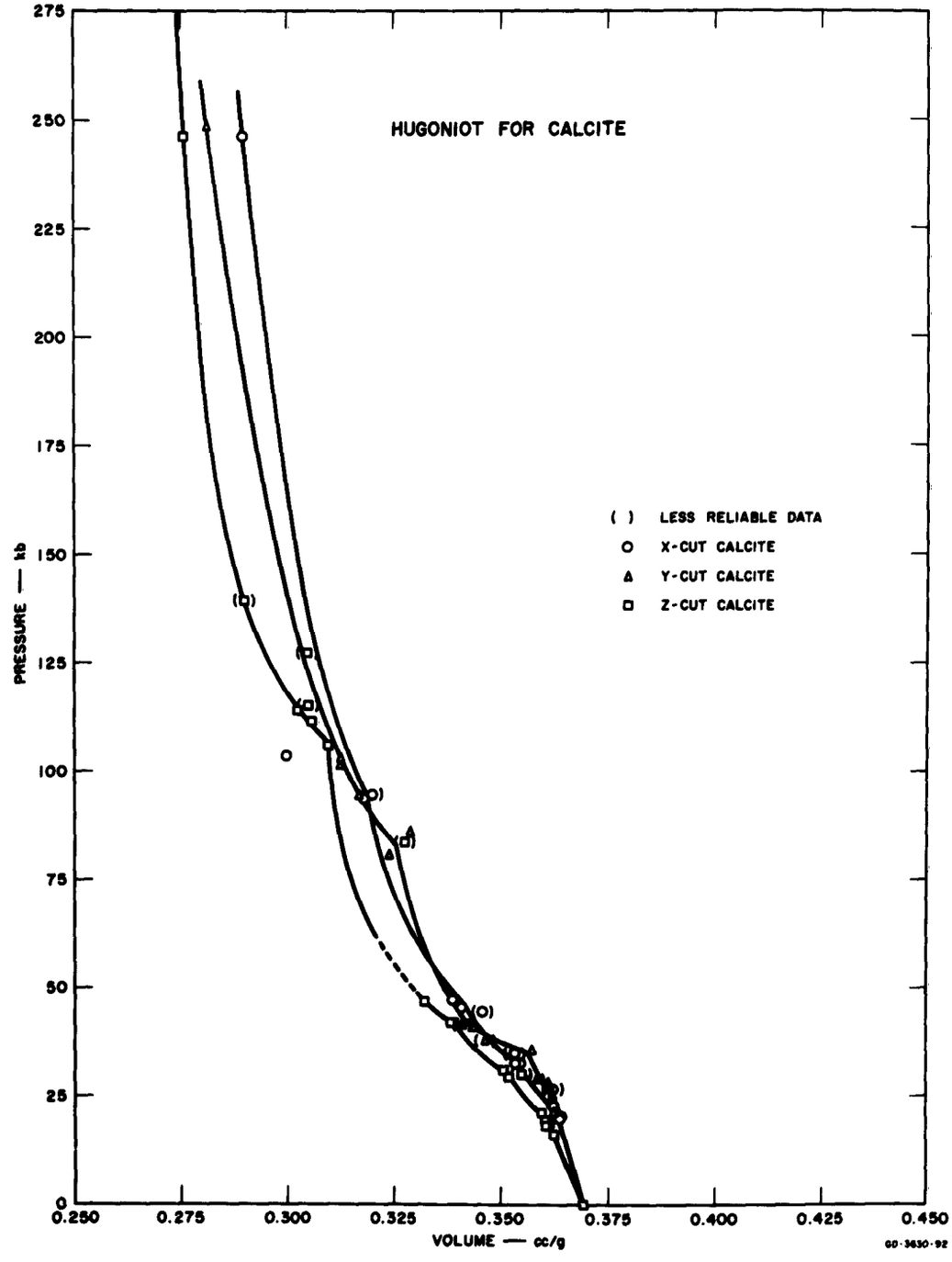

FIG. 18 HUGONIOT FOR CALCITE AND CARBONATES

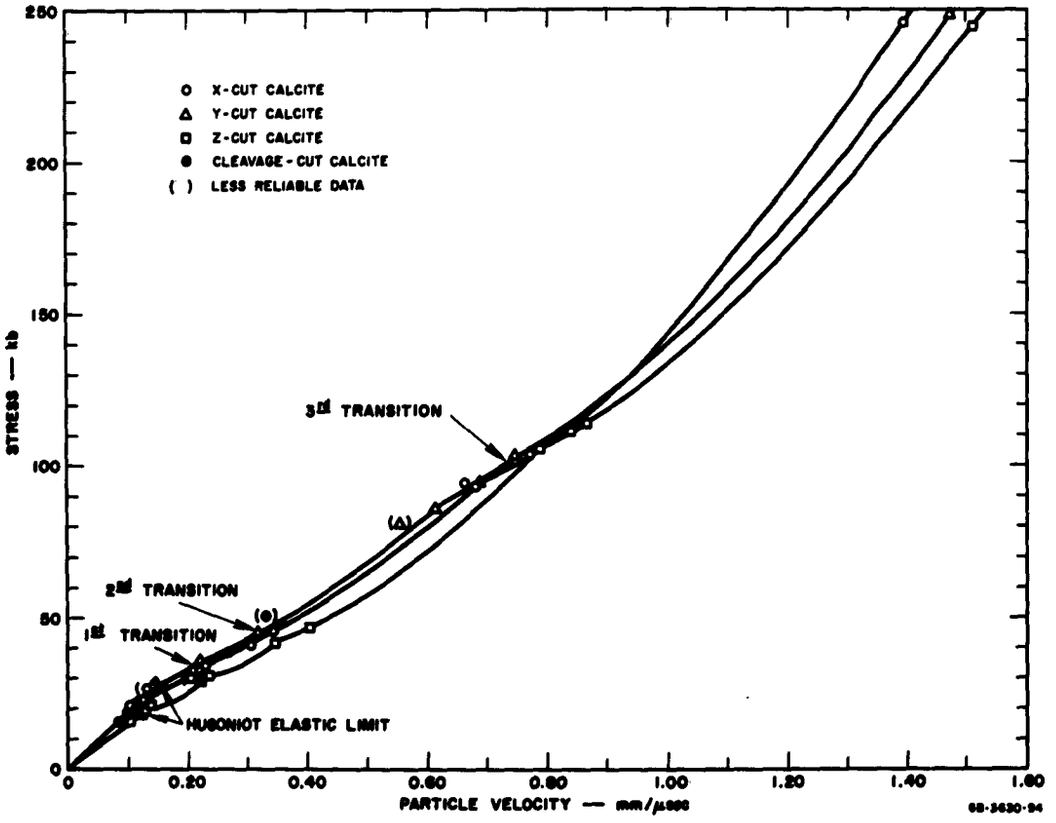

FIG. 19 STRESS-PARTICLE VELOCITY PLOT FOR CALCITE

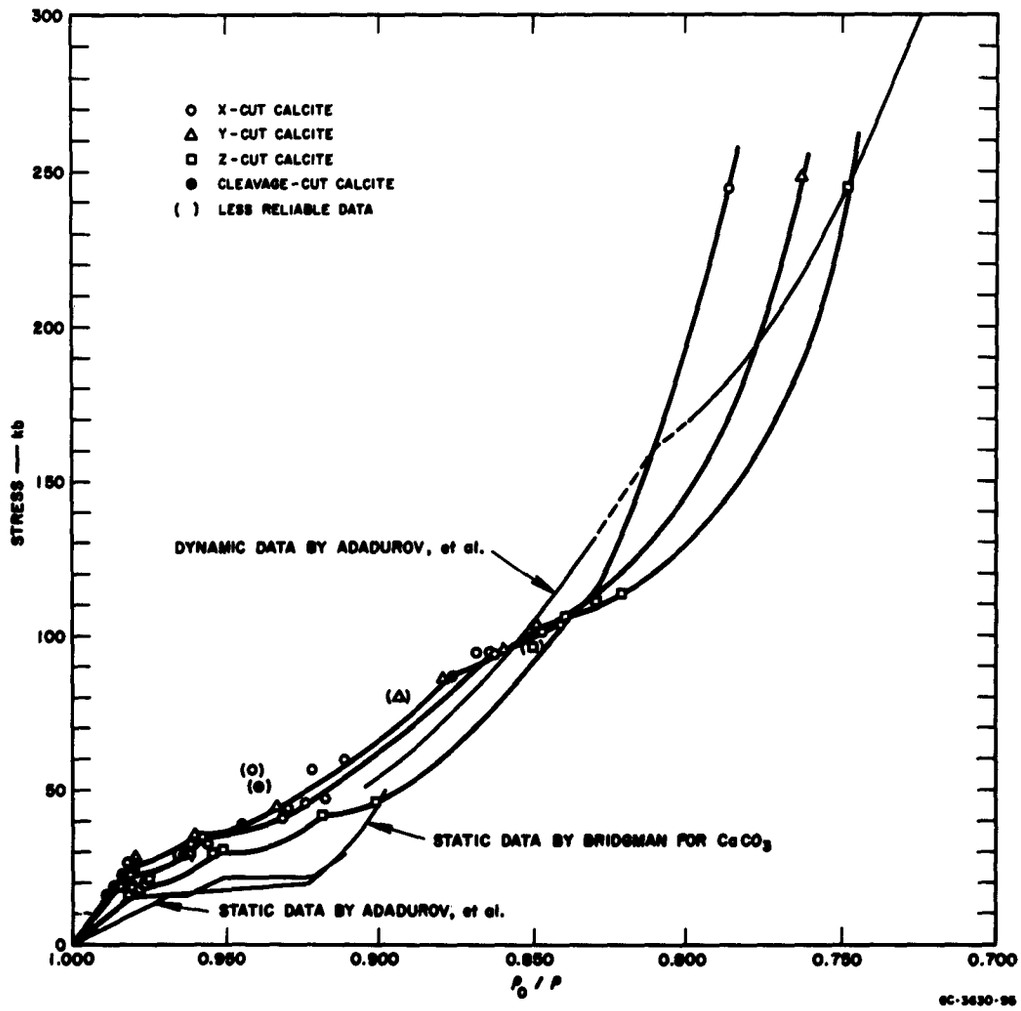

FIG. 20 STRESS-ρ_0/ρ PLOT FOR CALCITE

observe one at 95 kb. The 150 kb transition recorded by Adadurov *et al.*,[2] is probably the boundary between a double and single shock front produced by the 95 kb transition. If Rayleigh lines are constructed along the calcite Hugoniot, one can see that a single wave is stable for pressure states above 150 kb and a multiple front is stable below this region. The complicated shock front below 150 kb was not observed by Adadurov *et al.*, because the gap technique does not resolve such multiple wave fronts.

The differences in the data among the various crystal cuts at 250 kb are disturbing (a similar behavior is observed for the various cuts of quartz at these pressures). They imply that anisotropy is still important. It would be desirable to repeat these measurements since there exists only one experiment for each cut at these pressures.

2. Marbles and Limestones

Yule and Vermont marble, Solenhofen and Spergen limestones were used in the experiments to measure Hugoniot data for polycrystalline carbonate rocks. A petrographic description of these rocks follows:

a. Solenhofen Limestone

Solenhofen limestone is a massive, tan, lithographic limestone composed of 96% calcite.

The grain size of the calcite ranges from 0.005 to 0.015 mm in diameter and has a median diameter of 0.010 mm. There are occasional grains as large as 0.03 mm and an occasional quartz grain. A few percent of interstitial clay is present and the true porosity is a few tenths of a percent. The density is 2.581 g/cc.

b. Spergen Limestone

The Spergen limestone is a gray, well cemented, microcoquina composed of about 60% fossil fragments, 20% bioclastic debris including carbonate detritus, 20% calcite, and a percent or two of oolites.

The size of the sub-rounded fragments ranges from 0.1 to 0.7 mm with the average size being about 0.3 to 0.4 mm in diameter. The average grain size of the calcite matrix is 0.2 to 0.3 mm in diameter with an occasional grain as large as 1.0 mm in diameter.

The calcite matrix tends to have a "sub-poikiloblastic" texture. Some of the bioclastic fragments which are included in the grains of cementing calcite have the same optic orientation as the neighboring calcite grains.

The porosity is about 12%. The density ranges from 2.360 to 2.398 g/cc.

c. VERMONT MARBLE

Vermont marble is massive, white, fine-grained and composed of 95% calcite grains.

The calcite ranges from 0.05 to 0.2 mm in diameter and has a median diameter of 0.12 mm. Five percent secondary quartz occurs in occasional bands that are 1 mm thick. The quartz grains are 0.05 mm in diameter and are scattered among the calcite grains in the 1 mm band. The density is 2.687 cc/gm.

d. YULE MARBLE

Yule marble is a massive, white, homogeneous marble that is composed of 100% calcite.

The average grain size of the marble is between 0.2 and 0.4 mm with an occasional grain as large as 1.5 mm in diameter (apparent grain size in the thin section depends upon orientation as the grains are platy). The density is 2.697 cc/gm.

Table III compiles all plane-wave experimental data on carbonate rocks, including a reinterpretation of the plane-wave experiments listed in Semiannual Report No. 2. Figure 18 is a plot of the Hugoniot curves for the carbonates.

The Hugoniot for marble follows the Hugoniot for calcite. The Hugoniot elastic limit (10-15 kb) and 3 transitions (22, 40, and 95 kb) are observed.

For Vermont marble the Hugoniot elastic limit is about 10 to 15 kb and decays as the shock travels. Figure 21 shows Hugoniot elastic limits plotted as a function of specimen thickness. Data for ¼-inch and ½-inch specimens of Vermont marble are measured from a single experiment

Table III

HUGONIOT DATA FOR CARBONATE ROCKS

SPECIMEN	SPECIMEN THICKNESS (mm)	FIRST FRONT				FINAL STATE				EXPLOSIVE	DRIVER			SHOT NO.
		Particle Velocity (mm/μsec)	Shock Velocity (mm/μsec)	Stress (kb)	Volume (cc/g)	Particle Velocity (mm/μsec)	Shock Velocity (mm/μsec)	Stress (kb)	Volume (cc/g)		Material (inch)	Free-Surface Velocity (mm/μsec)	Stress (kb)	
Yule Marble	8.206[γ]	(0.396)	(4.63)	(49)	(0.339)					P-60	0.5 Al			8281
		(0.697)+	(4.21)	(83)	(0.313)	(0.782)	(3.537)	(91)	(0.303)					
	10.167	(0.103)	(5.73)	(16)	(0.36)					P-60	0.5 Al			8280
		(0.769)+	(4.94)	(104)	(0.31)	(1.024)	(4.478)	(134)	(0.293)					
	δ					(1.17)	(5.52)	(176)	(0.292)	P-60 + 1" Comp B	0.5 Al	(2.89)		7785
						(1.12)	(5.83)	(177)	(0.299)	P-60 + 1 Comp B	0.5 Al			7786
						1.59	5.91	253	0.271	P-60 + 2 Comp B	0.5 Al	(2.870)	292	8317
Vermont Marble	11.747[β]	0.086	5.262	12	0.366									
		0.165[α]	4.300	21	0.359	0.378	0.3791	43	0.338	P-60	0.5 Steel+	1.379	30	9257
		0.123	4.718	15	0.362						0.5 Lucite	1.429	32	
		0.190+	3.98	23	0.356									
		0.352[α]	3.73	39	0.340	0.443	3.284	47	0.329					
Solenhofen Limestone	6.215[δ]	0.073	5.330	10	0.382									
		1.108+	3.808	13	0.378					P-60	0.5 Steel+	1.363	29	9068
		0.163+	3.585	18	0.372	0.441	3.094	42	0.339		0.5 Lucite			
		0.223+	3.419	24	0.365									
		0.387+	3.342	38	0.346									
	6.278[δ]	0.820	4.572	97	0.318	(1.238)	(3.666)	(134)	(0.271)	P-60	0.5 Al	1.572	139	9066
Spergen Limestone	6.680[$]	0.046	3.888	4	0.428					P-60	0.5 Steel+	1.323	29	9067
		0.090+	2.939	7	0.422	0.481	2.634	31	0.358		0.5 Lucite			
	6.045[$]	0.224+	2.716	15	0.400									
						0.757	3.971	70	0.347	P-60	0.5 Al	1.572	139	9066
						(1.025)[Δ]	(4.00)	(95)	(0.319)					
	9.185[$]					0.789	3.38	62	0.324	P-60	0.5 Al	1.161	100	8150
	8[$]					0.965	3.94	90	0.318	P-60	0.5 Al	1.51		8075
						1.01	3.797	91	0.309	P-60	0.5 Al	1.54		8081
	12.405[$]					1.020	4.11	96.5	0.318	P-60	0.5 Al			8271
	14.488[$]													
	13.038[$]					0.965	3.94	90	0.318	P-60	0.5 Al	1.51	134	8079
	8[$]					1.62	5.21	201	0.291	P-60 + 1" Comp B	0.5 Al			8080
						1.790	5.23	221	0.278	P-60 + 2" Comp B	0.5 Al	2.94	298	8165

[δ] Plane-wave wedge experiment

[( )] Points in parenthesis are less reliable.

[+] Nonsteady—these states define the slow transition from the first front to the final state.

[$] Initial density 2.581 g/cc.

[$] Initial density 2.327 g/cc.

[Δ] Includes attenuation correction.

[α] Second front

[β] Initial density 2.687 g/cc

[γ] Initial density 2.697 g/cc

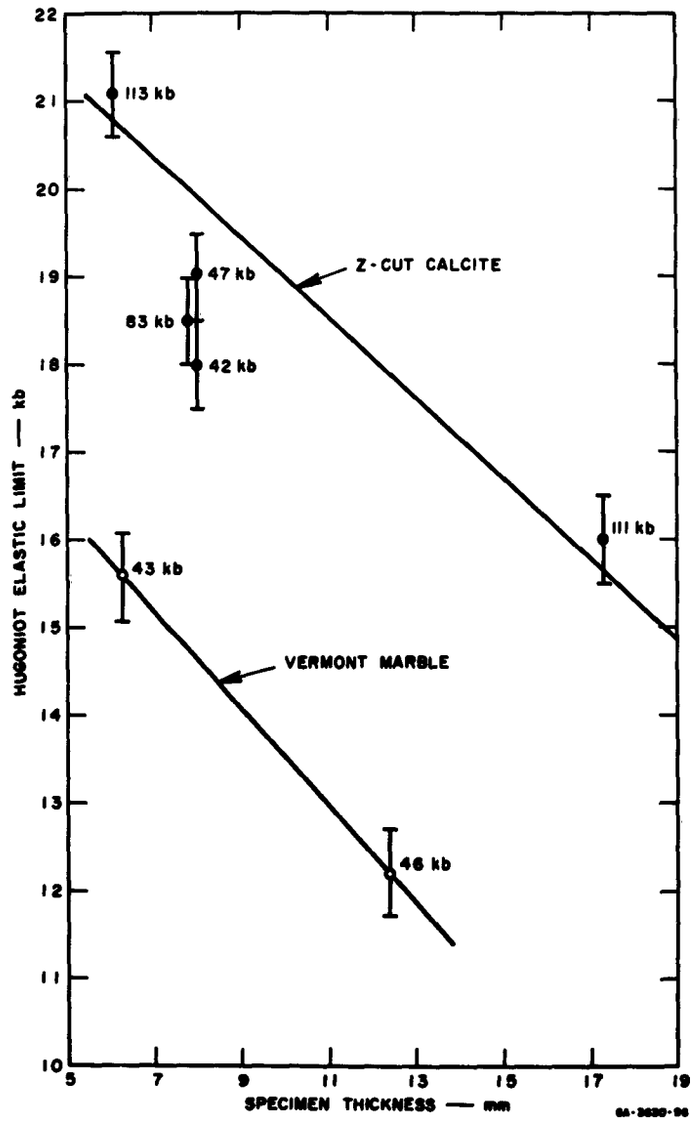

FIG. 21 DECAY OF HUGONIOT ELASTIC LIMITS
Final State Pressures are Indicated

and are considered reliable values. Data for *Z*-cut calcite are taken from several experiments. In general, both sets of data show that the Hugoniot elastic limit decays at about the same rate.

The experiment using a ¼-inch and a ½-inch specimen of Vermont marble also provides information about the behavior of transitions above the Hugoniot elastic limit. First consider what shock theory would predict.

A shock front may become unstable if a phase transition is present in the material. The phase transition may be either a first-order transition having a discontinuous change in volume, or a second-order transition having a discontinuous change in heat capacity, isothermal compressibility, or coefficient of thermal expansion.[22] If a shock front becomes unstable it will break up into two or more shock fronts, each stable for a certain range of pressures.

The necessary and sufficient condition for stability of a single shock transition between two arbitrary states, α and β should not intersect the Hugoniot at any intermediate point. If the Hugoniot is such that the Rayleigh line does intersect it at intermediate states, then the Rayleigh line must consist of segments, each segment corresponding to a wavefront (Fig. 22). For a material with several phase transitions, therefore, the wave structure can be somewhat complicated and can exhibit one or more wavefronts depending on the final pressure.

The intersection of the Rayleigh line with the Hugoniot indicates the pressure of the transition or final state, while the slope of the Rayleigh line is a measure of the velocity for a particular shock transition. In fact, it is easily shown that shock velocity is proportional to the square root of the negative slope of the Rayleigh line.

Figure 22 illustrates a Hugoniot for a material with two phase transitions in addition to a yield point. For final shock pressures greater than *I*, a single shock is stable. For final pressures between *I* and *E*, or between *B* and *D*, two waves will be present; the first is the elastic precursor wave whose amplitude is defined as the Hugoniot elastic limit, and the second is the final state. For final pressures between *D* and *E*, three waves will be present; the first is the elastic transition, the second is a phase transition, and the third is the final state. Note that the transition at *G* does not give rise to a separate wavefront. Note, too, that the region near Rayleigh line *BDE* would indicate the

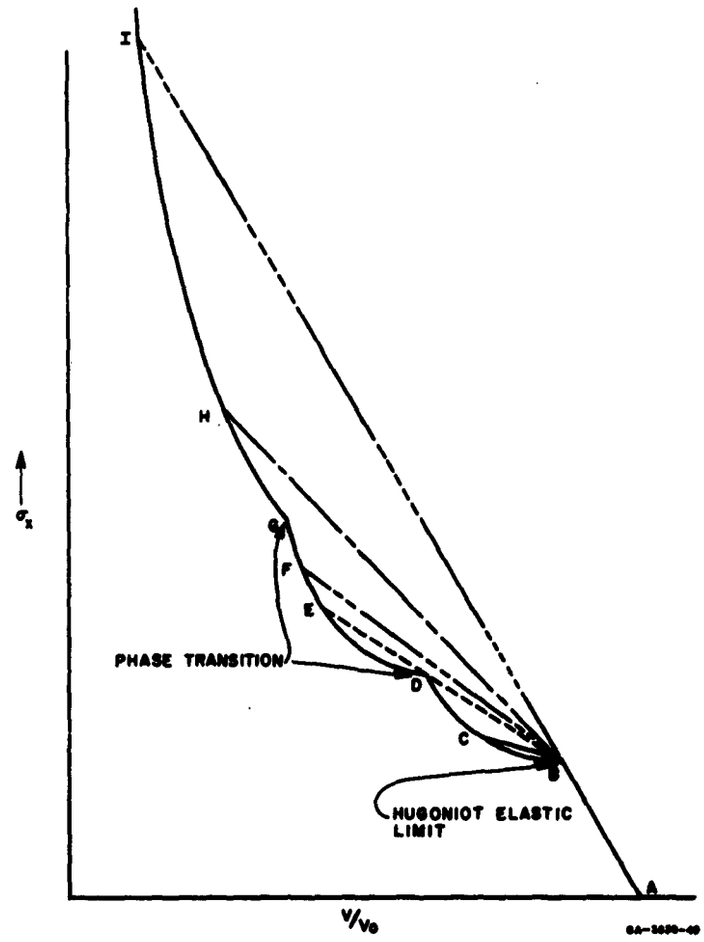

FIG. 22 HUGONIOT FOR A SOLID HAVING A YIELD POINT AND TWO PHASE TRANSITIONS

transition at *D* but it will take time until the fronts have traveled and separated sufficiently for the recording equipment to resolve the fronts.

For regions in which there are finite rise times to fronts, or for regions near the transition at *D* where the two fronts may not be completely resolved, the inclined-mirror trace appears as in Fig. 23. An inclined-mirror trace for a steep front appears as in Fig. 24.

For an inclined-mirror trace from a steep fronted shock, the arrival times and changes in trace angles are abrupt, but this is not so for shocks that have a finite rise time; the inclined-mirror traces

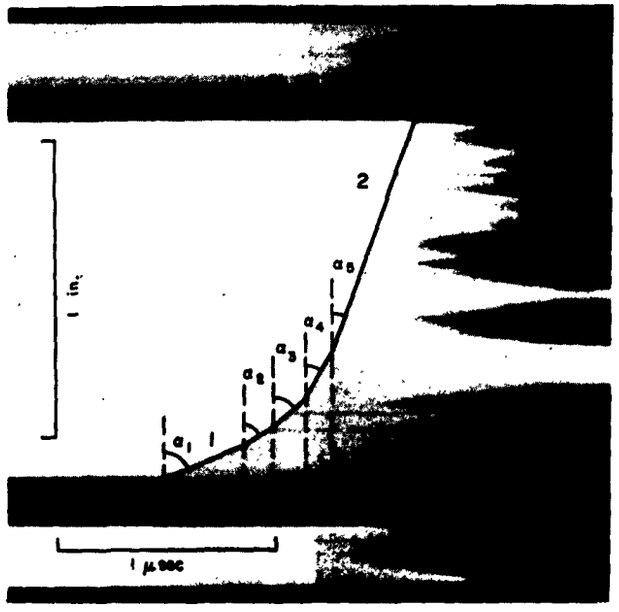

FIG. 23 INCLINED MIRROR TRACE FOR SOLENHOFEN LIMESTONE

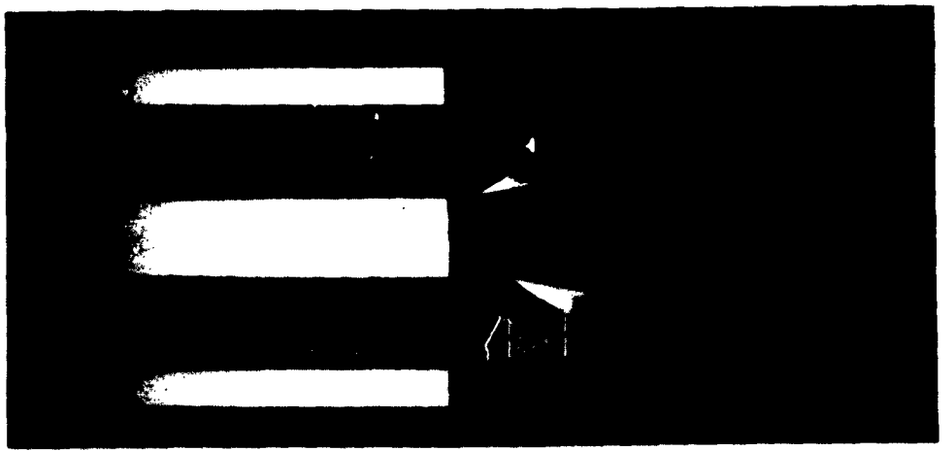

FIG. 24 INCLINED MIRROR TRACE FOR QUARTZ

appear curved. The Rankine-Hugoniot jump conditions are still valid in regions between initial and final states of a shock with a finite rise time and are used piecewise to obtain states between the final and initial states. Figure 23 shows how the curved inclined-mirror trace was approximated by a series of shock steps. The Rankine-Hugoniot jump conditions was applied to each step. In this case, the states between the initial (no. 1) and final (no. 2) in Fig. 23 are non-steady states and describe the path from the first state to the final state. Two of these paths are plotted in Fig. 18.

We stated that additional information is available for transitions above the Hugoniot elastic limit. The inclined-mirror trace for Vermont marble is shown in Fig. 25. The trace from the ½-inch specimen shows three distinct breaks indicating the front is composed of three shocks. The trace from the ¼-inch specimen shows breaks which are not as distinct and are curved—indicating that the front is composed of fewer shocks of *longer* rise times. Figure 26 is a diagram of these two fronts. The states in the ¼- and ½-inch-specimen are close to the Rayleigh line path *BDE* of Fig. 22 thus it takes some time for the shocks to separate sufficiently to show the transitions. Notice, that the Hugoniot elastic limit is decaying; however, the other two transitions do not appear to decrease appreciably—the observed variations are not experimentally significant.

Porous carbonates compact irreversibly and follow the marble calcite Hugoniot once they have compacted. Except for the elastic transition at 5 kb, other transitions are not observed because the thermodynamic path followed by the locking carbonate does not permit such resolution. This is a similar case to that part of Fig. 22 described by the Rayleigh line *BH* near the transition at *G*. The two dashed lines show such a particular path through which the porous carbonates compress to the final state. Note that the Solenhofen limestone behaves as if it were a pure carbonate rock with a 4% porosity. This is the first indication that, in some cases, minor impurities in the rocks may have considerable effect on propagation of shock waves.

In summary, then, we may describe the Hugoniots for carbonate rocks as follows:

The nonporous polycrystalline carbonates follow the Hugoniot of calcite. Transitions at 22, 42, and 95 kb are observed. The transition

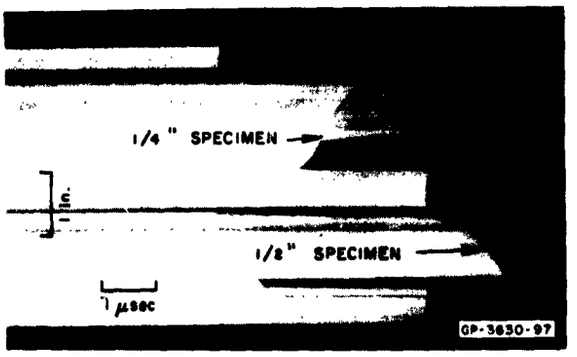

FIG. 25 INCLINED MIRROR TRACE FOR VERMONT MARBLE

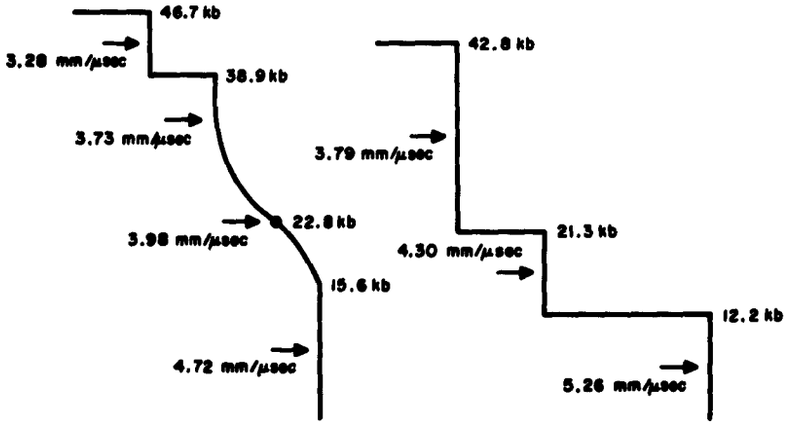

FIG. 26 IDEALIZED SHOCK FRONT FOR MARBLE

at 30 kb was not observed, but a special experiment would have to be designed since it is the most difficult to detect. The transition at 22 kb in marble is puzzling since this is the pressure of the calcite Hugoniot elastic limit. The 22 kb transition was also observed in the two-dimensional wedge data.[1] Hugoniot elastic limits are about 10 to 15 kb and decay.

The porous carbonates have Hugoniot elastic limits of about 5 kb and compress to states that lie along the calcite Hugoniot.

C. PLAGIOCLASE ROCKS AND BASALT

1. Plagioclase Rocks

Most experiments have used anorthosite. This is an igneous rock composed largely of the andesine member of the plagioclase series; our specimens were collected in the western San Gabriel mountains in southern California. The specimens were light bluish-gray. About 98% of the rock is andesine (An 43), and the remainder consists of apatite, zircon, chlorite, hornblende, biotite, and iron ore minerals scattered throughout. The andesine grains are anhedral to subhedral and range from about 8 mm to 1 mm in diameter; the average grain size is about 4 mm. The secondary minerals are usually imbedded in the andesine and range from 0.01 mm to 0.03 mm in size. Density is 2.662 g/cc.

Specimens of single crystal albite and labradorite were also used in one experiment.

Table IV presents all data on plagioclase. Hugoniots are plotted in Fig. 27, stress-particle velocity curves in Fig. 28. Figure 29 displays all known data for rocks which contain large amounts of plagioclase.

The main features of shock propagation in plagioclase are best demonstrated by the Hugoniot for anorthosite, and the Hugoniot for single crystal albite and labradorite, Fig. 27. We see that these rocks have a Hugoniot elastic limit at about 40 kb and, as yet, have no detectable transitions beyond this at least up to pressures of 250 kb. Composition and elastic wave decay govern the specific value of the Hugoniot elastic limit observed in a particular experiment.

In anorthosite evidence for elastic wave decay (stress relaxation) is indirect; the elastic wave amplitude was observed to increase as the amplitude of the second wave increased for the same specimen thickness. This effect was also observed in quartz by Fowles[6] and Wackerle.[9] One might speculate that if sufficient single crystal data for feldspar were available, the data would show elastic wave decay to be as important in feldspar as in quartz—a reasonable speculation since crystal structure for the two minerals is similar in many respects.

We stated that the Hugoniot elastic limit also depended upon the composition of the feldspar. Evidence for this is meager: one experiment.

Table IV

HUGONIOT DATA FOR PLAGIOCLASE

ROCK TYPE	SPECIMEN THICKNESS (mm)	FIRST FRONT				FINAL STATE				EXPLOSIVE SYSTEM P-60 +	DRIVER		SHOT NO.	NOTES
		Particle Velocity (mm/μsec)	Shock Velocity (mm/μsec)	Stress (kb)	Volume (cc/g)	Particle Velocity (mm/μsec)	Shock Velocity (mm/μsec)	Stress (kb)	Volume (cc/g)		Material (inch)	Free-Surface Velocity (mm/μsec)		
Anorthosite	5.885					1.517	5.63	227	0.275	2" Comp B	0.5 Al	2.955	9099	Initial density 2.662 g/cc
	12.484	(0.261)	(6.17)	(43)	(0.360)	1.320	5.59	198	0.288					
	5.880	0.286	5.66	43	0.356	0.406	3.75	55	0.344	--	0.5 Steel +			
	5.878	0.293	5.67	44	0.356						0.5 Lucite	1.404	9101	Initial density 2.662 g/cc
	5.880					0.858	5.34	122	0.315	1" Baratol	0.5 Al	1.560	9161	Initial density 2.662 g/cc
	12.474	0.317	5.86	50	0.355	0.812	5.28	118	0.320					
	6.340	0.403	5.40	58	0.348	1.029	5.18	144	0.302	0.5" Comp B +	0.5 Al	--	9230	Initial density 2.662 g/cc
	12.471	0.378	5.77	58	0.351	0.852	5.38	140	0.311	1" Baratol				
Labradorite	6.568	0.273	6.62	49	0.377	0.803	5.27	123	0.326	1" Baratol	0.5 Al	1.56	9231	Initial density 2.69 g/cc
Albite	6.314	0.188	6.60	32	0.357	0.802	4.80	106	0.319					Initial density 2.58 g/cc

( ) Parentheses indicate data less reliable.

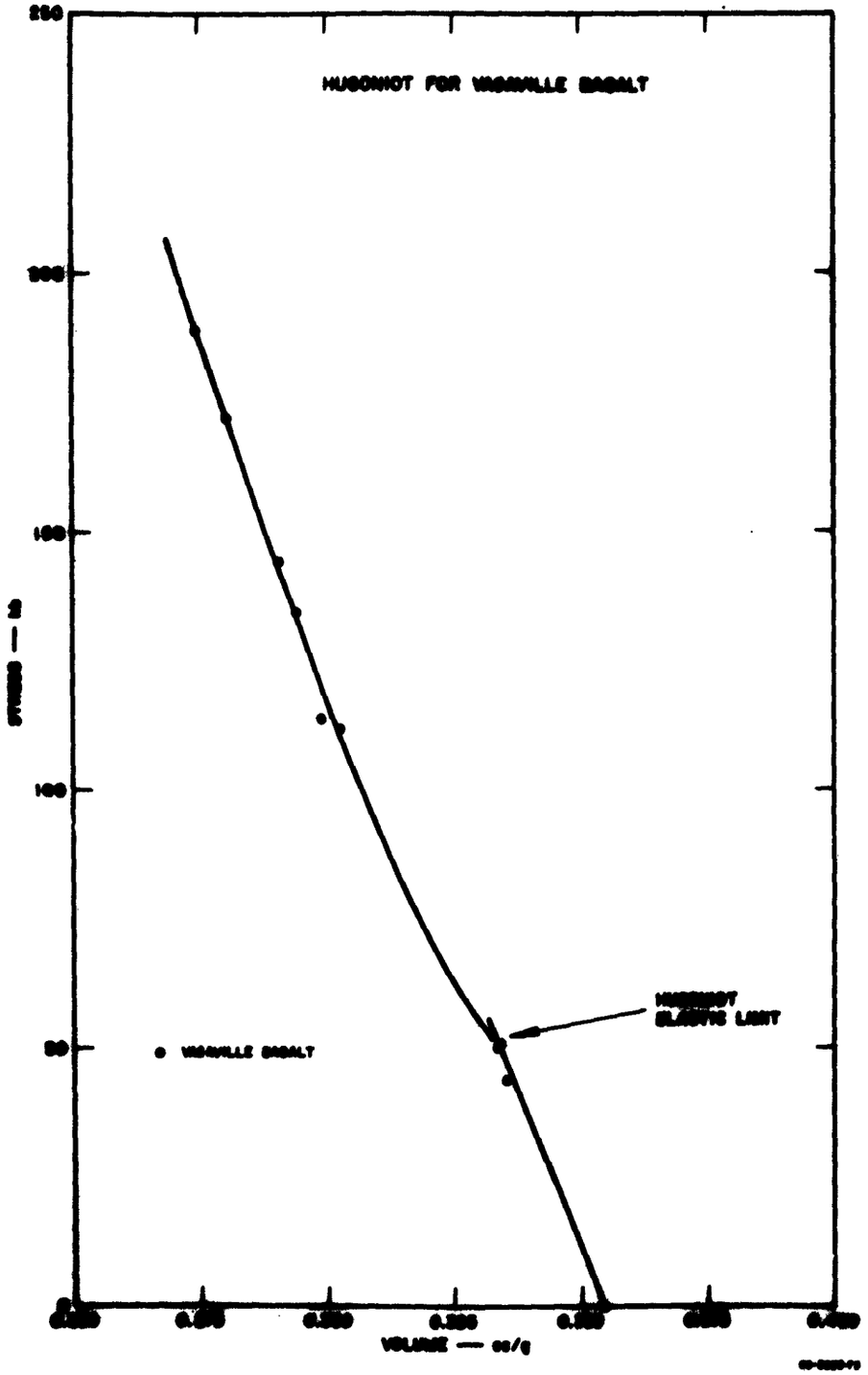
HUGONIOT FOR VASHVILLE BASALT
VOLUME — cc/g
VASHVILLE BASALT

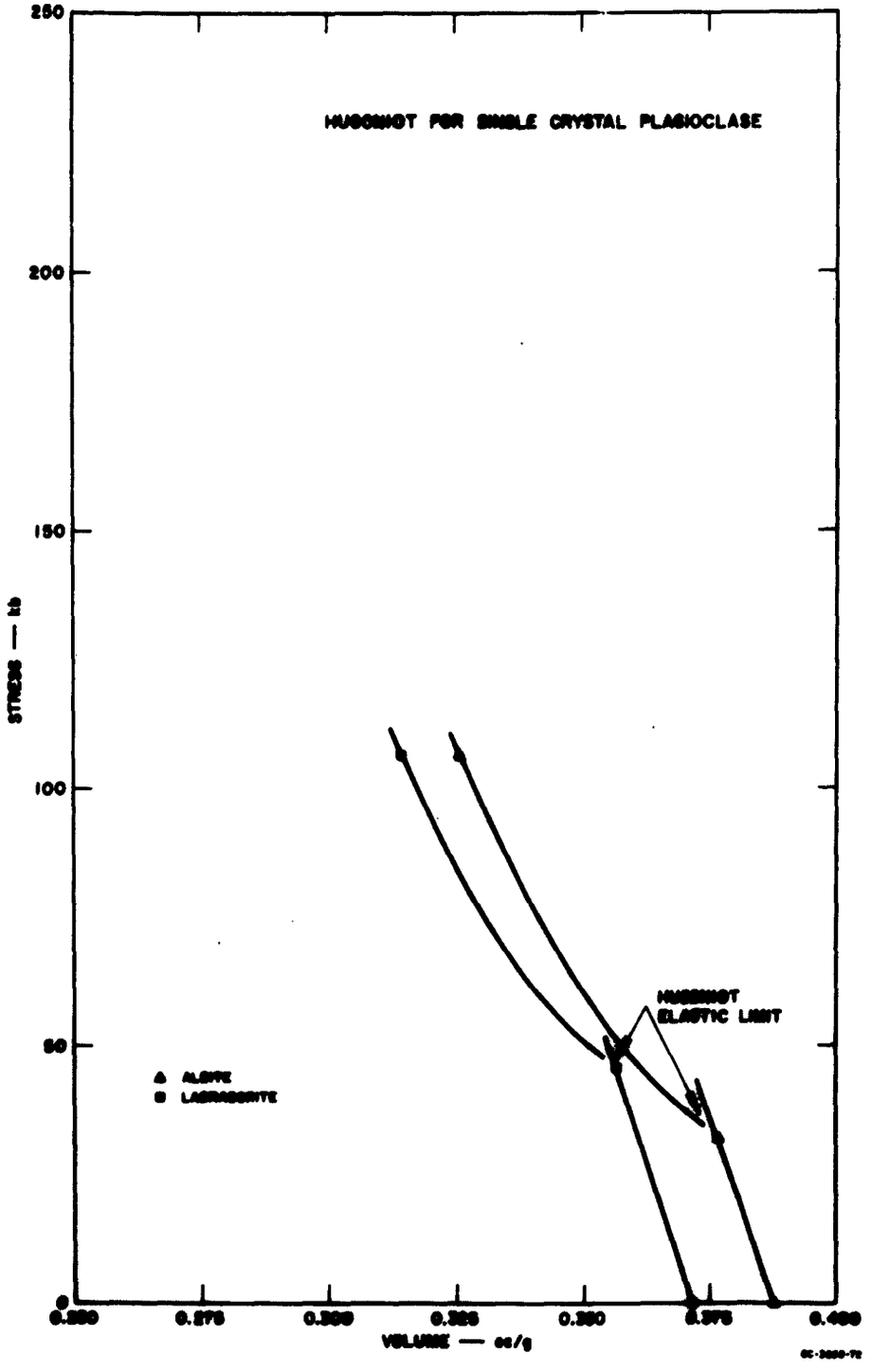
HUGONIOT FOR SINGLE CRYSTAL PLAGIOCLASE
250
200
150
100
50
0
STRESS — kb
HUGONIOT
ELASTIC LIMIT
ALBITE
LABRADORITE
0.350
0.375
0.400
VOLUME — cc/g

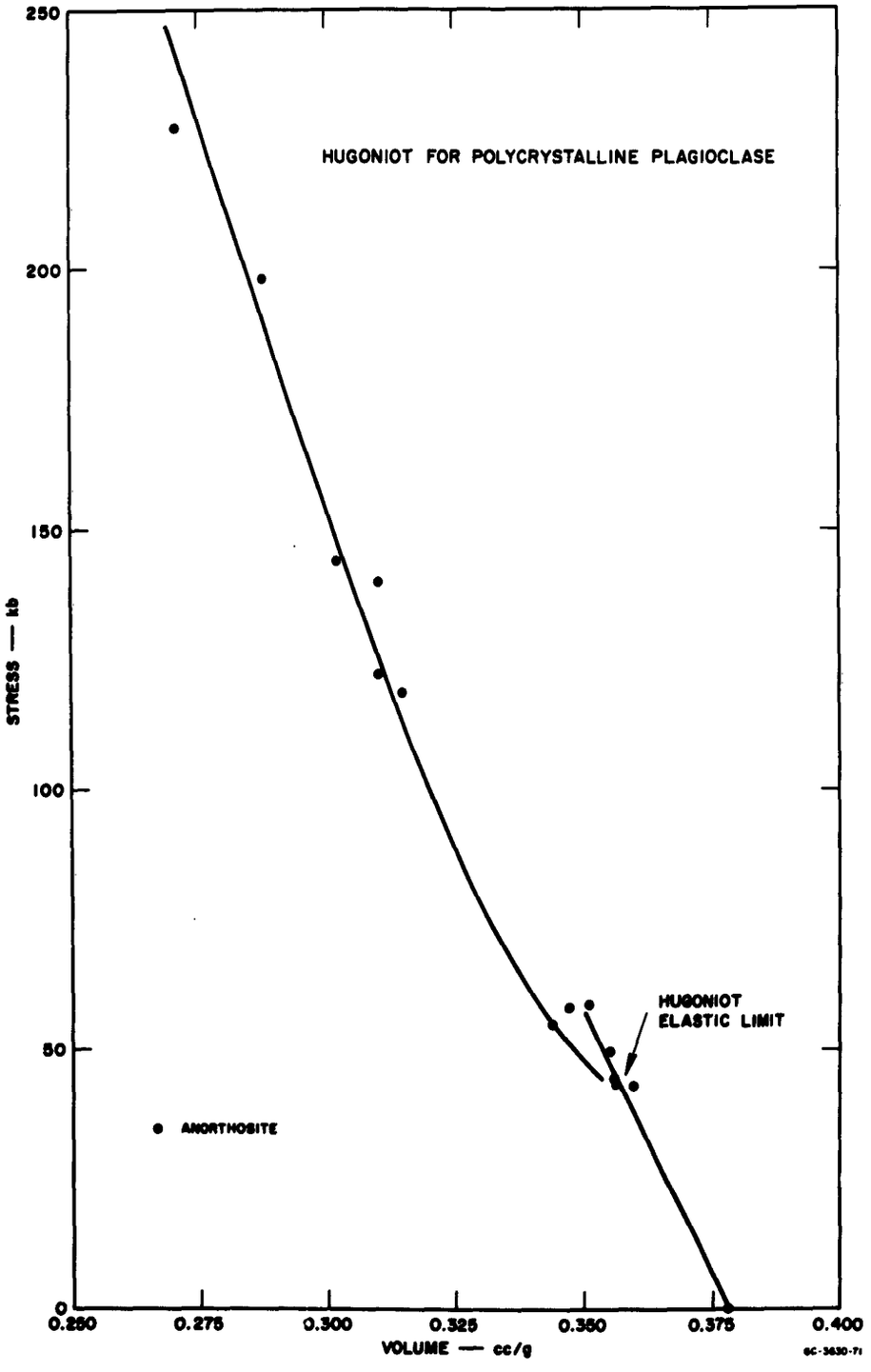

FIG. 27 HUGONIOT FOR PLAGIOCLASE AND BASALT

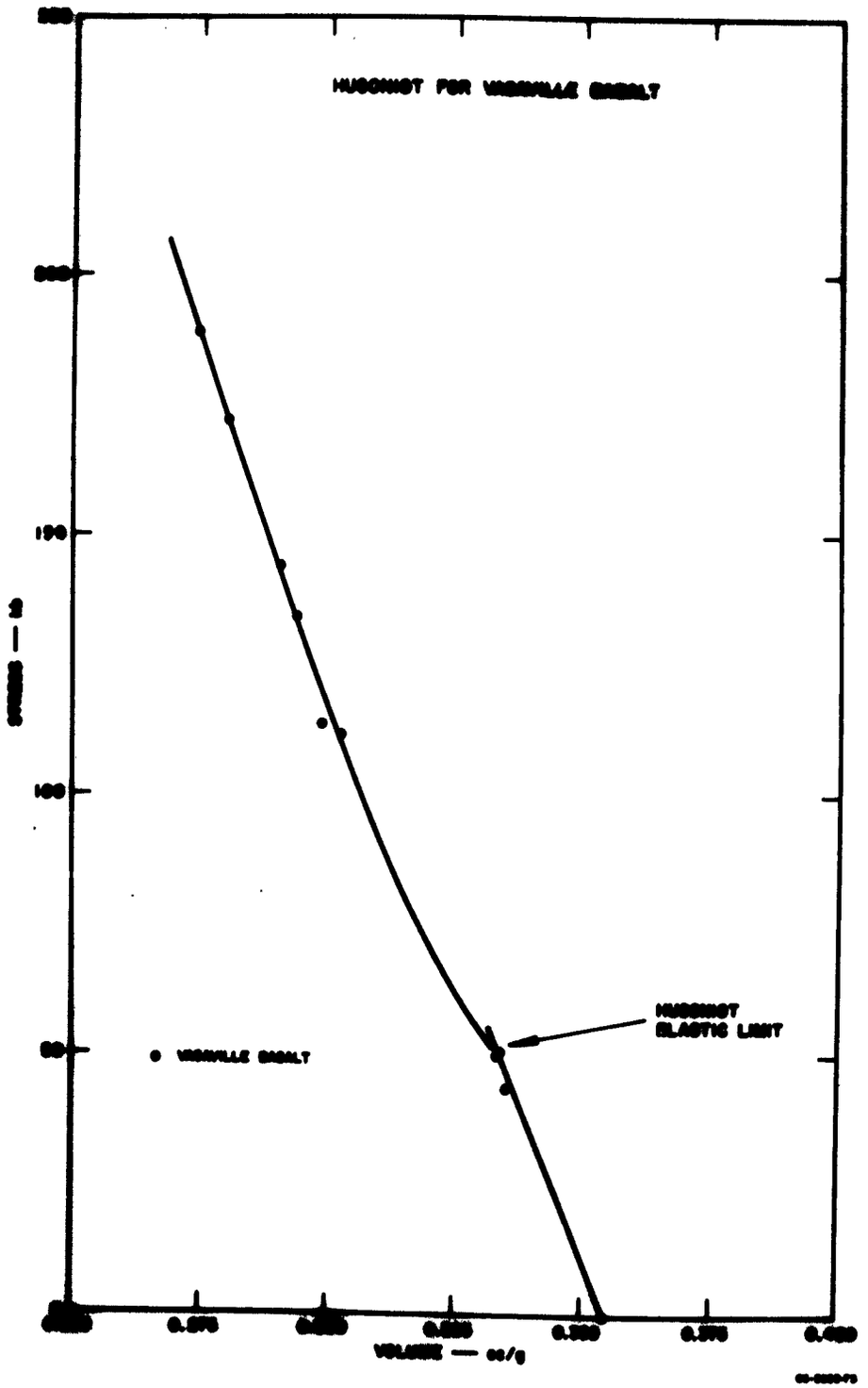
HUGONIOT FOR VESUVIUS BASALT
200
100
50
VESUVIUS BASALT
HUGONIOT
ELASTIC LIMIT

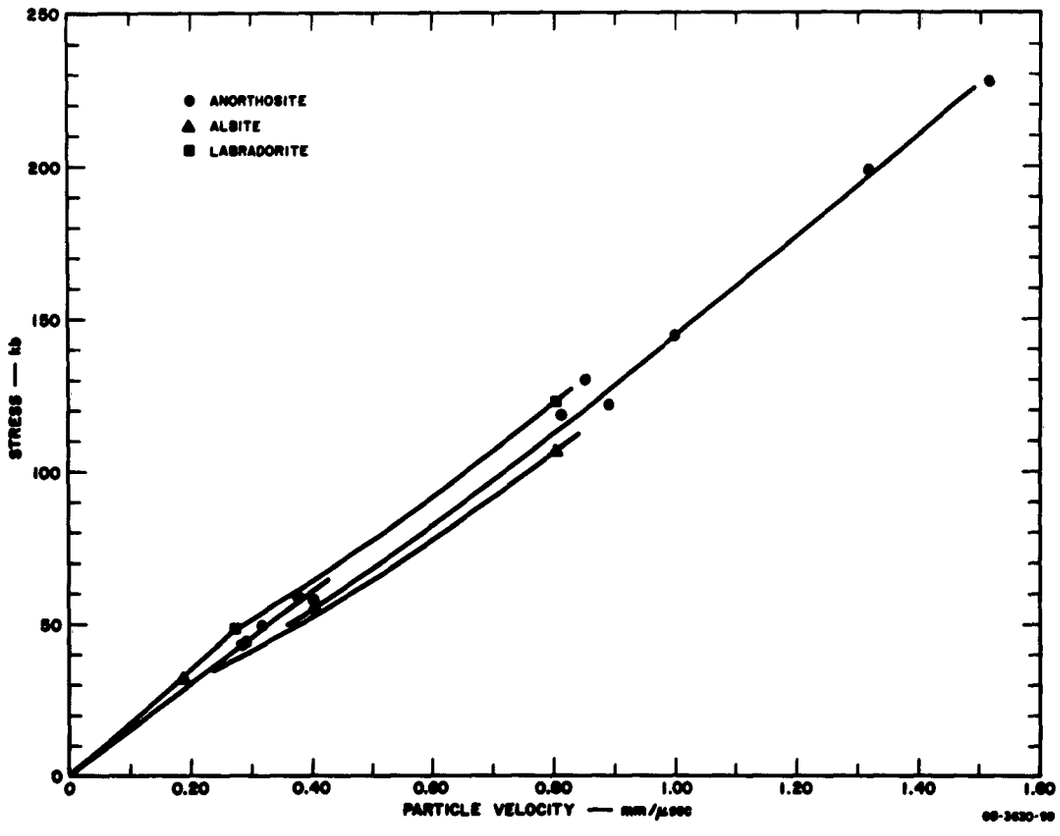

FIG. 28 STRESS-PARTICLE VELOCITY CURVE FOR PLAGIOCLASE

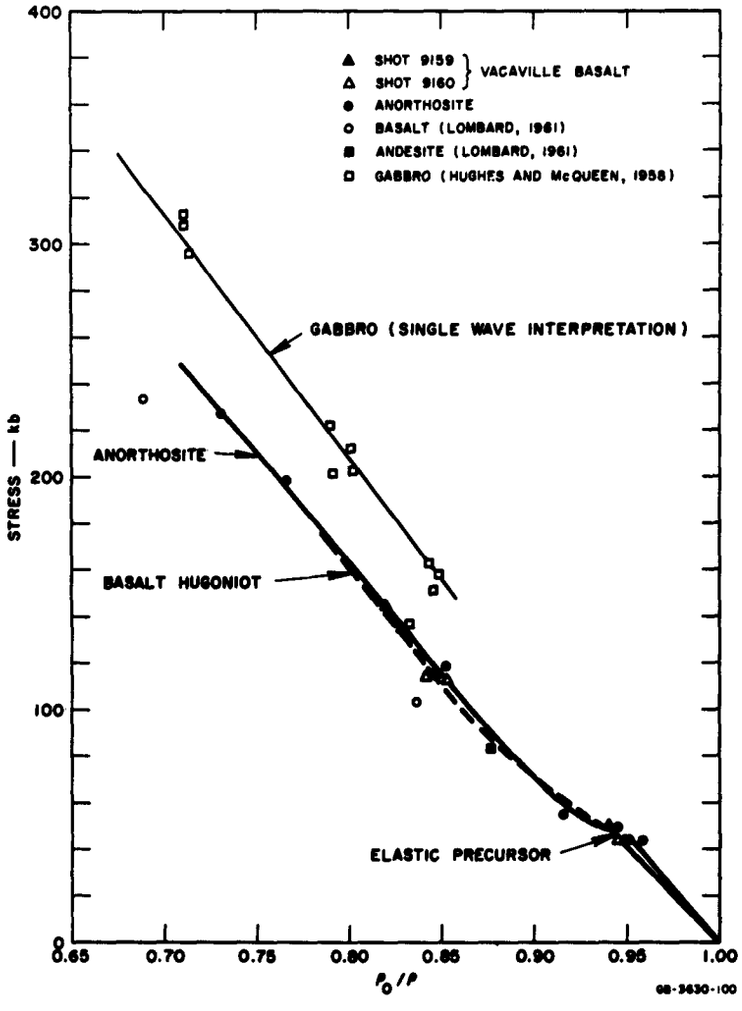

FIG. 29 STRESS-ρ_0/ρ PLOT OF FELDSPAR BEARING ROCKS

However, the two feldspars, labradorite and albite, have essentially the same thickness and crystal orientation and were shocked by the same input pressure. We recorded a difference of about 20 kb for their Hugoniot elastic limit. One would not expect elastic wave decay to be markedly different in comparing the adjacent specimens. Thus, it seems reasonable to expect Hugoniot elastic limits to increase from more sodic members to more calcic plagioclase members.

The feldspars are a complicated group of minerals but the above experiments have given us some insight into their behavior under shock loading. Much work should be done to obtain Hugoniot data for three crystallographic orientations for at least two end members of the plagioclase series and orthoclase. Additional work is needed to obtain values of stress-relaxation for plagioclase of a specific composition.

2. BASALT

Vacaville basalt is massive, dark gray basalt that can be classified as 2312E in the system of Johannsen. The mineral composition is 53% plagioclase (An_{53}-An_{45}), 31% augite, 9% magnetite-ilmenite, 5% celadonite, and 2% apatite. The basalt is composed essentially of equidimensional mineral grains with interstitial celadonite. The feldspars and augite crystallized penecontemporaneously, giving the rock an intergranular texture. Grain sizes are between 0.2 mm and 0.02 mm. The presence of some vesicules gives the rock a porosity of about 3%, Density is 2.82 g/cc.

Table V lists Hugoniot data. Figures 27 and 30 are plots of Hugoniot data and stress-particle velocity data for basalt. Figure 29 shows all available data for feldspar and basalt type rocks.

The Hugoniot shows two features of interest. The first is the Hugoniot elastic limit at about 50 kb with no other transitions evident to pressures as high as 190 kb. The second is that velocities of the main shock are close to elastic velocities. This makes interpretation of a multiple shock front difficult because of the time required for the fronts to separate. We do not have enough data to tell if the elastic wave in basalt decays with distance of travel.

The transition at about 150 kb reported by Hughes and McQueen[3] was not found in the anorthosite or the basalt. Moreover, a transition with

Table V

HUGONIOT DATA FOR BASALT

ROCK TYPE	SPECIMEN THICKNESS (mm)	FIRST FRONT				SECOND FRONT				EXPLOSIVE SYSTEM P-60 +	DRIVER		SHOT NO.	NOTES
		Particle Velocity (mm/μsec)	Shock Velocity (mm/μsec)	Stress (kb)	Volume (cc/g)	Particle Velocity (mm/μsec)	Shock Velocity (mm/μsec)	Stress (kb)	Volume (cc/g)		Material (inch)	Free-Surface Velocity (mm/μsec)		
Basalt	6.228					0.964	5.31	144	0.290	0.5" Comp B +	0.5 Al	1.968	9159	Initial density 2.82 g/cc
	12.456	0.328	5.43	50	0.333	0.906	5.19	134	0.294	1" Baratol				
Basalt	6.236					0.798	5.06	114	0.299	1" Baratol	0.8 Al	(1.64)	9160	
	12.454	0.291	5.33	44	0.335	0.764	5.12	112	0.302					
Basalt	6.134					1.232	5.44	189	0.274	1" Comp B	0.5 Al	--	9232	
	12.370	0.323	5.55	51	0.334	1.124	5.40	172	0.281					

( ) Parentheses indicate data less reliable.

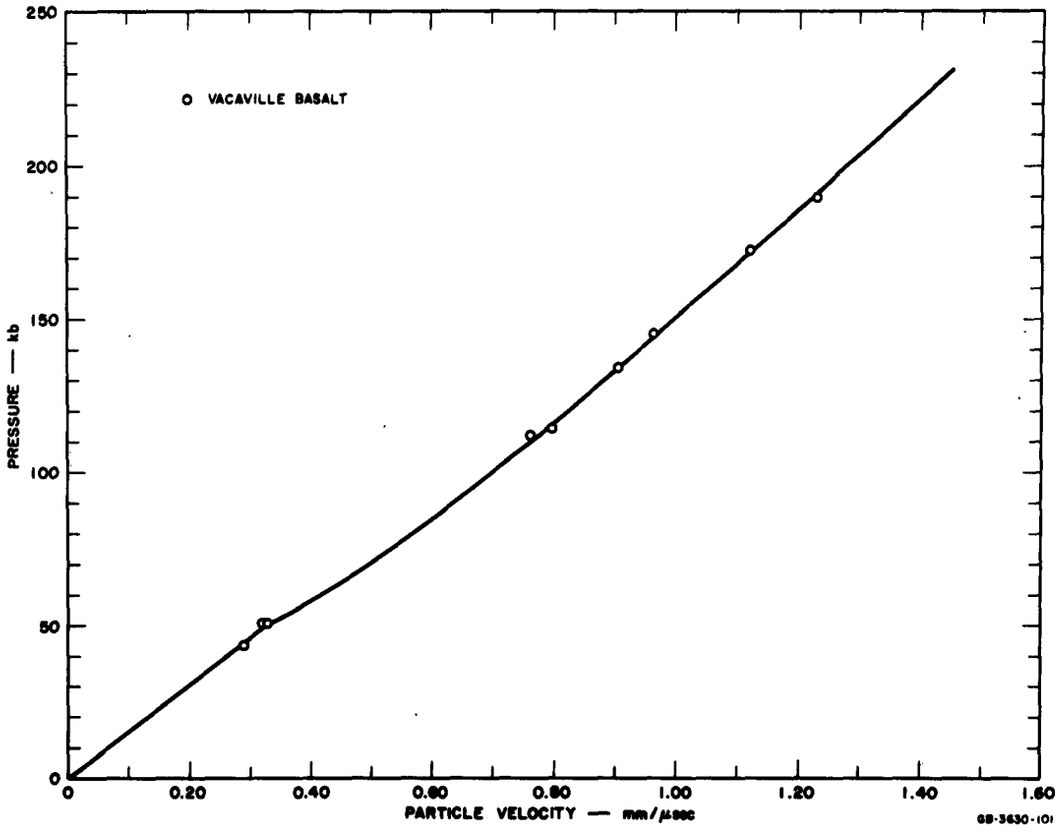

FIG. 30 PARTICLE VELOCITY CURVE FOR BASALT

magnitude of the large suggested volume change for gabbro seems unlikely in the feldspar rocks so far studied. The properties of the gabbro, which is composed of more than 50% plagioclase, are probably similar to those of anorthosite. A modified explanation is therefore proposed for the data presented by Hughes and McQueen. The extension of the Rayleigh line above the Hugoniot elastic limit intersects the Hugoniot curve at approximately 150 and 230 kb for anorthosite and basalt (Fig. 27). It seems reasonable to conclude that rocks with a high feldspar content would have a stable single shock front above a shock stress on the order of 150 to 230 kb, and a double shock front below this magnitude. Hughes and McQueen used a technique that recorded the shock velocity of the first front of a multiple shock until they exceeded 300 kb (Fig. 31).

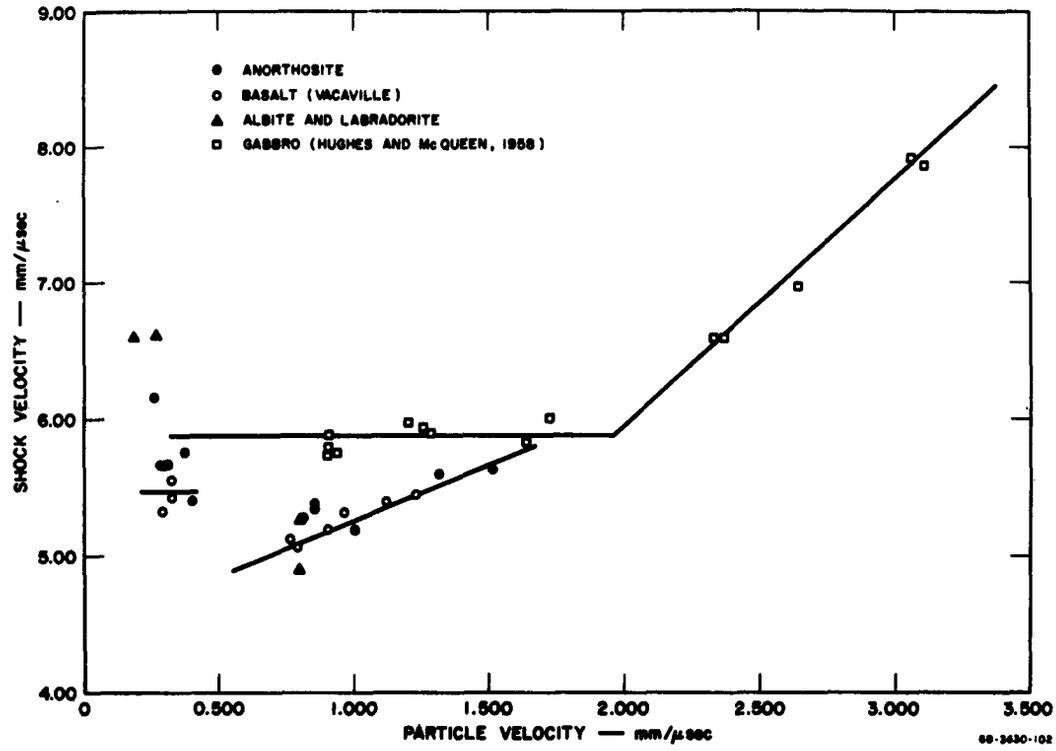

FIG. 31 SHOCK-PARTICLE VELOCITY CURVE FOR FELDSPAR BEARING ROCKS

Above about 300 kb a single shock again becomes the stable front and the shock velocity of a single front is measured. The effect recorded by Hughes and McQueen is, then, the boundary between regions of a stable single shock and a stable double shock. Their method is based on an impedance match solution which, as they point out, is invalid for a two-wave structure. If a two-wave structure is present, it cannot be observed directly but its presence can be inferred from the change in slope of the shock velocity-particle velocity curve.

Using their system, the transition point where the second wave begins cannot be precisely determined. They suggest that the transition is at 150 kb. However, the first wave through gabbro may be an elastic precursor of about 50 kb rather than the 150 kb state suggested. Although the material of the present investigation is not identical it appears likely that Hughes and McQueen recorded the elastic wave until it was overdriven at 300 kb, and not a polymorphic transition.

V STATIC MEASUREMENTS

A. EXPERIMENTS

(Portions of the following pages have been taken from another report prepared at these Laboratories for Vela-Uniform.[23])

The goal of the static experiments is to find some parameter which can be related to the Hugoniot elastic limit. Some of the rocks studied dynamically have been subjected to uniaxial compression, the same strain geometry that exists in the dynamic experiments. Length, compressional velocity, and shear velocity have been measured as a function of pressure. Present results indicate that strength under conditions of plane-strain may be directly related to the Hugoniot elastic limit for porous quartz sandstones.

The details of the theory, equipment, and techniques are described elsewhere.[23] Briefly, a cylindrical rock sample is placed in a steel pressure vessel (Fig. 32). Pressure is exerted in the axial direction by means of two steel pistons which have ultrasonic ceramic transducers bonded to the ends with phenylsalicylate. Lateral pressure is applied through a hole in the chamber wall and is controlled independently of the axial pressure (Fig. 33).

The specimen is fitted into a rubber sleeve with the ends of the sleeve wired firmly to ends of the steel pistons to prevent oil from penetrating the sample. This technique is quick and is usually quite successful.

For plane-strain, the relationship

$$\tau_{22} = [1 - 2(\beta/\alpha)^2]\tau_{11}$$

must be satisfied, where τ_{22} is the lateral pressure, τ_{11} is the longitudinal pressure, β is the shear velocity, and α is the compressional velocity. When this relationship is determined, the specimen can be compressed under conditions of plane-strain. In practice the shear velocity is quite difficult to determine accurately, especially for porous sandstones. At low pressures both velocities are extremely

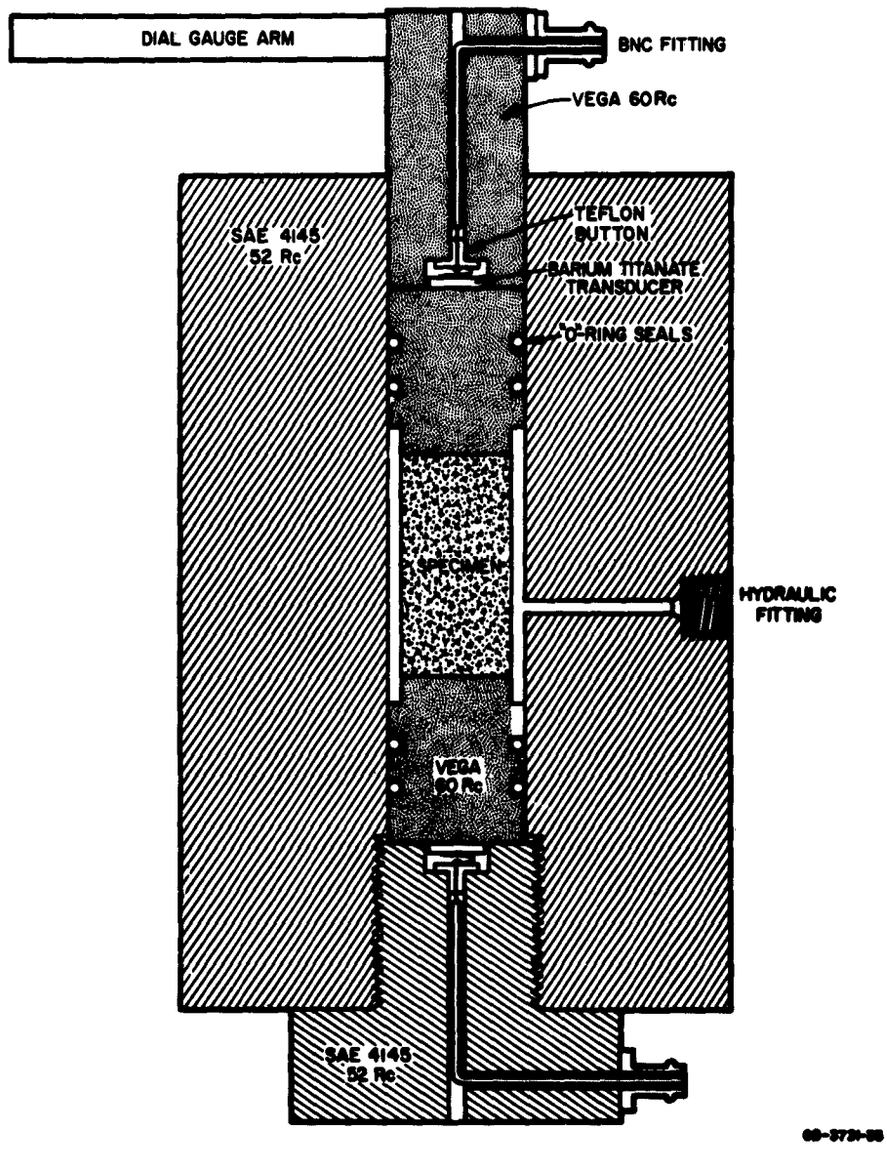

FIG. 32 EXPERIMENTAL PRESSURE VESSEL FOR ULTRASONIC MEASUREMENTS WITH TWO-DIMENSIONAL STRESS SYSTEMS

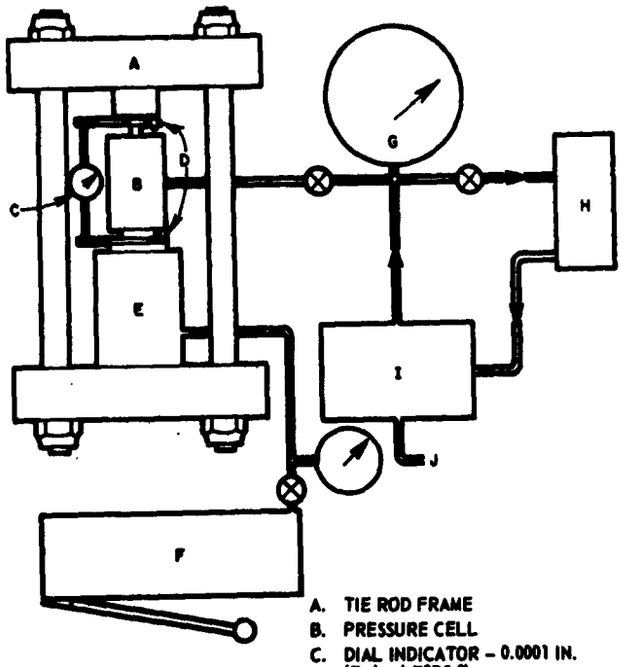

A. TIE ROD FRAME
B. PRESSURE CELL
C. DIAL INDICATOR – 0.0001 IN. (Federal E3BS-Z)
D. TRANSDUCER CONNECTION – BNC
E. RAM – 60 TON (Blackhawk – RC60)
F. HYDRAULIC PUMP (Blackhawk – P80)
G. PRESSURE GAUGE – 30 kpsi (Heise)
H. OIL RESERVOIR
I. AIR PUMP – (Sprague)
J. AIR LINE – 100 psi

FIG. 33 SCHEMATIC OF SYSTEM

sensitive to small changes in pressure. The plane-strain condition is best determined from values taken at pressures of about 0.3 kb or more. Care must be taken to measure both compressional and shear velocities at the same pressure since small differences in velocity can make a large difference in the plane-strain line.

A 1 μsec, 30-volt video pulse is applied to either of two 1 Mc/sec ceramic transducers. The transmitted signal from the receiving transducer is observed on the oscilloscope. Zero-pressure travel time measurements are obtained using the calibrated Tektronix Type 535A oscilloscope delay lines. As pressure is applied to the specimen, variations of

0.005 μsec in travel time can be measured by displacement of the signal on the oscilloscope face using a sweep speed of 0.1 μsec/cm.

Longitudinally polarized ceramic transducers are used to generate and detect longitudinal waves. Transverse velocities are measured in two ways: (1) A direct measurement can be made using square ceramic transducers, polarized parallel to their silvered faces. These transducers will produce a strong transverse pulse which is preceded by a weak longitudinal forerunning wave. (2) An indirect measurement depends on conversion of longitudinal waves to transverse waves at the specimen lateral boundary. The transverse waves (S) propagate across the specimen diameter and are again reflected as longitudinal waves (P). When a pulse is sent down the specimen by one transducer, the received signal at the other transducer consists of the direct P arrival followed by a train of pulses corresponding to paths of the type $P - nS - P$, where n is an integer. The delay time of these pulses is given by

$$\Delta t_s = nD\sqrt{\beta^{-2} - \alpha^{-2}}$$

where D is the cylindrical specimen diameter. The indirect measurement has the advantage that both α and β can be measured at the same time on the same sample, but suffers from the disadvantage noted by Hughes and Maurette[24] that it sometimes gives spurious results on coarse-grained rocks. In the present work, this method was not successful using porous sandstones and had limited success with other rocks. Another difficulty with the indirect measurement is that it is based on the assumption that the medium is homogeneously strained, as by hydrostatic pressure. In our experiment, the stress has a tensorial character and hence mode conversion at the boundaries becomes more complicated.

B. RESULTS

1. St. Peter Sandstone

Most of the study has been concentrated on St. Peter sandstone in an attempt to improve techniques and to obtain reliable data. The most interesting aspect proves to be the strength of the rock under conditions of plane-strain or near plane-strain. In seven runs, the sandstone has failed at 6.5 ± 0.3 kb. The conditions at failure are somewhat offset from plane-strain because the maximum longitudinal pressure obtainable along the St. Peter plane-strain line is about 5.7 kb with our equipment.

Our limiting factor is lateral stress, which cannot be raised much above 30,000 psi. The ratio of ram pressure to lateral pressure at failure was slightly greater than that calculated for plane-strain.* However, failure is obtained for several different values of ram to lateral pressure ratio, all larger than, but close to, the ratio for plane-strain. The strength does not vary significantly with the ratio over the small range studied. The conclusion is reached that the strength of St. Peter sandstone under conditions of plane-strain is close to 6.5 kb.

Only two values of the Hugoniot elastic limit have been measured in shock experiments 10.9 kb and 4.5 kb. The lower value is thought to be more reliable. The spread is large, but the agreement with the strength under static conditions is encouraging.

Two examples of specimens after failure are shown in Figs. 34 and 35. The 2-inch samples have a tendency to fail along a 45° plane, as shown. The 1-inch samples tend to fail in a conical manner with one end serving as the base of a cone, again at about 45° to the axis. Presumably, the shorter length does not allow a plane to form. In the pictures the rubber sleeve, of double thickness, has been slit lengthwise to expose the samples.

Measurements of the change in travel time of the compressional wave with increasing pressure are shown in Fig. 36. The values change in a characteristic and repeatable manner, but the magnitude of the change, especially over the initial kilobar or so, fluctuates from sample to sample. The method of analysis depends on correcting for times through the transducers and pistons by obtaining the difference in measurements on specimens of different lengths, usually 2 inches and 1 inch. Obviously, specimen to specimen variations are troublesome in this sort of analysis. In the present case the average values for three runs on 1-inch samples have been subtracted from the average of three runs on 2-inch samples.

The dial readings (Fig. 37), which measure change in length of the samples and pistons, are reduced in a similar manner to eliminate the effects of changes in the piston. The dial readings are subject to errors in friction and in alignment of the piston with the surface of the tie rod frame. In nearly all cases, the readings have changed with pressure in a linear fashion except near the beginning of the run where they deviate markedly, apparently through alignment effects and friction.

* An apparent excess in ram pressure may be partially offset by the friction in the "O" rings which seal the steel pistons (Fig. 32). This friction is thought to be small and will tend to reduce the actual stress, τ_{11}, applied to the specimen.

FIG. 34 TWO-INCH SPECIMEN OF ST. PETER SANDSTONE AFTER FAILURE

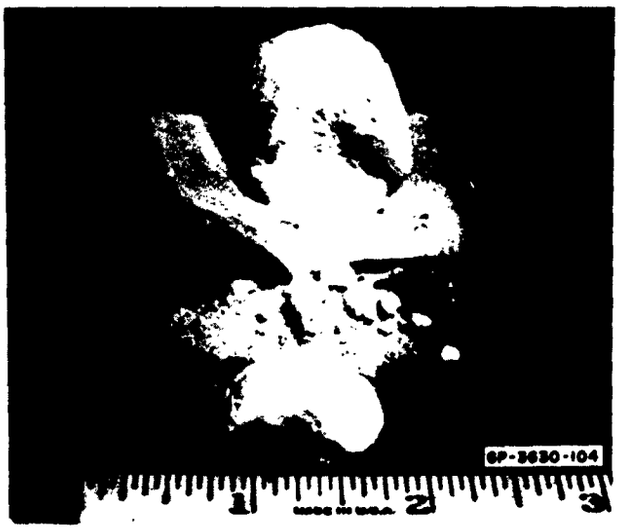

FIG. 35 ONE-INCH SPECIMEN OF THE ST. PETER SANDSTONE AFTER FAILURE

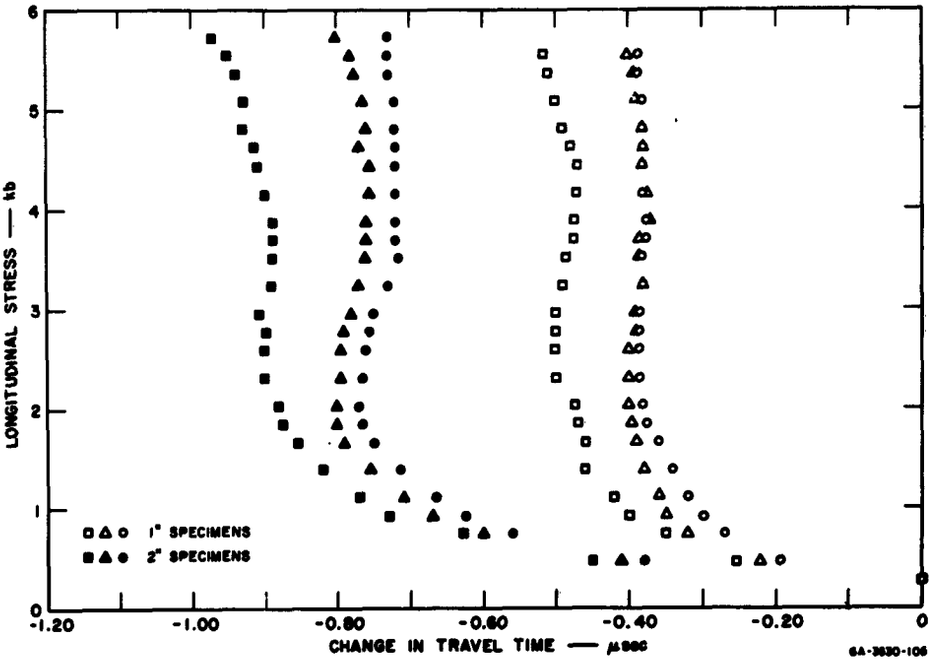

FIG. 36 ST. PETER SANDSTONE – RAW ULTRASONIC DATA FOR COMPRESSIONAL WAVE ARRIVALS

Because of errors at the beginning, slopes over the main portion of the plots are averaged and the average slope is extended back to zero pressure. The measured decrease in sample length shown in Fig. 6 is the difference between the average for three runs with 1-inch specimens and the average for three runs with 2-inch specimens obtained in this manner. Another run with a 2-inch sample has been disregarded because it differs substantially from the other three. The cause of the discrepancy is not certain, although some difference evidently arises because the dial gauge had been aligned somewhat differently. For future work the system of measuring sample lengths should be improved.

The length decrease of the sample may be calculated independently of the dial measurements, using the relationship

$$S = S_0 - \frac{1}{\rho_0 S_0} \int_0^{\tau_{11}} t_p^2 \, d\tau_{11}$$

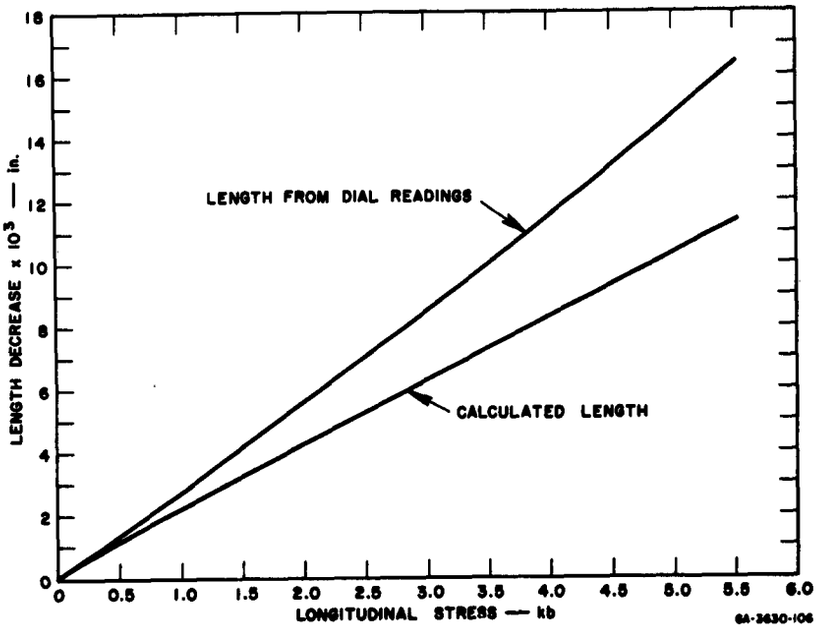

FIG. 37 ST. PETER SANDSTONE – CALCULATED AND MEASURED LENGTH DECREASE

where S is the specimen length, S_0 is the original length, ρ_0 is the original density, t_p is the travel-time through the specimen for the compressional wave, and τ_{11} is the longitudinal stress. This equation is derived elsewhere[28] and is only valid for conditions of plane-strain.

The calculated length decrease (Fig. 37) is in poor agreement with the length decrease as given by the dial measurements. As noted above, the dial measurements are subject to large errors in this analysis.

The measurements of length and travel-time permit the compressional velocity as a function of pressure to be plotted. The results are shown in Fig. 38. The velocity rises quite sharply from its initial value and reaches a maximum at about 2 kb pressure. As pressure is further increased, the velocity slowly decreases. The significance of this feature is not clearly understood, and its validity is not firmly established.

The question may be raised that errors in experiment and analysis are great enough so that the velocity actually reaches a constant value or perhaps even continues to increase very slowly, as is the expected

result. However, the change in travel-time plots (Fig. 36) indicates that the time through the sample and pistons reaches a nearly constant value after passing through a minimum. The time through the pistons is expected either to remain constant or to decrease at some linear rate. Also, the sample length decreases linearly. Therefore, from a qualitative point of view, it appears that the maximum in the compressional velocity-stress curve (Fig. 38) is controlled by raw travel-time data and not by errors in the analysis.

The compressional wave travel-time measurements as a function of pressure are thought to be quite accurate. Changes in travel-time can be measured to ±0.005 μs and ram pressure and lateral pressure can be regulated to ±20 psi. The uniaxial-strain line itself is not well-known but measurements on St. Peter sandstone using a significantly different uniaxial-strain line show similar results for change in travel-time. Sioux quartzite, Solenhofen limestone, Vermont marble, and Massillon sandstone do not show such a minimum in the travel-time data. For other

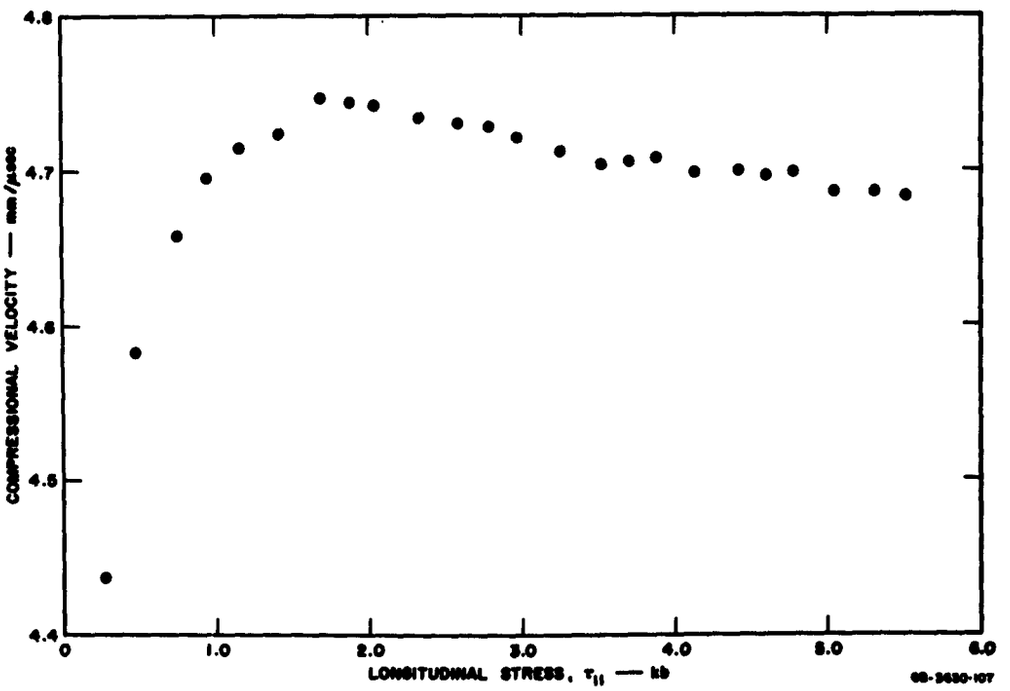

FIG. 38 ST. PETER SANDSTONE – COMPRESSIONAL VELOCITY MEASUREMENTS

rocks, time continues to decrease with the magnitude of decrease becoming smaller with increasing pressure.

Shear velocity measurements have been attempted using both the *PSP* technique and the shear transducers. Reliable measurements as a function of pressure are not obtained with either method. The most serious source of trouble is that an increase of pressure leads to a severe distortion of the waveform being observed. The *PSP* measurements are especially troublesome in this respect, and the method has been rejected for studying porous sandstones.

In the case of *S* measurements with shear transducers, the waveshape of the *S* arrival is affected by changes in the *P* precursor relative to the *S* arrival. The *P* precursor is very small at its beginning, but "noise" in the trace increases before the *S* arrival, presumably because of the arrival of waves which travel part of the distance as *P* waves and part as *S* waves. The *S* arrival itself also appears to change character sometimes as pressure increases. Getting enough energy through the sample is another source of difficulty with the *S* wave measurements—a difficulty that can be solved with a stronger pulse generator. The first problem will still remain but will then be easier to overcome. The shear velocity measurements are important because of the possibility that the uniaxial-strain ratio, τ_{22}/τ_{11}, may change with pressure. Such a change may be the cause of the compressional velocity decrease with pressure.

2. Massillon Sandstone

Four runs have been made with 1-inch specimens of Massillon sandstone. Failure occurs at 4.2, 4.0, 3.4, and 3.1 kb. A 2-inch specimen failed at 4.0 kb. The uniaxial-strain relationship, $\tau_{22} = 0.375\ \tau_{11}$, which had been found for the St. Peter sandstone, has been used for these measurements. It is thought that errors involved in this approximation are not much greater than uncertainties in the measurements, but for future work the proper relationship should be developed. Measurements of the Hugoniot elastic limit give values of 6.9, 6.4, and 4.2 kilobars, with the lower value being favored because it has been determined from a record of better quality.

The dial gauge readings are less linear than are those of the St. Peter sandstone. Some evidence of yielding has been noted long

before failure. The impurities in the Massillon probably make the stress-strain relation more complex.

The compressional wave travel-time behavior appears to be normal. The minimum that characterized the St. Peter does not appear in the Massillon except possibly just before failure. A sharp initial decrease is gradually attenuated until a nearly constant travel-time is reached towards the end of the run.

3. Coconino Sandstone

Two runs have been made with specimens of Coconino sandstone using the St. Peter uniaxial-strain relationship, $\tau_{22} = 0.375\ \tau_{11}$. Both failed at about 3.9 kb. Measurements of the Hugoniot elastic limit give values of ~2, 4.1, 5.1, and 8 kb. The middle two values are more reliable because of better record quality.

Five measurements taken at different ratios of lateral to longitudinal stress provide an indication of the error involved in using an incorrect uniaxial-strain relationship. Using the ratio $\tau_{22}/\tau_{11} = 0.23$, the specimens fail at ~2.6 kb; and using the ratio 0.47, they fail at ~4.4 kb.

The dial gauge readings are more linear than those of the Massillon, probably reflecting the relative lack of impurities in the Coconino. (See Section IV-A-2 for more detailed description of composition.)

4. Solenhofen Limestone

Six runs have been made with two specimens of Solenhofen limestone. The behavior appears quite normal with the compressional velocity increasing from 5.56 mm/μsec at zero-pressure to 5.76 mm/μsec at 5.2 kb. The rate of increase, as expected, lessens with pressure.

Two of the runs have been made with shear transducers. The behavior of the shear velocity is similar to that of the compressional velocity, but numerical agreement between runs is poor.

No extensive yielding or other anomalous behavior of the rock has been noted. This is in contrast with the Vermont marble which displays plastic yielding in the range 3.0 kb to 5.7 kb.

REFERENCES

1. Gregson, V. G. and D. R. Grine, "Vela-Uniform, Dynamic Properties of Rocks," Stanford Research Institute, PGU-3630, Semiannual Technical Report No. 2, 1962.

2. Adadurov, G. A., D. B. Balashor, and A. N. Dremin, "A Study of the Volumetric Compressibility of Marble at High Pressure," *Bull. Acad. Sci.*, USSR (Geophysics) 5, 443-446, 1961.

3. Hughes, D. S. and R. G. McQueen, "Density of Basic Rocks at Very High Pressures," *Trans. Am. Geophys. U.*, 39, 959-965, 1958.

4. Rice, M. H., J. M. Walsh, and R. G. McQueen, "Compression of Solids by Strong Shock Waves," *Solid State Physics*, 6, ed. by F. Seitz and D. Turnbull, Acad. Press Inc., New York, 1958.

5. Walsh, J. M., M. H. Rice, and R. G. McQueen, "Shock Wave Compression of 27 Metals—Equations of States of Metals," *Phys. Rev.*, 108, 196-216, 1957.

6. Fowles, G. R., "Shock Wave Compression of Quartz," Stanford Research Institute, Poulter Laboratories Technical Report 003-61, 1961.

7. Jones, O. E., F. W. Neilson, and W. B. Benedick, "Dynamic Yield Behavior of Explosively Loaded Metals Determined by a Quartz Transducer Technique," *J. Appl. Phys.*, 33, 3224-3232, 1962.

8. Halpin, W. J., O. E. Jones, and R. A. Graham, "Submicrosecond Technique for Simultaneous Observation of Input and Propagated Impact Stresses," Proc. of Conference on Dynamic Behavior of Materials, ASTM, Albuquerque, 1962.

9. Wackerle, J., "Shock Wave Compression of Quartz," *J. Appl. Phys.*, 33, 922-937, 1962.

10. Bridgman, P. W., "The Compression of 39 Substances to 100 000 kg/cm^2," *Proc. Am. Acad. Arts Sci.*, 76, 55-70, 1948.

11. McQueen, R. G., J. N. Fritz, and S. P. Marsh, "On the Equation of State of Stishovite," *J. Geophys. Research*, 68, 2319-2322, 1963.

12. Walsh, J. M. and R. H. Christian, "Equation of State of Metals from Shock Wave Measurements," *Phys. Rev.*, 97, 1544-1556, 1955.

13. Kormer, S. B., A. I. Funtikov, V. D. Urlin, and A. N. Kolesnikova, "Dynamic Compression of Porous Metals and the Equation of State with Variable Specific Heat at High Temperatures," Soviet Physics, *JETP*, 14, 477-488, 1962.

14. Birch, F., "Elasticity and Constitution of the Earth's Interior," *J. Geophys. Research*, 57, 227-286, 1952

15. Kelley, K. K., "Contributions to the Data on Theoretical Metallurgy," Bull. 476, Bureau of Mines, U.S. Dept. Interior, 1949.

16. Al'tshuler, L. V., S. B. Kormer, M. I. Brazhnik, L. A. Vladimirov, M. P. Speranskaya, and A. I. Funtikov, "The Isentropic Compressibility of Aluminum, Copper, Lead, and Iron at High Pressures," Soviet Physics, *JETP*, 11, 766-775, 1960.

17. Courant, R. and K. O. Fredericks, *Supersonic Flow and Shock Waves*, Interscience Publishers, Inc., New York, 1948.

18. Schall, Rudi, "High Speed Measurement of Shock Compressibility in the 1-Mb Range," *Proc. Int. Cong. on High-Speed Photography*, 184-187, Academic Press, New York, 1961.

19. Sclar, C. B., A. P. Young, L. C. Carrison, and C. M. Schwartz, "Synthesis and Optical Crystallography of Stishovite, a Very High Pressure Polymorph of SiO_2," *J. Geophys. Research*, 67, 4049-4054, 1962.

20. Gregson, V. G., C. F. Petersen, and J. C. Jamieson, Vela-Uniform, "Dynamic Properties of Rocks," Stanford Research Institute, PGU-3630, Semiannual Technical Report No. 3, 1962.

21. Dremin, A. N. and G. A. Adadurov, "Shock Adiabat for Marble," Soviet Physics, *Doklady*, Akad Nauk, USSR, **128**, 970-973, 1959.

22. Curran, D. R., "On the Possibility of Detecting Shock-Induced Second-Order Phase Transitions in Solids. The Equation of State of Invar," *J. Appl. Phys.*, **32**, 1811-1814, 1961.

23. Jamieson, J. C., T. J. Ahrens, and R. C. Alverson, "Fundamental Research in Support of Vela-Uniform," Stanford Research Institute PGU-3731, Semiannual Technical Report No. 3, 1963.

24. Hughes, D. S. and C. Maurette, "Elastic Wave Velocities in Granites," *Geophys.*, **21**, 275-284, 1956.

25. Yoder, H. S., Jr., "High-Low Quartz Inversion up to 10,000 Bars," *Trans. Am. Geophys. U.*, **31**, 827-835, 1950.

Poulter Laboratories, STANFORD RESEARCH INSTITUTE, Menlo Park, California.

DYNAMIC PROPERTIES OF ROCKS (U) by V. G. Gregson, T. J. Ahrens, C. F. Peterson August 15, 1963. 78 pp., 38 illus., 5 tables AFCRL-63-662 Unclassified Report

Hugoniot equation of state data in the pressure range 5 to 250 kb have been obtained for quartzite, sandstone, calcite, marble, limestone, plagioclase and basalt. The data were obtained by conventional shock wave techniques which measure shock and associated free-surface velocities. Impedance match solutions were obtained for porous rocks.

High values of the Hugoniot elastic limit were observed in solid rocks—50 to 100 kb in quartzite, 40 to 50 kb in feldspar and basalt, and 20 kb in calcite and marble. Porous rocks show considerably reduced values amounting to approximately 5 kb in sandstone and limestone.

UNCLASSIFIED

1. Hugoniot data for quartz rocks
2. Hugoniot data for carbonate rocks
3. Hugoniot data for plagioclase
4. Hugoniot data for basalt
5. Static uniaxial strain measurements for sandstones and limestones

I. Gregson, V. G., T. J. Ahrens and C. F. Peterson

Poulter Laboratories, STANFORD RESEARCH INSTITUTE, Menlo Park, California.

DYNAMIC PROPERTIES OF ROCKS (U) by V. G. Gregson, T. J. Ahrens, C. F. Peterson August 15, 1963. 78 pp., 38 illus., 5 tables AFCRL-63-662 Unclassified Report

Hugoniot equation of state data in the pressure range 5 to 250 kb have been obtained for quartzite, sandstone, calcite, marble, limestone, plagioclase and basalt. The data were obtained by conventional shock wave techniques which measure shock and associated free-surface velocities. Impedance match solutions were obtained for porous rocks.

High values of the Hugoniot elastic limit were observed in solid rocks—50 to 100 kb in quartzite, 40 to 50 kb in feldspar and basalt, and 20 kb in calcite and marble. Porous rocks show considerably reduced values amounting to approximately 5 kb in sandstone and limestone.

UNCLASSIFIED

1. Hugoniot data for quartz rocks
2. Hugoniot data for carbonate rocks
3. Hugoniot data for plagioclase
4. Hugoniot data for basalt
5. Static uniaxial strain measurements for sandstones and limestones

I. Gregson, V. G., T. J. Ahrens and C. F. Peterson

Poulter Laboratories, STANFORD RESEARCH INSTITUTE, Menlo Park, California.

DYNAMIC PROPERTIES OF ROCKS (U) by V. G. Gregson, T. J. Ahrens, C. F. Peterson August 15, 1963. 78 pp., 38 illus., 5 tables AFCRL-63-662 Unclassified Report

Hugoniot equation of state data in the pressure range 5 to 250 kb have been obtained for quartzite, sandstone, calcite, marble, limestone, plagioclase and basalt. The data were obtained by conventional shock wave techniques which measure shock and associated free-surface velocities. Impedance match solutions were obtained for porous rocks.

High values of the Hugoniot elastic limit were observed in solid rocks—50 to 100 kb in quartzite, 40 to 50 kb in feldspar and basalt, and 20 kb in calcite and marble. Porous rocks show considerably reduced values amounting to approximately 5 kb in sandstone and limestone.

UNCLASSIFIED

1. Hugoniot data for quartz rocks
2. Hugoniot data for carbonate rocks
3. Hugoniot data for plagioclase
4. Hugoniot data for basalt
5. Static uniaxial strain measurements for sandstones and limestones

I. Gregson, V. G., T. J. Ahrens and C. F. Peterson

Poulter Laboratories, STANFORD RESEARCH INSTITUTE, Menlo Park, California.

DYNAMIC PROPERTIES OF ROCKS (U) by V. G. Gregson, T. J. Ahrens, C. F. Peterson August 15, 1963. 78 pp., 38 illus., 5 tables AFCRL-63-662 Unclassified Report

Hugoniot equation of state data in the pressure range 5 to 250 kb have been obtained for quartzite, sandstone, calcite, marble, limestone, plagioclase and basalt. The data were obtained by conventional shock wave techniques which measure shock and associated free-surface velocities. Impedance match solutions were obtained for porous rocks.

High values of the Hugoniot elastic limit were observed in solid rocks—50 to 100 kb in quartzite, 40 to 50 kb in feldspar and basalt, and 20 kb in calcite and marble. Porous rocks show considerably reduced values amounting to approximately 5 kb in sandstone and limestone.

UNCLASSIFIED

1. Hugoniot data for quartz rocks
2. Hugoniot data for carbonate rocks
3. Hugoniot data for plagioclase
4. Hugoniot data for basalt
5. Static uniaxial strain measurements for sandstones and limestones

I. Gregson, V. G., T. J. Ahrens and C. F. Peterson

Four phase transitions, indicated by multiple shock fronts, are observed in calcite. No simple relation between these and the reported transitions observed in static experiments is evident. An indication of a phase transition in sandstone at 68 kb was also obtained and is interpreted as the quartz-stishovite transition. Decay of the elastic precursor wave amplitude, implying a time-dependent yield stress, is observed in quartzite, calcite, and marble.	UNCLASSIFIED	Four phase transitions, indicated by multiple shock fronts, are observed in calcite. No simple relation between these and the reported transitions observed in static experiments is evident. An indication of a phase transition in sandstone at 68 kb was also obtained and is interpreted as the quartz-stishovite transition. Decay of the elastic precursor wave amplitude, implying a time-dependent yield stress, is observed in quartzite, calcite, and marble.	UNCLASSIFIED
Four phase transitions, indicated by multiple shock fronts, are observed in calcite. No simple relation between these and the reported transitions observed in static experiments is evident. An indication of a phase transition in sandstone at 68 kb was also obtained and is interpreted as the quartz-stishovite transition. Decay of the elastic precursor wave amplitude, implying a time-dependent yield stress, is observed in quartzite, calcite, and marble.	UNCLASSIFIED	Four phase transitions, indicated by multiple shock fronts, are observed in calcite. No simple relation between these and the reported transitions observed in static experiments is evident. An indication of a phase transition in sandstone at 68 kb was also obtained and is interpreted as the quartz-stishovite transition. Decay of the elastic precursor wave amplitude, implying a time-dependent yield stress, is observed in quartzite, calcite, and marble.	UNCLASSIFIED

STANFORD
RESEARCH
INSTITUTE

MENLO PARK
CALIFORNIA

Regional Offices and Laboratories

Southern California Laboratories
820 Mission Street
South Pasadena, California

Washington Office
808–17th Street, N.W.
Washington 6, D.C.

New York Office
270 Park Avenue, Room 1770
New York 17, New York

Detroit Office
1025 East Maple Road
Birmingham, Michigan

European Office
Polikanstrasse 37
Zurich 1, Switzerland

Japan Office
911 Iino Building
22, 2-chome, Uchisaiwai-cho, Chiyoda-ku
Tokyo, Japan

Representatives

Toronto, Ontario, Canada
Room 710, 67 Yonge St.
Toronto 1, Ontario, Canada

Milan, Italy
Via Macedonio Melloni, 49
Milano, Italy